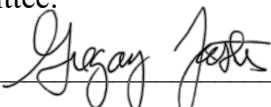


NONCOVALENT BINDING OF ANTHRACENE AND CIPROFLOXACIN WITH
MOLECULAR PSEUDOPHASE: FLUORESCENCE AND PH STUDIES

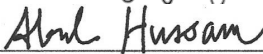
by

Carol Ajjan
A Dissertation
Submitted to the
Graduate Faculty
of
George Mason University
in Partial Fulfillment of
The Requirements for the Degree
of
Doctor of Philosophy
Chemistry and Biochemistry

Committee:



Dr. Gregory D. Foster, Committee Chair



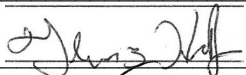
Dr. Abul Hussam, Committee Member



Dr. Gerald Weatherspoon, Committee Member



Dr. Mikell Paige, Committee Member



Dr. Thomas Huff, Committee Member



Dr. Gerald Weatherspoon, Department Chairperson



Dr. Donna M. Fox, Associate Dean,
Office of Student Affairs & Special
Programs, College of Science



Dr. Ali Andalibi, Interim Dean, College of
Science

Date: May 6, 2020

Spring Semester 2020
George Mason University
Fairfax, VA

Noncovalent Binding of Anthracene and Ciprofloxacin with Molecular Pseudophase:
Fluorescence and pH Studies

A Dissertation submitted in partial fulfillment of the requirements for the degree of
Doctor of Philosophy at George Mason University

by

Carol A. Ajjan
Bachelor of Science
George Mason University, 2015

Director: Gregory D. Foster, Professor
Department of Chemistry and Biochemistry

Spring Semester 2020
George Mason University
Fairfax, VA

Copyright 2020 Carol A. Ajjan
All Rights Reserved

DEDICATION

This is dedicated to my parents, Mirvat and Alexander Ajjan, and brothers, Michel and Joseph Ajjan. Thank you for everything you have done and sacrificed to help me become the person I am today. I love you.

ACKNOWLEDGEMENTS

Thank you to the Department of Chemistry and Biochemistry for funding my research and graduate education.

Thank you to the Office of the Provost for funding with the Dissertation Completion Grant.

Dr. Gregory Foster for your positivity, support and being an amazing mentor.

I would like to thank Dr. Abul Hussam for your patience, mentorship and dedication throughout this process.

Dr. Gerald Weatherspoon for always doing what you could to make things happen and encouraging me to pursue my doctorate. I would not have been in the position I am in today without your support and seeing the potential I didn't see in myself.

My committee members Dr. Mikell Paige and Dr. Tom Huff for their time serving on the committee and support throughout this process.

Thank you, Dr. Megan Erb for being a great mentor and friend.

Mrs. Melissa Hayes for being an angel and making the impossible, possible. Thank you for your encouragement, kindness and support.

My friends Arion Leahigh, Elizabeth Lang, Kathryn Holguin, Megan Devine, James Sadighian, Jen Jones and Andrew Evangelista. Graduate school would not have been the

same without you and I am thankful to have friends that supported, guided and kept me sane throughout these five years.

TABLE OF CONTENTS

	Page
List of Tables	x
List of Figures.....	xii
List of Equations.....	xvi
List of Abbreviations and Symbols	xviii
Abstract.....	xxi
INTRODUCTION	1
1.1 Introduction	1
1.1.1 Overview of Fluoroquinolones and surfactants.....	1
1.1.2 Introduction of Surfactants	4
1.1.3 Sodium Dodecyl Sulfate (SDS).....	5
1.1.4 Perfluorooctanesulfonic Acid (PFOS).....	6
1.1.5 DL- α -Tocopherol succinate (TPGS-750M).....	7
1.1.6 Myelin basic protein (MBP).....	9
1.2 Instrumental techniques employed to study binding	10
1.3 Theories: Binding Equilibria in Solution	15
1.3.1 Monomer Complexes	15
1.3.2 Aggregate complexes	21
THEORY SECTION	28
2.1 Theory.....	28
EXPERIMENTAL	39
3.1 Experimental.....	39
3.1.1 Chemicals	39
3.1.2 Instrumentation	39
3.1.3 The operation of the CFCLS	41
3.1.4 Measurement of equilibrium mixing time	44
3.1.5 Fluorophore and surfactant combinations	46

3.1.5.1	Anthracene and TPGS	46
3.1.5.2	pH titrations of CPF	47
3.1.5.3	CPF and SDS Additions	47
3.1.5.3.1	CPF and SDS batch experiments with Shimadzu RF-6000	47
3.1.5.3.2	CPF and SDS titration experiments with CFCLS	48
3.1.5.4	CPF and PFOS additions	49
3.1.5.4.1	CPF and PFOS batch experiments with Shimadzu RF-6000	49
3.1.5.4.2	CPF and PFOS titration experiments with CFCLS	49
3.1.5.5	CPF and TPGS-750M titration experiments with CFCLS	50
3.1.5.6	CPF and MBP titration experiments with CFCLS	51
3.1.6	Data Analysis.....	51
DETERMINATION OF ANTHRACENE AND DL- α - TOCOPHEROL SUCCINATE (TPGS-750M) COMPLEXATION		54
4.1	Anthracene and TPGS-750M complexation	54
4.1.1	The fluorescence spectrum of anthracene	54
4.1.2	The effect of TPGS-750M on anthracene fluorescence	55
4.1.3	Determination of the critical aggregation concentration of TPGS-750 M	56
4.1.4	Binding Constants	58
4.1.1.1	A literature survey of anthracene binding with other pseudophase aggregates	60
THE EFFECT OF pH ON CIPROFLOXACIN (CPF) SPECIATION AND FLUORESCENT PROPERTIES		64
5.1	The effect of pH on CPF speciation and fluorescent properties.....	64
5.1.1	The effect of pH on the fluorescence spectra of CPF species	70
5.1.2	Concentration calibration of CPF: Effect of speciation	72
DETERMINATION OF CIPROFLOXACIN (CPF) AND SODIUM DODECYL SULFATE (SDS) PSEUDOPHASE INTERACTIONS		74
6.1	The determination of CPF and SDS pseudophase interactions	74
6.1.1	CPF and SDS monomer and pseudophase interactions in the presence of phosphate buffer.....	77
6.1.1.1	CPF and SDS monomer and pseudophase interactions at pH 7.00	77
6.1.1.2	CPF and SDS monomer and pseudophase interactions at pH 8.33	84
6.1.1.3	CPF and SDS monomer and pseudophase interactions at pH 4.00	90

6.1.2	CPF and SDS monomer and pseudophase interactions in the absence of phosphate buffer.....	96
6.1.2	Conclusion of CPF and SDS binding	104
Determination of Ciprofloxacin (CPF) AND Perfluorooctanesulfonic Acid (PFOS) Pseudophase Interactions.....		106
7.1	Determination of CPF and PFOS pseudophase interactions	106
7.1.1	Acid dissociation properties of PFOS	106
7.1.2	Effect of PFOS on CPF Fluorescence	107
7.1.2.1	Determination of CPF and PFOS interactions in the presence of phosphate buffer	107
7.1.2.2	Comparison of binding when CPF is tetraprotic versus triprotic	110
7.1.2.2.1	<i>The effect of protonation on fluorescence intensity.....</i>	112
7.1.2.2.2	<i>The effect of protonation of CPF on the binding with PFOS.....</i>	114
7.1.2.2.3	<i>Determination of CPF and PFOS monomer and pseudophase binding</i>	116
7.1.3	Determination of CPF and PFOS binding in the absence of phosphate buffer	117
7.1.3.1.1	<i>Determination of CPF and PFOS monomer and pseudophase binding</i>	122
7.1.3.1.2	<i>Analysis of preaggregate and postaggregate binding between CPF and PFOS</i>	122
7.1.3.2	Binding of CPF and PFOS in the preaggregate phase in the absence of phosphate buffer	123
7.1.4	Conclusion of CPF and PFOS binding	128
DETERMINATION OF CIPROFLOXACIN (CPF) AND DL- α -TOCOPHEROL SUCCINATE (TPGS-750M) PSEUDOPHASE INTERACTIONS		133
8.1	The binding of DL- α -tocopherol succinate (TPGS-750M) and Ciprofloxacin (CPF)	133
8.1.1	Effect of TPGS-750M on CPF fluorescence	133
8.1.1.1	Concentration of TPGS-750M on fluorescence emission of CPF.....	133
8.1.2	Evaluation of CPF-TPGS-750M binding constants	139
8.1.2.1	Determination of the preaggregate and postaggregate binding of CPF with TPGS-750M	139
8.1.2.2	The analysis of CPF and TPGS-750M monomer and pseudophase binding	140

CONCLUSIONS AND FUTURE OUTLOOK.....	142
9.1 Conclusion and Future Outlook.....	142
References	147
Biography	155

LIST OF TABLES

Table	Page
Table 1.1.1 The physical and chemical properties of fluoroquinolones.....	2
Table 1.1.2 Physiochemical properties of Ciprofloxacin (CPF)	3
Table 1.1.3 The chemical properties of the pseudophase compounds	10
Table 1.2.1 A compilation of techniques used to study CPF-surfactant interactions and their characteristics	11
Table 3.1.1 The experimental parameters of CFCLS to determine the ideal mixing time	45
Table 4.1.1 The literature critical aggregation concentration of other surfactants.....	57
Table 4.1.2 The binding of anthracene and TPGS-750M at 25°C. The literature aggregation number of 41 was used to determine K_{n1}	59
Table 4.1.3 Literature binding constants of anthracene with other pseudophase aggregates. cmc- critical micelle concentration, n- aggregation number of the surfactant not the quencher, K_{11} is the 1:1 binding constant, K_b - binding constant (water), K_{sv} - Stern-Volmer constant. a. listed in Table 4.1.4, b. N/L = not listed, c. detection limit in nM not a binding constant, d intensity ratio between sodium taurocholate (NaTC)-metal to NaTC alone.....	60
Table 4.1.4 Equations used to determine the binding constants in Table 4.1.3	61
Table 5.1.1 The literature protonation and pKa values reported for ciprofloxacin using various experimental methods.	64
Table 6.1.1 The literature binding constants of SDS and SLS with CPF using various experimental methods and parameters.	74
Table 6.1.2 The fraction of CPF speciation present in solution at pH 7.00	79
Table 6.1.3 The fluorescence efficiency of free CPF, CPF-monomer (CS) and CPF-pseudophase (CS_n) complexes at pH 7.00 and 25°C.	80
Table 6.1.4 Summary of preaggregate and postaggregate binding constants for CPF and SDS complexation extracted from the slope and intercept of Figure 6.1.3 (a-e) at pH 7.00. The literature aggregation number of 60 was used to determine K_{n1}	83
Table 6.1.5 The fraction of CPF speciation present in solution at pH 8.33	85
Table 6.1.6 The fluorescence efficiency of free CPF, CPF-monomer (CS) and CPF-pseudophase (CS_n) complexes at pH 8.33 and 25°C	86
Table 6.1.7 Summary of preaggregate and postaggregate binding constants for CPF and SDS complexation extracted from the slope and intercept of Figure 6.1.6 (a-e) at pH 8.33. The literature aggregation number of 60 was used to determine K_{n1}	89
Table 6.1.8 The fraction of CPF speciation present in solution at pH 4.00	92
Table 6.1.9 The fluorescence efficiency of free CPF, CPF-monomer (CS) and CPF-pseudophase (CS_n) complexes at pH 4.00 and 25°C	93

Table 6.1.10 Summary of preaggregate and postaggregate binding constants for CPF and SDS complexation extracted from the slope and intercept of Figure 6.1.9 (a-e) at pH 4.00. The literature aggregation number of 60 was used to determine K_{n1} .	95
Table 6.1.11 The fluorescence efficiency of free CPF, CPF-monomer (CS) and CPF-pseudophase (CS_n) complexes at 25°C	98
Table 6.1.12 The fluorescence efficiency ratios obtained from the data in Table 6.1.11	100
Table 6.1.13 The determination of preaggregate and postaggregate binding constants for CPF and SDS complexation using the CFCLS extracted from the slope and intercept Figure 6.1.12 (a) – (e). The literature aggregation number of 60 was used to determine K_{n1} .	102
Table 7.1.1 The literature pK_a values of PFOS.	106
Table 7.1.2 Data obtained for CPF with PFOS additions using Shimadzu RF-6000 and pH measurement	109
Table 7.1.3 Binding constants for tetraprotic and triprotic CPF species with PFOS surfactant and PFOS-pseudophase at 25.0 °C. The literature aggregation number 7 was used to determine K_{n1} .	116
Table 7.1.4 The change in pH and concentration of PFOS obtained with the CFCLS at 25°C.	118
Table 7.1.5 Binding constants K_{11} and K_{n1} for CPF species with PFOS surfactant and PFOS pseudophase at 25°C. The literature aggregation number of 7 was used to determine K_{n1} .	122
Table 7.1.6 Determination of preaggregate binding constant K_{11} for CPF species with PFOS surfactant extracted from the slope of Figure 7.1.14 (a) - Figure 7.1.14 (f) at 25°C.	128
Table 8.1.1 Calculated K_{11} and K_{n1}/n binding constants of CPF and TPGS-750M at 25°C extracted from the slope and intercept of Figure 8.1.4 (a) – (e). The literature aggregation number of 41 was used to determine K_{n1} .	139

LIST OF FIGURES

Figure	Page
Figure 1.1.1 The chemical structure of sodium dodecyl sulfate (SDS).....	6
Figure 1.1.2 The chemical structure of perfluorooctanesulfonic acid (PFOS).....	7
Figure 1.1.3 The chemical structure of DL- α -tocopherol succinate (TPGS-750M).....	8
Figure 1.1.4 A portion of the chemical structure of myelin basic protein (MBP) responsible for fluorescence	9
Figure 3.1.1 Schematic of a Continuous Flow Closed Loop System (CFCLS). TC: Thermo-stated mixing cell (35.0 mL), PH- pH probe, T- thermostat, PELS5B: Perkin-Elmer Mode 5B spectrofluorometer, Autoburet: RAZEL precision syringe pump, P: Peristaltic pump controlled by computer, MC 1208 FS-Plus: Measurement Computing data acquisition card (PMD 1208, Measurement Computing Inc., USA).....	41
Figure 3.1.2 An example of CFCLS program	43
Figure 3.1.3 The calibration of the pH probe used in CFCLS using buffer pH 4.00, 7.00, and 10.00	44
Figure 3.1.4 The fluorescence intensity versus volume flow to determine the ideal mixing time of reagents in the whole flow system in the CFCLS	45
Figure 4.1.1 An emission spectrum of 0.023 μ M anthracene in distilled water + 300 μ L of methanol without TPGS – 750 M at 25°C. The excitation wavelength = 270 nm.....	55
Figure 4.1.2 Fluorescence Intensity \pm 5 of anthracene versus the concentration of TPGS – 750M at 25°C.	56
Figure 4.1.3 The figure shows an emission ratio vs. [TPGS] μ M added. The critical aggregation concentration, 1512 μ M, is found from the intersection of initial slopes as shown.....	57
Figure 4.1.4 Figure shows a portion of the emission ratio when $S_T - c_{ac}$ is greater than or equal to 0. The intercept and the slope were used to calculate K_{11} and K_{n1}/n	59
Figure 5.1.1 CPF dissociation and the corresponding species (left to right) with designated fractions α_0 , α_1 , α_2 , α_3 , and α_4 for CPF as a tetraprotic acid.	66
Figure 5.1.2 Fractional distribution (alpha) of CPF species as a function of pH for a tetraprotic acid. The pK_a values used were 3.64, 5.05, 6.95 and 8.95.....	69
Figure 5.1.3 Distribution of CPF species (alpha) as a function of pH for a triprotic acid. The pK_a values used were -0.21, 6.30 and 8.61.	69
Figure 5.1.4 The excitation (a) and emission (b) spectra of 31.2 μ M CPF from pH 1-11 using Shimadzu RF-6000 at 25°C. $\lambda_{excitation}$ = 270 nm, excitation slit = 3.0 nm; emission slit = 3.0 nm	71

Figure 5.1.5 The experimental fluorescence intensity vs pH of CPF at $\lambda_{\text{emission}}$ of 448 nm and 416 nm. The fluorescence intensity maximums between the two wavelengths correspond to the experimental pK_a values.	72
Figure 5.1.6 Calibration of CPF in water. The measured fluorescence intensity is shown in blue. The tetraprotic CPF distribution curve (Figure 5.1.2) was used to calculate the contribution of the species to the measured fluorescence e.g., CPFH_2^+ (alpha-2) (grey) and CPFH^+ (alpha-3) (orange).	73
Figure 6.1.1 Emission spectrum of SDS additions into 31.2 μM of CPF at pH 7.00. The excitation wavelength = 270 nm and the excitation and emission slits were 3.0 nm.	78
Figure 6.1.2 The fluorescence intensity versus concentration of SDS added to 31.2 μM CPF at pH 7.00 and $\lambda_{\text{emission}} = 448 \text{ nm}$	79
Figure 6.1.3 The equation of $(F_T - F_0)/(C_T \cdot \alpha) = 1 + k_C + k_{11} K_{11}[S] + (k_{n1} K_{n1}/n)(S_T - \text{cac})$ was used. A plot of $(F_T - F_0)/(C_T \cdot \alpha)$ versus $S_T - \text{cac}$ for CPFH_4^{+3} (a), CPFH_3^{+2} (b), CPFH_2^+ (c), CPFH^+ (d), and CPF^- (e) at 25°C and pH 7.00. The K_{n1} and K_{11} were extracted from the slope and intercept of the plots.	82
Notes: The equation $(F_T - F_0)/(C_T \cdot \alpha) = 1 + k_C + k_{11} K_{11}[S] + (k_{n1} K_{n1}/n)(S_T - \text{cac})$ was used to extract the K_{11} and K_{n1} binding constants from the intercept and slope of Figure 6.1.3 (a) – (e). * K_{11} was negative for CPFH_4^{+3} (-52), CPFH_3^{+2} (-50), and CPF^- (-51).	83
Figure 6.1.4 Emission spectrum of SDS additions into 31.2 μM of CPF at pH 8.33. The excitation and emission slits were 3.0 nm.	84
Figure 6.1.5 The fluorescence intensity versus concentration of SDS added to 31.2 μM CPF at pH 8.33 and $\lambda_{\text{emission}} = 448 \text{ nm}$	85
Figure 6.1.6 The equation of $(F_T - F_0)/(C_T \cdot \alpha) = 1 + k_C + k_{11} K_{11}[S] + (k_{n1} K_{n1}/n)(S_T - \text{cac})$ was used. A plot of $(F_T - F_0)/(C_T \cdot \alpha)$ versus $[S_T - \text{cac}]$ for CPFH_4^{+3} (a), CPFH_3^{+2} (b), CPFH_2^+ (c), CPFH^+ (d), CPF^- (e) at 25°C and pH 8.33.	88
Figure 6.1.7 Emission spectrum of SDS additions into 31.2 μM of CPF at pH 4.00. The excitation and emission slits were 3.0 nm.	91
Figure 6.1.8 Fluorescence intensity versus concentration of SDS added to CPF at pH 4.00 and $\lambda_{\text{emission}} = 448 \text{ nm}$	92
Figure 6.1.9 The equation of $(F_T - F_0)/(C_T \cdot \alpha) = 1 + k_C + k_{11} K_{11}[S] + (k_{n1} K_{n1}/n)(S_T - \text{cac})$ was used. A plot of $(F_T - F_0)/(C_T \cdot \alpha)$ versus $S_T - \text{cac}$ for CPFH_4^{+3} (a), CPFH_3^{+2} (b), CPFH_2^+ (c), CPFH^+ (d) and CPF^- at 25°C and pH 4.00.	94
Notes: The equation $(F_T - F_0)/(C_T \cdot \alpha) = 1 + k_C + k_{11} K_{11}[S] + (k_{n1} K_{n1}/n)(S_T - \text{cac})$ was used to extract the K_{11} and K_{n1} binding constants from the intercept and slope of Figure 6.1.9 (a) – (e). * K_{11} binding was negative for CPFH_4^{+3} (-52), CPFH_3^{+2} (-7.0), CPFH_2^+ (-80), CPFH^+ (-87) and CPF^- (-87).	96
Figure 6.1.10 The fluorescence intensity versus concentration of SDS added with 31.2 μM of CPF flushed with N_2 (g) without added phosphate buffer	97
Figure 6.1.11 The distribution of CPF speciation from pH 7.60 – 8.20 \pm 0.01	98
Figure 6.1.12 The equation $[(F_T)/(F_0 \cdot \alpha)] - 1 = (k_{11}/k_C)K_{11}S + (k_{n1}/k_C)(K_{n1}/n)(S_T - \text{cac})$ was used. A plot of $[(F_T)/(F_0 \cdot \alpha)] - 1$ versus $[S_T - \text{cac}]$ for CPFH_4^{+3} (a), CPFH_3^{+2} (b), CPFH_2^+ (c), CPFH^+ (d), and CPF^- (e) at 25°C and pH 7.61 – 8.20.	101

Figure 7.1.1 The fractional distribution of PFOS when the pKa is -3.3.....	107
Figure 7.1.2 The excitation (a) and emission (b) spectra for 31.2 μ M of CPF upon addition of PFOS. $\lambda_{\text{excitation}} = 270$ nm and $\lambda_{\text{emission}} = 416$ nm and excitation and emission slits were 3.0 nm, respectively.....	109
Figure 7.1.3 Plot of intensity vs concentration of PFOS added into 31.2 μ M of CPF at excitation maximum $\lambda_{\text{excitation}} = 270$ nm (a) and emission maximum $\lambda_{\text{emission}} = 416$ nm (b)	110
Figure 7.1.4 Fractional distribution of CPF species as (a) tetraprotic acid and (b) triprotic acid	111
Figure 7.1.5 The observed fluorescence intensity (orange) versus the concentration of PFOS added to CPF. The calculated intensities due to CPFH ₂ ⁺ (blue) and CPFH ⁺ (grey) account for CPF being a tetraprotic acid. The error bars in the diagram show the error within the fluorescence measurement. The error is the greatest when 50 mM of PFOS was added because it precipitated out.	112
Figure 7.1.6 The observed fluorescence intensity (orange) versus the concentration of PFOS added to CPF. The calculated intensities due to CPFH ₂ ⁺ (blue) and CPFH ⁺ (grey) accounts for CPF being a triprotic acid.	113
Figure 7.1.7 The equation $F_0/F_T = 1 + K_{11}[S] + (K_{n1}/n)(S_T - \text{cac})$ was used. A plot of (F_0/F_T) versus [$S_T - \text{cac}$] for no speciation, CPFH ₂ ⁺ and CPFH ⁺ when CPF is tetraprotic, where CPFH ₂ ⁺ (orange) and CPFH ⁺ (grey)	115
Figure 7.1.8 The equation $F_0/F_T = 1 + K_{11}[S] + (K_{n1}/n)(S_T - \text{cac})$ was used. A plot of (F_0/F_T) versus [$S_T - \text{cac}$] for no speciation, CPFH ₂ ⁺ and CPFH ⁺ when CPF is triprotic, where species CPFH ₂ ⁺ (orange) and CPFH ⁺ (grey).	115
Figure 7.1.9 The fluorescence intensity versus the concentration of PFOS added to 31.2 μ M CPF without added phosphate buffer flushed with N ₂ (g).....	118
Figure 7.1.10 Distribution diagram of CPF at experimental pH	119
Figure 7.1.11 The equation $F_0/F_T = 1 + K_{11}[S] + (K_{n1}/n)(S_T - \text{cac})$ was used. A plot of (F_0/F_T) versus [$S_T - \text{cac}$] for no speciation of CPF (a), CPFH ₄ ⁺³ (b), CPFH ₃ ⁺² (c), CPFH ₂ ⁺ (d), CPFH ⁺ (e), and CPF ⁻ (f) at 25°C.	121
Figure 7.1.12 A plot of fluorescence intensity versus concentration of PFOS added to CPF at 25°C flushed with N ₂ (g).	124
Figure 7.1.13 The distribution of CPF speciation from pH 7.75 – 8.25 \pm 0.01.....	125
Figure 7.1.14 The equation $(F_0/F_T) = 1 + K_{11}[S]$ was used to determine K ₁₁ . A plot of (F_0/F_T) versus [S_T] for no speciation of CPF (a), CPFH ₄ ⁺³ (b), CPFH ₃ ⁺² (c), CPFH ₂ ⁺ (d), CPFH ⁺ (e), CPF ⁻ (f) at 25°C.....	127
Figure 7.1.15 2:1 complex of water hydrogen binding with nearby PFOS in aqueous solution. The number of water molecules shown are much less for clarity.	130
Figure 7.1.16 Figure shows a conceptual depiction of the pseudophase aggregate. A hemispherical part of the PFOS aggregate showing the shell and the core. At low pH (<7) CPFH ₂ ⁺ species remains in the outer edge while CPFH ⁺ is weakly bound in the inside edge. This is speculated from the weak binding constants. The PFOS is shown as completely deprotonated base due to its low pKa (-3.3)	131

Figure 8.1.1 The fluorescence intensity versus concentration of TPGS-750M added to CPF.	134
Figure 8.1.2 The distribution of CPF speciation at pH $7.60 - 7.77 \pm 0.01$	135
Figure 8.1.3 The determination of the experimental cac for TPGS-750M.....	136
Figure 8.1.4 The equation $F_0/F_T = 1 + K_{11}[S] + (K_{n1}/n)(S_T - cac)$ was used to determine K_{11} and K_{n1} . (F_0/F_T) versus $[S_T - cac]$ with no speciation of CPF (a) $CPFH_4^{+3}$ (b) $CPFH_3^{+2}$ (c), $CPFH_2^+$ (d), $CPFH^{+-}$ (e) and CPF^- (f) at 25°C	138

LIST OF EQUATIONS

Equation	Page
Equation 1.3.1 Mass Action Equation of monomer:monomer complex	15
Equation 1.3.2 Equilibrium Constant K_{11} for monomer:monomer complex.....	16
Equation 1.3.3 Mass Balance for Surfactant	16
Equation 1.3.4 Mass Balance for Fluorophore	16
Equation 1.3.5 Observed Fluorescence	16
Equation 1.3.6 Initial Fluorescence Intensity of the Fluorophore	17
Equation 1.3.7 Difference in fluorescence intensity.....	17
Equation 1.3.8 Expanded difference in fluorescence intensity	17
Equation 1.3.9 Substitution of fluorescence efficiency.....	18
Equation 1.3.10 Substitution of the concentration of monomer: monomer complex	18
Equation 1.3.11 monomer:monomer binding constant	18
Equation 1.3.12 K_{11} expanded equation	18
Equation 1.3.13 Expanded equation of 1.3.12.....	19
Equation 1.3.14 Scott Equation	19
Equation 1.3.15 Benesi – Hildebrand (BH) equation.....	19
Equation 1.3.16 Concentration of the aggregate	21
Equation 1.3.17 Mass balance of monomer:aggregate complex.....	21
Equation 1.3.18 monomer:aggregate equilibrium expression.....	22
Equation 1.3.19 Concentration of the aggregate	22
Equation 1.3.20 Determination of binding by De La Guardia et. al.....	23
Equation 1.3.21 Concentration of the micelle	23
Equation 1.3.22 Determination of binding in the postaggregate phase by De La Guardia et. al.	23
Equation 1.3.23 Literature binding constant of the quencher.....	24
Equation 1.3.24 Total concentration of the quencher.....	25
Equation 1.3.25 Concentration of the quencher within the micelle	25
Equation 1.3.26 Linear relationship of postaggregate binding by Encinas et. al.	25
Equation 1.3.27 Variation of the Benesi-Hildebrand equation	26
Equation 1.3.28 Determination of postaggregate binding by Khan et. al.	26
Equation 1.3.1 Mass balance of monomer : monomer complex	28
Equation 1.3.2 Equilibrium expression of the monomer : monomer complex	29
Equation 1.3.3 Mass balance of monomer : pseudophase complex	29
Equation 1.3.4 Equilibrium expression	29
Equation 1.3.5 Concentration of the aggregate	29
Equation 1.3.6 Total concentration of the fluorophore	30

Equation 1.3.7 Total fluorescence intensity	30
Equation 1.3.8 Fluorescence of the individual fluorophore	30
Equation 1.3.9 Determination of total fluorescence	31
Equation 1.3.10 Expanded equation of the total fluorescence	31
Equation 1.3.11 Expanded equation of the total fluorescence to account for the aggregation number	31
Equation 1.3.12 Determination of binding constants for FQ like behavior	32
Equation 1.3.13 Dilution factor	32
Equation 1.3.14 Determination of binding constants for FQ like behavior with the dilution factor	33
Equation 1.3.15 Expanded total fluorescence intensity.....	33
Equation 1.3.16 Expanded total fluorescence intensity to account for K_{11} and K_{n1}/n	33
Equation 1.3.17 Determination of binding constants for FQ like behavior accounting for the fluorescence efficiency and total concentration of the fluorophore	34
Equation 1.3.18 Total fluorescence intensity when k is not constant	35
Equation 1.3.19 Expanded total fluorescence intensity when k is accounted for	36
Equation 1.3.20 Total Fluorescence intensity to account for all species of the fluorophore in solution	37
Equation 1.3.21 Substitution of F_T and F_j	37
Equation 1.3.22 Determination of K_{11} and K_{n1} to account for fluorescence enhancement	37
Equation 1.3.23 Determination of K_{11} and K_{n1} to account for FE, a revision of Equation 1.3.22	99
Equation 9.1.1 Fluorescence quenching (FQ)	143
Equation 9.1.2 Fluorescence enhancement (FE)	143

LIST OF ABBREVIATIONS AND SYMBOLS

-OH	Hydroxyl Functional Group
ΔA	Differential Absorbance in Micellar-Bound and Free Forms of CPF
ΔA_{∞}	Differential Absorbance
$\lambda_{\text{emission}}$	Emission Wavelength
$\lambda_{\text{excitation}}$	Excitation Wavelength
ΔG	Gibbs Free Energy
μg	Microgram
μL	Microliter
μM	Micromolar
μM	Micromolar
$[\text{H}]^+$	Hydrogen Concentration
$[\text{M}]$	Micelle Concentration
$[\text{Q}]_{\text{M}}$	Quencher Concentration in Micellar Phases
$[\text{Q}]_{\text{T}}$	Total Quencher Concentration
$[\text{Q}]_{\text{w}}$	Quencher Concentration in Aqueous Phases
$[\text{S}]$	Stoichiometric Concentration of Surfactant
$^{\circ}\text{C}$	Temperature, Degrees Centigrade
$\Delta\epsilon$	Difference in Absorption Coefficients (1 is the Pathlength of the Cell)
AB	Auto-buret
ADC	Analog to digital Converter
Ar	Argon Gas
BH	Bensei-Hildebrand Equation
C	Fluorophore
C_0	Initial Fluorophore Concentration
cac	Critical Aggregation Concentration
CFCLS	Continuous Flow Closed Loop System
C_i	Concentration of the individual fluorophore
C_j	Concentration of the fluorophore of a particular species
Cl^-	Chloride Ion
CMC	Critical Micelle Concentration
CPC	Cetylpyridinium Chloride
CPF	Ciprofloxacin
CPF^-	Anionic Ciprofloxacin
CPF-HCl	Ciprofloxacin-Hydrochloric Acid Mixture
CPFH^+	Zwitterionic Ciprofloxacin
CPFH_2^+	Diprotic Ciprofloxacin

CPFH ₃ ⁺²	Triprotic Ciprofloxacin
CPFH ₄ ⁺³	Tetraprotic Ciprofloxacin
CS	Fluorophore:Surfactant Complex
CS _n	Fluorophore:aggregate complex
C _T	Total fluorophore Concentration
CTAB	Cetyltrimethyl Ammonium Bromide
d _f	Dilution Factor
e.g	For Example
EPA	Environmental Protection Agency
<i>f</i>	Fraction of Quencher Occurring in Dissolved Water Phase
F	Observed Fluorescence, total fluorescence intensity
F ₀	Initial fluorescence intensity
FE	Fluorescence Enhancement
F _j	Fluorescence of specific species
FQ	Fluorescence Quenching
F _T	Total Fluorescence Intensity
FTIR	Fourier Transform Infrared Spectroscopy
g	Grams
H ₂ SO ₄	Sulfuric Acid
HCl	Hydrochloric Acid
HNO ₃	Nitric Acid
HPLC	High Performance Liquid Chromatography
i.e.	That Is
I ₂	Iodine Gas
K ₁₁	Monomer Binding Constant
K _a	Acid Dissociation Constant
K _b	Water Binding Constant, Binding/Association Constant
k _C	Fluorescence Efficiency of C
k _{CS}	Fluorescence Efficiency of CS
k _D	Dynamic Quenching Constant
k _i	Individual Fluorescence Efficiency
K _{n1}	Aggregate Binding Constant
K _{ow}	Octanol-water partition coefficient
k _s	Fluorescence Efficiency of S
K _{sv}	Stern-Volmer Constant
L	Liter
Log	Logarithm
m	Meters
M	Molarity
MBP	Myelin Basic Protein
mg	Milligram
min	Minute
mL	Milliliter
mM	Millimolar

mol	Moles
ms	Millisecond
mV	Millivolts
MW	Molecular Weight
n	Aggregation Number
\bar{n}	Mean Occupation Number, Number of Species Occupied in the Micelle
N/A	Not Applicable
N/L	Not Listed
N1	Quinolone Nitrogen
N1'	First Piperazine Nitrogen
N ₂	Nitrogen Gas
N4'	Second Piperazine Nitrogen
NaCl	Sodium Chloride
NaOH	Sodium Hydroxide
nm	Nanometers
NMR	Nuclear Magnetic Resonance Spectroscopy
NOM	Natural Organic Matter
O ₂	Oxygen
PAH	Polycyclic Aromatic Hydrocarbon
PFAS	Perfluoroalkyl Substances
PFOA	Perfluoroactanoic Acid
PFOS	Perfluorooctanesulfonic Acid
pK _a	Acid dissociation constant
Q	Quencher
RSD	Relative Standard Deviation
s	Second
S	Surfactant (mass balance equation)
SDS	Sodium Dodecyl Sulfate
S _n	Aggregate concentration
S _T	Total Surfactant Concentration
SV	Stern-Volmer equation
T	Temperature, Degrees Kelvin
TPGS-750M	DL- α -Tocopherol Methoxypolyethylene Glycol Succinate
UV-Vis	Ultraviolet Visible Spectroscopy
V	Volume

ABSTRACT

NONCOVALENT BINDING OF ANTHRACENE AND CIPROFLOXACIN WITH MOLECULAR PSEUDOPHASE: FLUORESCENCE AND PH STUDIES

Carol A. Ajjan, Ph.D.

George Mason University, 2020

Dissertation Director: Dr. Gregory D. Foster

Pseudophase compounds are molecular or micellar self-assembled aggregates that form in many natural aquatic environments. Pseudophase chemistry offers distinct advantages in modeling phase distributions or complexation in water-colloid and water-surfactant systems where the phases or microemulsions cannot be physically separated to assess binding constants. The goal of the present study was to determine binding constants in preaggregate and postaggregate phases for the solutes ciprofloxacin (CPF) and anthracene, with selected pseudophase compounds. The pseudophase compounds tested included sodium dodecyl sulfate (SDS), DL- α -Tocopherol methoxypolyethylene glycol succinate (TPGS-750M), perfluorooctanesulfonic acid (PFOS), and myelin basic protein (MBP). In order to fully understand the pseudophase interactions, the key equations represented either fluorescence enhancement (FE) or fluorescence quenching (FQ).

Equilibrium binding models for anthracene and ciprofloxacin with the pseudophase compounds were derived as:

$$\text{FQ: } F_0/F_T = 1 + K_{11} S + (K_{n1}/n)(S_T - \text{cac})$$

$$\text{FE: } (F_T - F_0) / (C_T \cdot \alpha) = [(k_C + (k_{11} \cdot K_{11}) S] + (k_{n1} \cdot K_{n1}/n) (S_T - \text{cac})]$$

Where F_T is the total fluorescence intensity while F_0 is the initial fluorescence of solute. C_T is the total concentration of solute and α is the fraction of the solute present at the corresponding pH. S_T is the total surfactant concentration, S is the monomer surfactant concentration, n is the aggregation number and cac is the critical aggregation concentration. k_C , k_{11} and k_{n1} are the fluorescence efficiencies of the free solute, bound solute in the preaggregate phase and bound solute in the postaggregate phase. K_{11} is the binding constant for the monomer-monomer complex and K_{n1} is the binding constant for the monomer-pseudophase complex. K_{11} , K_{n1} and cac were extracted from the intercept and slope from the equations above. The fluorescence efficiencies, k_C , k_{11} and k_{n1} , were obtained directly from the experimental data. K_{11} and K_{n1} were obtained for SDS, TPGS-750M and PFOS. The change in the fluorescence intensity was too low to measure reliable binding constants for the CPF-MBP system.

The equations were evaluated experimentally using both static and continuous-flow fluorometric titrations. The influence of pH on CPF fluorescence was rigorously evaluated at pH 1-11 where CPF speciation was calculated based on CPF as a tetraprotic

acid. It was determined that the interactions between CPF and the pseudophase compounds were dependent on properties such as pH, salt concentration, and quenching compounds like O₂ radical and Cl⁻. FE was observed when CPF interacted with SDS while overall FQ was observed with PFOS and TPGS-750M.

The binding of the anthracene-TPGS-750M system was significant where K_{11} was $292 \pm 8 \text{ M}^{-1}$ and K_{n1} was $(2.8 \pm 0.05) \times 10^4 \text{ M}^{-1}$. The binding was higher when CPF is considered a tetraprotic acid compared to a triprotic acid with PFOS where K_{n1} was $438.2 \pm 56 \text{ M}^{-1}$ and $175.7 \pm 14 \text{ M}^{-1}$ respectively for the zwitterionic species. The highest interactions occurred with CPF- SDS complexation in the postaggregate phase with a K_{n1} of $1780 \pm 71 \text{ M}^{-1}$. The highest binding in the preaggregate phase occurred with the CPF-PFOS tetraprotic complex where K_{11} was $160 \pm 3 \mu\text{M}^{-1}$. The most significant variables to consider are pH, and ionic strength. The highest binding occurred at neutral pH and the lowest in acidic pH. These factors significantly influence the interactions or lack of interactions that occur with the molecular pseudophase. By fully understanding the interactions between the preceding compounds, this in turn provides a greater understanding in the fate and effects and potential removal from the environment.

INTRODUCTION

1.1 Introduction

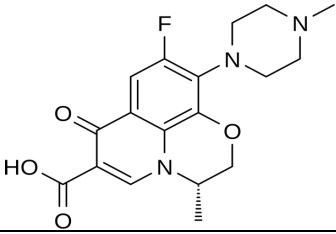
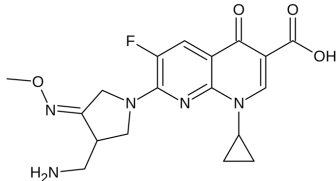
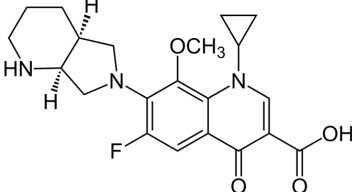
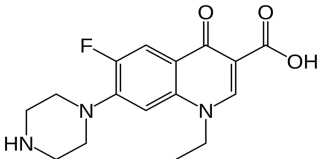
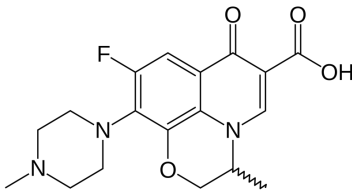
A particular challenge in environmental chemistry is to quantify the distribution and binding of micropollutants in water with non-filterable dispersed phases such as aquatic colloids or surfactants. Antibiotics are micropollutants of particular concern in water quality because of the potential development of widespread microbial resistances to contemporary drugs. Ciprofloxacin (CPF) is a commonly prescribed fluoroquinolone antibiotic in both humans and animals¹ that is routinely detected in the aquatic environment.² CPF is regarded as an emerging concern of pharmaceutical contaminant or micropollutant. By understanding more about fundamental binding properties of CPF with surfactants, it is hoped new discoveries can be used to create and implement better management strategies to safeguard our environment. The goal of this section is to show how the binding of ciprofloxacin (CPF) to surfactants has been modeled, with the emphasis on experimental and theoretical methods previously used to evaluate the relevant binding constants between CPF and various surfactants.

1.1.1 Overview of Fluoroquinolones and surfactants

Fluoroquinolones are a class of antibiotics that target gram-negative bacteria. They are important drugs for the treatment of respiratory tract, urinary tract, skin and

skin-structure infections.³ The properties of commonly used fluoroquinolones are expressed in Table 1.

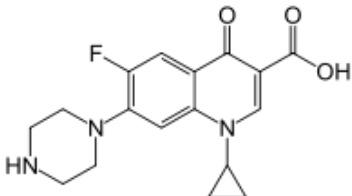
Table 1.1.1 The physical and chemical properties of fluoroquinolones

Antibiotic	Molecular Weight (g/mol)	Solubility	pK _a	Melting Point (°C)
Levofloxacin⁴ 	361.37	>54.2 (µg/mL)	6.50	225-227
Gemifloxacin⁵ 	389.387	1.31x10 ⁴ (mg/L)	6.40 9.00	235-237
Moxifloxacin⁶ 	401.438	1146 (mg/L)	6.31 9.35	238-242
Norfloxacin⁷ 	319.336	0.28 (mg/mL)	6.34 8.75	227-228
Ofloxacin⁸ 	361.373	28.3 (mg/mL)	6.05 8.11	250-257

The fluoroquinolone of interest in this study is CPF. Its properties are shown separately in Table 1.1.2. With the increasing CPF use, the occurrence and health risk of CPF in the environment is of concern as well as the potential of antibiotic resistance because of its presence. The bioavailability of CPF to aquatic organisms in surface waters is dependent on its multimedia distribution between water and colloids. Surfactants represent an important colloid phase in the aquatic environment, and little is known regarding the binding mechanisms of micropollutants in surfactants in colloids. Thus, surfactants influence the toxicity of CPF along with other fluoroquinolones. An important mode of fluoroquinolone toxicity is phototoxicity.^{9,10} Phototoxicity can range from mild erythema to severe bullous eruptions in sun-exposed skin areas as well as photomutagenic and photocarcinogenic potential, which has been observed in animals.¹⁰ With this in mind, it is important to understand the binding of CPF with other compounds and their properties so that the fate of CPF in the aquatic environment can be better predicted.

Table 1.1.2 Physiochemical properties of Ciprofloxacin (CPF)

Antibiotic	Molecular Weight (g/mol)	Solubility	pK_a	Melting Point (°C)	Log K_{ow}
Ciprofloxacin ¹¹	331.34	<1 (mg/mL)	3.64 5.05 6.95 8.95	225-227	0.28

					
---	--	--	--	--	--

1.1.2 Introduction of Surfactants

In nature, the transport and fate of many micropollutants are facilitated by binding with synthetic and natural organic matter (NOM) present in the aquatic environment. Aquatic NOM is comprised of many natural and synthetic bio-surfactants, including naturally occurring humic acids and fulvic acids derived from the diagenesis of plant matter. Additionally, synthetic surfactants derived from human use (e.g., detergents, cosmetics, flame retardants, food additives, formulations) are discharged into surface waters through wastewater treatment in large amounts. The presence of surfactants in natural water bodies has a profound influence on the biological fate of many micropollutants such as CPF. Synthetic surfactants may also inhibit the natural attenuation processes in the environment such as biodegradation through colloidal-phase sequestration into refractory organic matter as well as being toxic or inhibitory to microorganisms.¹² This induces anaerobic conditions with a negative influence on the bio-oxidation of certain substances.¹²

Surfactants are chemicals characterized by having a polar head and a non-polar tail. The polar moiety is hydrophilic while the non-polar moiety is hydrophobic¹³. They can be characterized as cationic, anionic, nonionic and zwitterionic. It is important to note

that the structures of surfactants change once the critical aggregation concentration (cac) is reached, which is the concentration at which the surfactant spontaneously reorganizes from a monomer to aggregate forms through self-assembly. The aggregate or micellar structure was first proposed by Hartley.¹⁵ In the colloidal micellar phase Hartley describes the aqueous micelle structure as having a polar or ionic head group oriented outward towards water, and non-polar paraffinic tails in the center having the least possible interaction with water. Surfactants, specifically anionic surfactants, are commonly used in many household products, such as detergents, water-repellants and cosmetics.¹⁴ The surfactants of interest for my study included those previously investigated for binding with CPF or other related fluoroquinolones, namely, sodium dodecyl sulfate (SDS), along with several novel surfactants and a protein, perfluorooctanesulfonic acid (PFOS), DL- α -tocopherol succinate (TPGS-750M), and myelin basic protein (MBP).

1.1.3 Sodium Dodecyl Sulfate (SDS)

Sodium dodecyl sulfate (SDS) is an anionic surfactant that is one of the most widely used surfactants in many personal care products with excellent foaming, cleansing, and rinsing properties.¹⁶ This is due to its amphiphilic properties. It has been shown to have potential for direct largescale environmental applications due to it being the main ingredient in oil dispersant and minor ingredient in other formulations.¹⁴ The structure of SDS is shown in Figure 1.1.1.

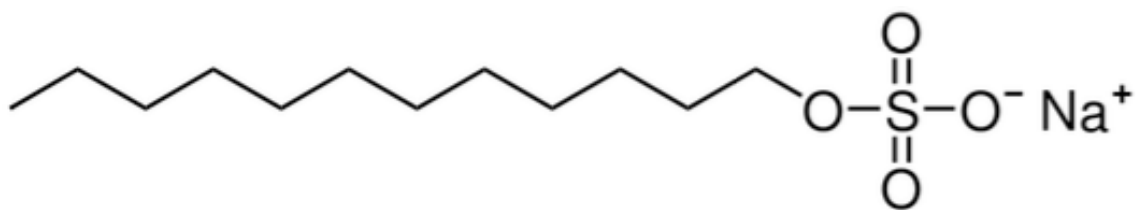


Figure 1.1.1 The chemical structure of sodium dodecyl sulfate (SDS)

SDS is one of the surfactants whose binding has been studied the most with CPF and other fluoroquinolones. However, the binding constants reported as well as the binding models used have varied greatly within the literature. The reason SDS was chosen for this study was to allow comparison of my binding constants to those obtained in previous literature.

1.1.4 Perfluorooctanesulfonic Acid (PFOS)

Perfluoroalkyl substances (PFAS) are a broad class of high production volume compounds used as flame retardants and water-repellants.^{17,18} PFAS persistence in the environment has detrimental effects.¹⁹ The two most well-known PFAS include perfluorooctanoic acid (PFOA) and perfluorooctanesulfonic acid (PFOS). PFOS is an anionic surfactant that exhibits environmental persistence, bioaccumulation and potential toxicity.^{19,20} Several studies have shown that PFOS interferes with fatty acid metabolism and can cause liver toxicity.¹⁹

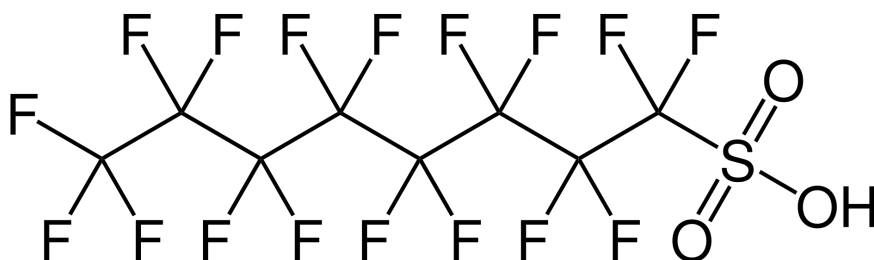


Figure 1.1.2 The chemical structure of perfluorooctanesulfonic acid (PFOS)

In the United States, there have been trace levels of PFOS found in drinking water, which can be transported from mothers to newborns via breastfeeding.²³ PFOS has been known to be transmitted to the fetus through umbilical cord blood, newborns through breast milk and has been found in the bloodstream of Americans since 2009^{19,23}. The EPA has issued a lifetime drinking water health advisory for PFOS of 70 nanograms per liter (or 70 parts per trillion)²³. Due to the extremely low concentration and the effects, PFOS has become of particular interest recently and a great concern in public health. While there have been previous studies of small molecules binding to PFOS in the aggregate phase^{19,20,24,25} there have not been any known reports of binding between CPF and PFOS or any other PFAS.

1.1.5 *DL- α -Tocopherol succinate (TPGS-750M)*

Biosurfactants like DL- α -tocopherol succinate (TPGS-750M) are a class of environmentally benign compounds used in green organic synthesis and drug delivery.^{26,27} It is a derivative of vitamin E.²⁸ In these nonionic surfactants the nearly equal ratio between the hydrophilic and hydrophobic portions allows it to solubilize a broad array of chemical reactions in water^{4, 18,19}. They are a balanced solvent

pseudophase for a sustainable organic synthesis in presence of bulk water, specifically transition metal-catalyzed cross couplings.²⁹ This is due to the surfactant having both polar and nonpolar entities in the structure. allowing it to be soluble in many solvents. The structure of TPGS-750M is shown in Figure 1.1.3.

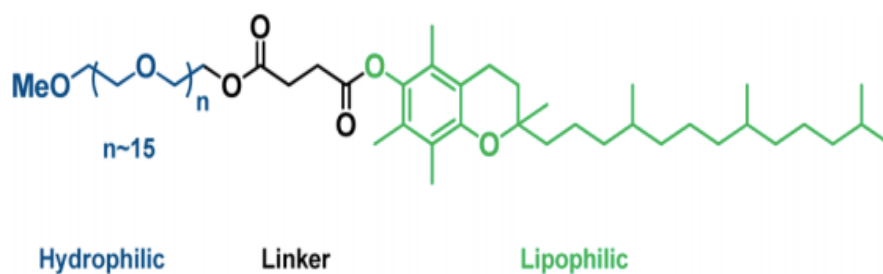


Figure 1.1.3 The chemical structure of DL- α -tocopherol succinate (TPGS-750M)

It has also been determined that TPGS-750M aggregation is not affected by temperature or concentration, which makes it ideal as a drug carrier for water insoluble compounds.²⁸ It is an attractive surfactant due to the availability from commercial suppliers at low cost. There is a lack of information on reliable critical aggregation concentration (cac) and aggregation number for this surfactant. The reported cac values have ranged from 20 to 1510 mM.³⁰ In addition, there are limited data available for the binding constants of small molecules with TPGS-750M, including partition coefficients, intraggregate activity coefficients, and water-surfactant distributions of species of small molecules, which are all essential to understand the basic solution thermodynamics and reactions related to solute-surfactant binding.^{28,30,31}

1.1.6 Myelin basic protein (MBP)

Myelin basic protein (MBP) is the second most abundant protein in the mammalian central nervous system.³² The charge of MBP is considered to be overall cationic due to the high content of arginine, lysine and histidine amino acid residues present.³³ MBP is the only aqueous pseudophase-forming substance tested that is not classified as a surfactant. However, under physical changes such as pH MBP has been observed to aggregate in water.³⁴ MBP (Figure 1.1.4) has fluorescence properties derived from tryptophan and tyrosine amino acid residues in the protein. There are four tyrosine and one tryptophan amino acids in the primary structure of MBP.³⁵

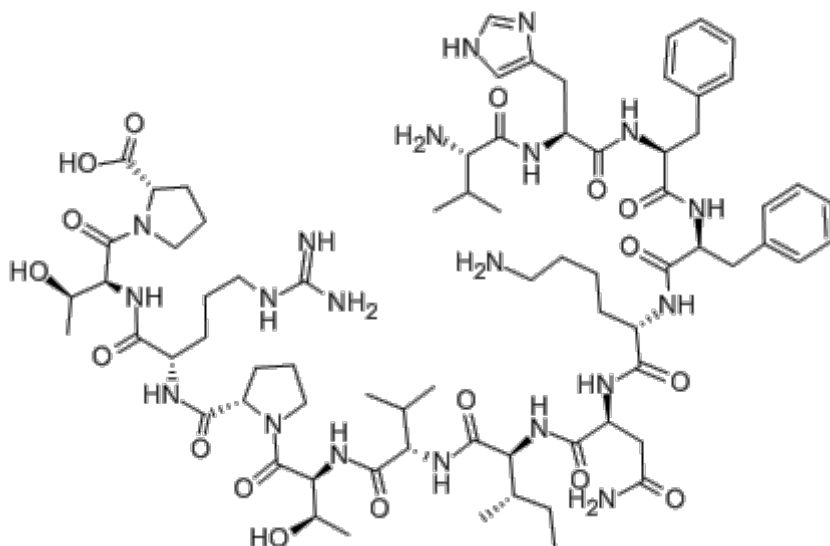


Figure 1.1.4 A portion of the chemical structure of myelin basic protein (MBP) responsible for fluorescence

The stability of the MBP is dependent on the interactions that occur from the 169 amino acids within the protein. The amino acid residues in MBP maximize

intramolecular electrostatic repulsions within the protein and decreases the stability in the compound with the increase in pH.³⁴ This is what initiates the aggregation of the protein. The protein has also shown hydrophobic and hydrophilic regions due to protein folding in water³⁶, similar to the pseudophase behavior described for surfactants. A summary of the aggregate properties is expressed in Table 1.1.3 below.

Table 1.1.3 The chemical properties of the pseudophase compounds

Compound	Molecular Weight (g/mol)	Critical Aggregation Concentration (mM)	Aggregation Number (n)
SDS ³⁷	288.38	8.0	60
PFOS ^{19,38}	500.13	8.0	7
TPGS-750M ³⁰	1250-1340	20 - 1510	41
MBP ³³	18,200	N/A	N/A

1.2 Instrumental techniques employed to study binding

To study the binding between CPF or other fluoroquinolones with surfactants, there have been various instrumental techniques employed (Table 1.2.1). These include high performance liquid chromatography (HPLC), ultraviolet visible spectroscopy (UV-Vis), fluorescence spectroscopy, Fourier transformed infrared spectroscopy (FTIR), and nuclear magnetic resonance (NMR) spectroscopy. Each technique is unique in selectivity and sensitivity in order to determine and understand different aspects of binding or partitioning between these compounds. However, in order to minimize the error in binding constant measurement, the techniques must measure free concentration of the

solute without interference and obtain maximum precision and accuracy. Here, I review the merits of some techniques for the measurement of binding constants.

Table 1.2.1 A compilation of techniques used to study CPF-surfactant interactions and their characteristics

Technique	Principle
High Performance Liquid Chromatography (HPLC) ^{4,39,40}	Measure the change in retention factor or the signal intensity and relate to concentration in the binding model.
Fluorescence spectroscopy ^{7,41–43}	Measure the change in the signal intensity compared to the concentration of surfactant added
Nuclear Magnetic Resonance (NMR) ^{44–47}	Observe structural changes in the fluorophore by observing the changes in peaks
Ultraviolet-visible spectroscopy (UV-vis) ⁴⁸	Measure the change in absorbance compared to the concentration of surfactant added
Fouier Transformed Infrared Spectroscopy (FTIR) ⁴⁸	Observe structural changes in the fluorophore by observing the intensity of the peaks

HPLC^{4,39,40}: From the literature, in order to determine binding of surfactants with CPF and other fluoroquinolones, it was imperative to have a fluorescent probe for the detection. In HPLC, the binding of a probe to a surfactant is characterized by the change in retention time and signal intensity of the peak. However, it is important to note that in a reversed phase HPLC using surfactant in the mobile phase, the probe is in equilibrium among the three phases: aqueous mobile phase, the nonpolar stationary phase, and the surfactant aggregate phase. The literature used cetyltrimethyl ammonium bromide (CTAB) and acetonitrile to prepare the mobile phase. Potassium dihydrogen phosphate was used to prepare the CTAB solution. However, depending on the volume of acetonitrile added to CTAB, this effects the critical aggregation concentration (cac).⁴⁹

The interactions in these three phase systems complicate the measurement of binding constants, especially with compounds as complex as CPF and PFOS. Therefore, it is not a direct and simple technique for the evaluation of binding constants.

*FTIR*⁴⁸: In order to observe the structural changes of CPF, Khan et al used FTIR in order to search of key functional groups. It is important to specify, before discussing the results, that the CPF used was CPF-HCl and not pure CPF. While the HCl allows for the compound to be soluble in water, this in turn could affect the obtained IR peaks. The paper specifies the complexity of CPF as a structure in terms of its behavior under different pH conditions. However, while they specified functional groups present such as -OH and NH, they fail to mention under what conditions they were found under.

Also due to the structure of CPF and its protonation or deprotonation, certain peaks should be disappearing as the pH increases such as the -OH peak. From the literature, it appears that FTIR would not be the ideal method in order to determine binding or partitioning between CPF and surfactants.

*NMR*⁴⁴⁻⁴⁷: In order to observe binding as well as determine dissociating and associating protons in CPF, NMR is a method that has been used.⁵⁰ Proton NMR will aid in the determination of the change in connectivity between CPF and surfactants or simply which protons are dissociating. NMR has also been used to determine the surfactant aggregate size and structure.^{44,46} However, depending on the compound's solubility in a solvent, limits the application. NMR has also been used to better observe structural changes within micelles.³⁷

*UV-Vis*⁴⁸: UV-vis is a commonly used technique that can determine the absorbance or also known as the excitation spectrum of a compound. This technique was used extensively for compounds with significant molar extinction coefficient in the UV-vis range. Khan et al used UV-vis along with FTIR to observe the effects of pH on the partitioning of CPF with SDS. However, unlike in fluorescence methods, UV-vis is a less sensitive technique for weakly absorbing species. Compounds cannot be distinguished based on the absorbances obtained. Therefore, with a compound like CPF, which has many different structures depending on pH, as well as what it is bound or partitioned to, the results obtained from UV-vis may not be as precise. Therefore, it could be utilized for simple systems with high concentrations of donor and acceptor with high molar absorptivities. While CPF in the environment remains at very low concentration and has strong emission in the visible region the fluorescence spectroscopy appears to be the technique of choice.

Fluorescence^{7,41–43}: Many compounds emit characteristic electromagnetic radiation after absorbing light in the UV region. The resulting emission is characterized by the fluorescence spectrum. Fluorescence spectroscopy is a good method to study binding or partitioning for multiple reasons. It can be used to measure binding directly, meaning it can be observed without the need to filter or otherwise separate the solute and surfactant in the original solution. Fluorescence is far more sensitive in comparison to UV-vis, FTIR and NMR, and has the ability to determine emission and excitation spectra simultaneously. The concentrations needed to complete fluorescence experiments are extremely low (down to sub-micromolar concentrations), and therefore overcomes

common problems such as the low solubility of the fluorophore in the solvent, self-association of the compound of interest (CPF), and self-quenching.

An important variable in fluorescence is the presence of quenching agents in solution with the fluorophore. For example, if CPF is used in the form of one of its chloride salts (e.g., CPF-HCl) or HCl is added to facilitate dissolving CPF in water, Cl⁻ can account for quenching. It would be difficult to determine whether quenching was attributed to the surfactant or chloride ion. Therefore, it is important to avoid the use of any additional quenching agents such as chloride ion when making CPF solutions. Another important quenching agent is oxygen from the atmosphere, which can decrease the total fluorescence intensity unintentionally. Atmospherically derived oxygen can be removed by sparging the solution initially with either Ar or N₂ gas.⁵¹ Unfortunately, no previous studies were found to have sparged their systems with an inert gas prior to making fluorescence measurements.

The existing literature clearly shows fluorescence spectroscopy is best suited to study binding of photoactive molecules at a very low concentrations approximating infinite dilution experimental conditions for the evaluation of meaningful thermodynamic binding constants. The infinite dilution condition is defined as the aqueous concentration of the solute (i.e., CPF) below the solubility limit where solute-solute interactions are negligible and only solute-water intermolecular attractive forces exist for the solute in the absence of colloid. We note that pH measurement in binding studies were often ignored in the literature or did not have a wide range of pH values. There are factors that can influence the strength of the binding between compounds, other than covalent and ionic

bonds. These include noncovalent and electrostatic attraction or repulsion (intermolecular forces) modulated by solvent, ionic strength, and pH.

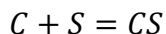
1.3 Theories: Binding Equilibria in Solution

The Spectrophotometric titration has been successfully developed as a means to directly measure the binding constants between low-molecular weight molecules and surfactants⁵² without the need to isolate the water and dispersed phases for independent analysis. Fluorescence is a particularly beneficial spectroscopic technique because of its selectivity and sensitivity. CPF is a fluorophore. The mathematical relationships between fluorescence and CPF binding to surfactants are described further below.

1.3.1 *Monomer Complexes*

It is first important to establish the fundamental mathematical equations of solute binding to surfactants to establish the best model. The derivations begin by first defining the reactants and products of the system through a mass action equation:

Equation 1.3.1 Mass Action Equation of monomer:monomer complex



The extent of the mass-action equation above equilibrium can be defined by the following equilibrium constant:

Equation 1.3.2 Equilibrium Constant K_{11} for monomer:monomer complex

$$K_{11} = \frac{CS}{C \cdot S}$$

K_{11} is defined as the binding constant of the monomer:monomer (1:1) complex between the fluorophore and the surfactant. The terms C and S can be further expressed in mass balance equations to account for the total surfactant (S_T) and total CPF (C_T) concentrations below:

Equation 1.3.3 Mass Balance for Surfactant

$$S = S_T - CS$$

Equation 1.3.4 Mass Balance for Fluorophore

$$C = C_T - CS$$

All of the concentrations are expressed in molarity units (mol/L). Assuming all three species, C, CS, and S are fluorescent, in this simple monomer system the observed fluorescence (F) can be expressed using the equation below assuming the path length of the cell is equal to 1:

Equation 1.3.5 Observed Fluorescence

$$F = k_S S + k_C C + k_{CS} CS$$

Equation 1.3.6 Initial Fluorescence Intensity of the Fluorophore

$$F_0 = k_C C_0$$

The k_S , k_C and k_{CS} terms above represent the fluorescence efficiency of the compounds of S, C and CS, respectively. C_0 is the initial concentration of CPF. If the surfactant S is not fluorescent (generally the case), the total fluorescence is only due to C and CS. It is important to note that C is the free and unbound fluorophore, therefore, it can be used interchangeably with C_0 .

By incorporating Equation 1.3.4 into Equation 1.3.5, then the following equation can be expressed:

Equation 1.3.7 Difference in fluorescence intensity

$$F - k_C C = (k_{CS} - k_C)CS$$

The excess fluorescence using the term ΔF , can be expanded in the following manner when substituting F_0 from Equation 1.3.6:

Equation 1.3.8 Expanded difference in fluorescence intensity

$$\Delta F = F - F_0 = F - k_C C$$

It is important to note that the excess fluorescence in Equation 1.3.8 is invalid unless C_T is constant. A new fluorescence term, q , can be defined to shorten the fluorescence efficiency expression:

Equation 1.3.9 Substitution of fluorescence efficiency

$$q = k_{CS} - k_C$$

The term CS can be expressed in the following manner:

Equation 1.3.10 Substitution of the concentration of monomer: monomer complex

$$CS = \frac{\Delta F}{q}$$

The binding constant K_{11} can be determined using the following equation:

Equation 1.3.11 monomer:monomer binding constant

$$K_{11} = \frac{CS}{\left(S_T - \frac{\Delta F}{q}\right) \left(C_T - \frac{\Delta F}{q}\right)}$$

Equation 1.3.11 can be rewritten below:

Equation 1.3.12 K_{11} expanded equation

$$K_{11} = \frac{\Delta F q}{(q S_T - \Delta F)(q C_T - \Delta F)}$$

Equation 1.3.13 Expanded equation of 1.3.12

$$\frac{S_T C_T}{\Delta F} + \frac{\Delta F}{q^2} = \frac{1}{q K_{11}} + \frac{S_T + C_T}{q}$$

If it is assumed that $S_T \gg C_T$, which is often the case at ambient solute and surfactant concentrations, and $S_T C_T / \Delta F \gg \Delta F / q^2$ then:

Equation 1.3.14 Scott Equation

$$\frac{S_T C_T}{\Delta F} = \frac{1}{q K_{11}} + \frac{S_T}{q}$$

Equation 1.3.14 is known as the Scott equation. If both sides of Equation 1.3.14 are divided by S_T , then the alternative Benesi-Hildebrand (BH) equation can also be expressed below:

Equation 1.3.15 Benesi – Hildebrand (BH) equation

$$\frac{C_T}{\Delta F} = \frac{1}{q K_{11} S_T} + \frac{1}{q}$$

If a plot of $C_T / \Delta F$ versus S_T , the slope of the graph would equal $1 / (q \cdot K_{11})$. It is important to note that the derivations assume no aggregation of S i.e., prior to the cac. It

also assumes either one of the reactants is present in excess the characteristic of the absorption or emission of the other reactant will be transparent in the range of the reaction system.⁵³

The Scott and Benesi-Hildebrand (BH)⁵² equations were extensively used with UV-vis and fluorescence spectroscopy for the measurement of binding derivations with simple systems. It was first developed to explain a phenomenon where iodine changes color in various aromatic solvents, which was attributed through I₂-solvent complex formation which could be determined spectroscopically.⁵⁴

However, the key assumption where the initial concentration of the solute is significantly greater than the initial concentration host cannot apply past the cac. Due to the aggregation number, $n > 1$, the concentration of the aggregate would significantly increase and could not be explained by the equations. Due to the noncovalent binding between the fluorophore and the aggregate, it is possible that intermediate (2:1) complexes to form in solution if they have significantly different association constants.

Scott criticized the BH equation assumption the equilibrium constant is concentration independent is inherent is difficult to justify.⁵⁵ Different results have been obtained when the assumption of K_{11} is not equal to the concentration of the acid. In Scott's derivations, he accounts for the concentration activity of the species of interest. The concentration activity accounts for the initial concentration of S and the fluorescence intensity.

Scott assumes the equilibrium constants are at infinite dilution which redefines the K_{11} binding constant in comparison to the BH equation. At infinite dilution, it assumes solute- solute interactions are negligible as stated earlier.

The Scott and BH equations have been the most successful when spectrophotometric measurement was conducted for acid-base complexes in inert solvents. However, it is not ideal for monomer-aggregate complexes as neither account for the structural changes once a monomer becomes the aggregate.

1.3.2 Aggregate complexes

Surfactants form aggregates (S_n) from monomers after the cac is reached, and the aggregation number (n) is assumed to be relatively constant for a particular surfactant.

Equation 1.3.16 Concentration of the aggregate

$$nS(\text{monomer}) = S_n(\text{aggregate})$$

Equation 1.3.1, Equation 1.3.2, and Equation 1.3.3 can be expanded to include the surfactant aggregate forms:

Equation 1.3.17 Mass balance of monomer:aggregate complex

$$C + S_n = CS_n$$

Equation 1.3.18 monomer:aggregate equilibrium expression

$$K_{n1} = \frac{CS_n}{C \cdot S_n}$$

Equation 1.3.19 Concentration of the aggregate

$$S_n = \frac{S_{T-cac}}{n}$$

Equation 1.3.17 Equation 1.3.18, and Equation 1.3.19 now account for the aggregate form of the surfactant, which can also serve as a binding agent. The aggregation number (n) is also critical in determining binding.

The following papers below have applied various modifications to the Scott and BH equations in combination with equations similar to Equation 1.3.17 Equation 1.3.18, and Equation 1.3.19 above to determine the binding between CPF or other fluorophores and aggregated surfactants or micelles.

De La Guardia et. al.⁵⁶ used the following derivations to determine binding constants between fluorescent molecules like 1-naphthol with cationic, anionic and nonionic surfactants and β -cyclodextrin⁵⁶ which is the fluorophore. To determine the binding constants, this was done using variations are from the Benesi-Hildebrand equation. Since the authors were trying to observe the binding of a solute in the micelle, the binding constant K_{n1} is introduced yielding Equation 1.3.20.

Equation 1.3.20 Determination of binding by De La Guardia et. al.

$$\left[\left(\frac{F}{F_0}\right) - 1\right]^{-1} = \left[\left(\frac{F_M}{F_0}\right) - 1\right]^{-1} \left[1 + \frac{1}{\gamma K_{n1} C}\right]$$

In Equation 1.3.20, γ is the ratio between the fluorophore extinction coefficient, at the excitation wavelength, in the presence and the absence of the surfactant. The paper also states that the concentration of the micelle (M) can be expressed in the following manner:

Equation 1.3.21 Concentration of the micelle

$$M = S_T - CMC$$

Equation 1.3.21 includes the micellar region of the solute without the aggregation number, therefore, K_{n1} is actually K_{n1}/n (an error not recognized by the authors) more specifically via Equation 1.3.20.

Equation 1.3.22 Determination of binding in the postaggregate phase by De La Guardia et. al.

$$\left[\left(\frac{F}{F_0}\right) - 1\right]^{-1} = \left[\left(\frac{F_M}{F_0}\right) - 1\right]^{-1} \left[1 + \frac{1}{\gamma K_{n1} (S_T - CMC)}\right]$$

In Equation 1.3.22, γ is equal to one when the extinction coefficients are equal in both micellar and solution media or when there is no emission by the micellar bound solute. A plot of $[(F/F_0)-1]^{-1}$ versus $1/(S_T- CMC)$ yields a straight line. By dividing the

intercept and the slope of the line, K_{n1} can be determined. Since the following equation does not account for the aggregation number, the binding constant K_{n1} is K_{n1}/n . While the authors account for the formation of the surfactant micelle through the critical micelle concentration (CMC), they do not, however, account for the aggregation number after the micelle is formed.

Encinas et. al.⁵⁷ observed in detail the partitioning of fluorescence quenching systems. K in the paper was described as a partition constant. However, the authors used Stern-Volmer plots in order to obtain these values. Stern-Volmer, while commonly used, has been proven to be an inaccurate method in order to determine binding constants using fluorescence spectroscopy.⁵⁸ Based on the derivation, it appears that the authors were trying to determine K_{n1} upon accounting for the micelle. This is particularly important due to the nature of surfactants and their structural change after the cac. The binding presented between these systems was not linear.

Equation 1.3.23 Literature binding constant of the quencher

$$K_{n1} = \frac{[Q]_M}{[Q]_w M}$$

$[Q]_M$ and $[Q]_w$ are the quencher concentrations in both micellar and aqueous phases, respectively. If $[Q]_T$ is defined as the total quencher concentration, then the following equation can be derived:

Equation 1.3.24 Total concentration of the quencher

$$[Q]_T = [Q]_M + f[Q]_w$$

Here, f was defined as the fraction of the quencher that occurs in the water (dissolved) phase. $[Q]_M$ was further defined by the following equation

Equation 1.3.25 Concentration of the quencher within the micelle

$$[Q]_M = \tilde{n}[M]$$

where \tilde{n} is defined as the mean occupation number. The mean occupation number is defined as the number of species occupied in the micelle. This term represents a factor proportional to the concentration of solute inside the micelle. This is the first paper to account for a type of aggregation number in the equation. In micellar systems, the number of aggregates present in the system also influences the strength of the binding or non-covalent interactions in the system. From this equation, Equation 1.3.24 can be rewritten in the following manner:

Equation 1.3.26 Linear relationship of postaggregate binding by Encinas et. al.

$$\frac{[Q]_T}{f} = \frac{\tilde{n}}{K_{n1}} + \frac{\tilde{n}[M]}{f}$$

A plot of $[Q]_T/f$ versus $[M]/f$ that allows for the determination and evaluation of K_{n1} and \tilde{n} for each value of F/F_0 .

Khan et. al.⁴⁸ and Banipal et. al.⁵⁹ used UV-vis spectroscopy to determine binding between CPF and SDS through a variation of the BH equation below:

Equation 1.3.27 Variation of the Benesi-Hidebrand equation

$$\frac{1}{\Delta A} = \frac{1}{\frac{K_{n1}}{n\Delta A_{\infty}} \times (C + (S_T - CMC))} + \frac{1}{\Delta A_{\infty}}$$

In Equation 1.3.27, ΔA_{∞} is defined as the differential absorbance when $S = 0$ (in absence of S), and ΔA is the differential absorbance in the micellar-bound and free forms of CPF. The authors further calculated the Gibbs free energy for the formation of K_{n1} as $\Delta G = -RT(\ln K_{n1})$. The following equation below was used to determine the binding constant between CPF or C and the micellar-phase surfactant:

Equation 1.3.28 Determination of postaggregate binding by Khan et. al.

$$\frac{[C][S]}{\Delta A} = \frac{[S]}{\Delta \epsilon l} + \frac{1}{\frac{K_{n1}}{n\Delta \epsilon l}}$$

$\Delta \epsilon$ was the difference in the absorption coefficients while l was the pathlength of the cell. It can be observed that Equation 1.3.28 closely resembles the Scott equation in order to determine binding. By plotting $[C][S]/\Delta A$ versus $[S]$, the value of K_{n1}/n was determined. However, the authors only accounted for the K_{n1} in acidic (pH 0.5-1) and basic conditions (pH 9) but collected data at pH 0.5-1, 5.0-6.0, 7.0. 9.2 and 13-14. This

could be due to obtaining negative binding constants in the other pH ranges. The authors also considered CPF to be a triprotic acid instead of a tetraprotic acid. Therefore, the results considered only two CPF acid-base species instead of all five potential species.

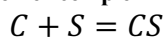
THEORY SECTION

2.1 Theory

The binding (equilibrium partitioning) of ciprofloxacin with surfactant-like substances was evaluated experimentally by using fluorimetry, specifically the reduction in fluorescence of a solute (i.e., ciprofloxacin) upon binding to a surfactant species that is either non-fluorescent or has wavelengths orthogonal with CPF fluorescence emission. Ciprofloxacin (CPF) binds to the surfactant noncovalently in both monomeric (1:1 in S:C) and aggregate forms (n:1 in $S_n:C$), and, therefore, requires the evaluation of two binding constants simultaneously (K_{11} and K_{n1}) along with the aggregation number n of the surfactant. Furthermore, the influence of pH must be incorporated into the ciprofloxacin binding model because of the importance of pH as an environmental variable and the pH-dependent speciation of ciprofloxacin. CPF has 4 acid dissociation (K_a) constants. The objective was to develop a fluorescence model capable of evaluating CPF binding to surfactants that included the important variables K_{11} , K_{n1} , n and pH. The new model used in my study is derived below.

As shown in previous literature⁶⁰⁻⁶², freely dissolved CPF (C) undergoes equilibrium binding to the surfactant (S) to yield the complexes C-S (1:1 form) and C- S_n (aggregate form of surfactant) according to following mass-action laws:

Equation 1.3.1 Mass balance of monomer : monomer complex



Equation 1.3.2 Equilibrium expression of the monomer : monomer complex

$$K_{11} = \frac{[CS]}{[C][S]}$$

Equation 1.3.3 Mass balance of monomer : pseudophase complex

$$C + S_n = CS_n$$

Equation 1.3.4 Equilibrium expression

$$K_{n1} = \frac{[CS_n]}{[C][S_n]}$$

All concentrations are molar (mol/L). S_n is the molar concentration of the aggregate (e.g., micellar) surfactant, which may be evaluated as

Equation 1.3.5 Concentration of the aggregate

$$S_n = \frac{S_T - cac}{n}$$

where S_T is the total concentration of S, cac is the critical aggregation concentration (mol/L) of the aggregate and n is the aggregation number. For many surfactants, cac and n are known at specific conditions but are dependent on temperature,

the presence of salt (buffer) or a change in pH. For example, sodium dodecyl sulfate, a common anionic surfactant, has a cac of 8 mM at 25°C with an aggregation number of 62³⁷ at zero ionic strength and neutral pH. Total C (total fluorophore concentration) in the system subject to fluorescence emission is defined in terms of its mass balance of complexation as

Equation 1.3.6 Total concentration of the fluorophore

$$C_T = C + CS + CS_n$$

The total fluorescence (F_t) for all species of C in (Equation 1.3.6) is defined additively as

Equation 1.3.7 Total fluorescence intensity

$$F_T = F_C + F_{CS} + F_{CS_n}$$

Furthermore, the fluorescence of any particular species of C, C_i , can be defined below according to its concentration and individual fluorescence efficiency k_i (1/M).

Equation 1.3.8 Fluorescence of the individual fluorophore

$$F_i = k_i C_i$$

Combining the mass balance equation expressed in Equation 1.3.6 with Equation 1.3.7 and Equation 1.3.8 yield a description of total fluorescence emission for all species in terms of an overall fluorescence efficiency k_c .

Equation 1.3.9 Determination of total fluorescence

$$F_T = k_c(C + CS + CS_n)$$

k_i is the fluorescence efficiency of C, CS and CS_n . They are assumed equal due to all of the species fluorescing at the same wavelength. Therefore, the total fluorescence, F_T , can be derived from Equation 1.3.9 with substitution of Equation 1.3.1 and Equation 1.3.2 for C-S and C- S_n , respectively.

Equation 1.3.10 Expanded equation of the total fluorescence

$$F_T = k_c[C] + k_{CS}K_{11}[C][S] + k_{CS_n}K_{n1}[C][S_n]$$

It is assumed all three species have the same fluorescence efficiency where $k_i = k_C = k_{CS} = k_{CS_n}$.

Equation 1.3.11 Expanded equation of the total fluorescence to account for the aggregation number

$$F_T = k_i[C] + k_iK_{11}[C][S] + k_iK_{n1}[C] \left[\frac{S_{T-cac}}{n} \right]$$

Assuming C is a solute monomer and F_t in the absence of S is designated as F_o (where $F_o = k_o C_o$) then fluorescence of the fluorophore is evaluated from the observed fluorescence (F_T) as

Equation 1.3.12 Determination of binding constants for FQ like behavior

$$\frac{F_o}{F_T} = 1 + K_{11}S + \left(\frac{K_{n1}}{n}\right)(S_{T-cac})$$

A plot of F_o/F_T versus $S_t - cac$ yields a straight line where the slope is (K_{n1}/n) and the intercept is $(1+K_{11}S)$.

When C is the only fluorescence emitting species in its monomeric free state, then as C is progressively bound to S, the total fluorescence emission decreases, due to the loss of C and the production of C-S and C-S_n, which are not fluorescent species. This can be viewed as a form of static quenching. Experimentally a finite yet small volume of S is added to the initial concentration of C_o. Assuming linearity of concentration calibration for free C, a dilution factor, d_f , can be introduced:

Equation 1.3.13 Dilution factor

$$d_f = \frac{V_o}{V_o + V_s}$$

Equation 1.3.14 Determination of binding constants for FQ like behavior with the dilution factor

$$\frac{F_0 d_f}{F_T} = 1 + K_{11}S + \left(\frac{K_{n1}}{n}\right)(S_{T-cac})$$

Equation 1.3.12 and Equation 1.3.14 are independent of the concentration of solute emitting species. Equation 1.3.14 is general for binding that reduces the total fluorescence emission due to the loss of C, which emulates Stern-Volmer (SV) quenching behavior.

The above derivations account for the noncovalent interactions between C and S. If it is assumed that the bound C species is not fluorescence emitting after the i^{th} addition of S to the system, then the total fluorescence is described by

Equation 1.3.15 Expanded total fluorescence intensity

$$F_T = k_C C = k_C(C_T - CS - CS_n)$$

Equation 1.3.16 Expanded total fluorescence intensity to account for K_{11} and K_{n1}/n

$$F_T = k_C \left([C] - K_{11}[C][S] - [C] \left(\frac{K_{n1}}{n} \right) [S_{T-cac}] \right)$$

If given freely dissolved $C = C_T \cdot \alpha$, where α is the fraction of the CPF speciation in the system, then Equation 1.3.16 can be recast as:

Equation 1.3.17 Determination of binding constants for FQ like behavior accounting for the fluorescence efficiency and total concentration of the fluorophore

$$\frac{F_T}{k_C \cdot C_T \cdot \alpha} = 1 - K_{11}[S] - \left(\frac{K_{n1}}{n}\right)[S_{T-cac}]$$

A plot of $F_T/(k_C C_T \cdot \alpha)$ versus $[S_t - cac]$ yields a straight line of the slope (K_{n1}/n) and intercept $(1-K_{11} S)$. The equation now allows the change in C_t due to dilution and accounts for the specification fraction, α , of C at the experimental pH. Equation 1.3.14 is valid at a single fluorescence wavelength or λ_{max} where the species of interest has the maximum absorption or emission intensity. If the fluorophore is an acid or base and pH is known, the α -s can be used to factor the total fluorescence emission intensity at given pH into those intensities associated with the particular species predominating.

Equation 1.3.14 and Equation 1.3.17 are better suited for determining binding between ionizable fluorophores and surfactants compared to the Scott and BH equations discussed in the literature review. Furthermore, many previous experiments yielding binding constants have been inaccurate because the presence of some quenching agents (e.g., Cl^- and O_2 -derived substances) were not adequately addressed. Since the surfactant also acts as a quencher, the presence of multiple quenchers likely means inaccurate values of K_{11} and K_{n1} have been assigned to the surfactants under study. The difference between these equations is that Equation 1.3.17 accounts for the total concentration of ciprofloxacin within the system as well as the fluorescence efficiency of CPF. F_T is the total fluorescence which accounts for an increase in fluorescence as the aggregate is titrated into the solution.

Equation 1.3.14 can be used to determine the binding of ciprofloxacin with the surfactants in the preaggregate and the postaggregate phases. In Equation 1.3.14, if the fluorophore is acidic or basic and pH varies the fractional concentration of the relevant species can be used to correct the emission intensity. The equation also accounts for the initial fluorescence intensity is greater than the total fluorescence as the aggregate is added into the solution.

To account for the fluorescence enhancement once complexation occurs, a new assumption is made where the fluorescence efficiency k , is not a constant all the species, rather the fluorescence efficiency of the monomer:monomer complex (k_{11}), aggregate:monomer complex (k_{n1}) and the free fluorophore (k_C) are included. Therefore Equation 1.3.18 can be expressed below:

Equation 1.3.18 Total fluorescence intensity when k is not constant

$$F_T = k_C + k_{11}CS + k_{n1}CS_n$$

Combining Equation 1.3.1, Equation 1.3.3, Equation 1.3.5, and Equation 1.3.7, Equation 1.3.19 is expressed:

Equation 1.3.19 Expanded total fluorescence intensity when k is accounted for

$$F_T = k_C + k_{11}K_{11}CS + k_{n1}K_{n1}C \frac{S_{T-cac}}{n}$$

Therefore, the observed total emission due the presence of three species, C + CS + CS_n, is related to binding constants, concentration of free C, the emission constants, cac, and n. Among these, the cac can be found from a characteristic inflection point of the observed emission. The concentration of free solute, C, is not easily obtained unless the solute is volatile, or its spectrum is clearly discernible from its complexes. If C is acidic or basic and its dissociation constants are known, preferably, with the same measurement technique, then the concentration of free C can be calculated from the fractional distribution of species vs. pH diagram. Therefore, the measurement of pH during the experiment is critically important. Species concentrations are given by

$$C_j = C_T \alpha_j$$

Here, α_j , is the fraction of j-th species e.g., of a multiprotic acid to calculated from the corresponding equilibrium constants. Therefore, Equation 1.3.20 can be expanded for all other species generated from the same compound with change in the conformation due to pH or other factors.

Equation 1.3.20 Total Fluorescence intensity to account for all species of the fluorophore in solution

$$F_T = \sum [F_j]$$

Equation 1.3.21 Substitution of F_T and F_j

$$\sum \left[\frac{F_j}{C_T \cdot \alpha_j} \right] = \sum \left[\left(k_j + ((k_{11}K_{11})_j S) + \left(k_{n1} \frac{K_{n1}}{n} \right)_j (S_{T-cac}) \right) \right]$$

For a single major species

Equation 1.3.22 Determination of K_{11} and K_{n1} to account for fluorescence enhancement

$$\frac{F_j}{C_T \cdot \alpha_j} = \left[\left(k_j + ((k_{11}K_{11})_j S) + \left(k_{n1} \frac{K_{n1}}{n} \right)_j (S_{T-cac}) \right) \right]$$

Equation 1.3.21 is the general expression for the model. The sum sign is over the number of species 0- j. Equation 1.3.21 is valid at a fixed wavelength where the emission intensity is measured. For a tetraprotic acid j=4 and there are five species. Since pH determines the abundance of species, α_j , the emission is mostly determined by the specific species in question unless the emission constants are significantly different from each other. Equation 1.3.22 was tested with the major species present at the indicated pH, specifically CPF and SDS complexation. Clearly, the model is explicit compared to that of single species approximate models like BH, and Scott described earlier, except there is

no simple way to get the aggregation number, n , other than literature values or ultrafast emission decay experiments.⁶³

EXPERIMENTAL

3.1 Experimental

3.1.1 *Chemicals*

Ciprofloxacin (CPF), sodium hydroxide, hydrochloric acid, perfluorooctane-1-sulfonic acid (PFOS), anthracene (97% purity), DL- α -tocopherol methoxypolyethylene glycol succinate (TPGS-750M) and myelin basic protein (MBP) were purchased from Sigma Aldrich (St. Louis, MO). Monosodium phosphate and disodium phosphate were purchased from Fisher Scientific (Hampton, NH). Sodium dodecyl sulfate (SDS) (98% purity), NaOH and HNO₃ were available without purchase. Chemicals were not further purified prior to use.

3.1.2 *Instrumentation*

Two spectrofluorometers were employed to measure fluorescence. The first was a Shimadzu (Columbia, MD) Model RF-6000 spectrofluorometer. Various sample dilutions were manually prepared in the quartz, 2.0 mL and 1.0 cm pathlength cuvette prior to measurement and manually added into instrument. The RF-6000 was used for the batch experiments of ciprofloxacin (CPF) pH experiments, CPF with sodium dodecyl sulfate (SDS) and perfluorooctanesulfonic acid (PFOS) in addition to scanning the absorption and emission fluorescence spectra of CPF and anthracene to select the wavelengths of maximum emission for equilibrium studies.

The second spectrofluorometer was custom built. To obtain reliable emission intensities at selected wavelengths while the solute probe (e.g., CPF) was added to the ligand (e.g., SDS) without having to manually replace the cuvette each time an addition of a flow-through attachment to a Perkin-Elmer LS-5B fluorescence spectrometer (Waltham, MA) was custom assembled. This feature allowed for the simultaneous data collection of fluorescence intensity and pH without manipulating the cuvette. The components of the flow cell apparatus consisted of a RAZEL Scientific precision syringe pump (Fairfax, VT), thermo-stated water bath at $(25 \pm 0.1)^\circ\text{C}$, a thermo-stated mixing cell, pH probe (Vernier, Beaverton, OR), a peristaltic pump, with Teflon tubing and a cuvette with the spectrofluorometer. The instrument is a Continuous Flow Closed Loop System (CFCLS). The CFCLS was designed and assembled by Dr. Abul Hussam. A schematic diagram of the apparatus is shown in Figure 3.1.1.

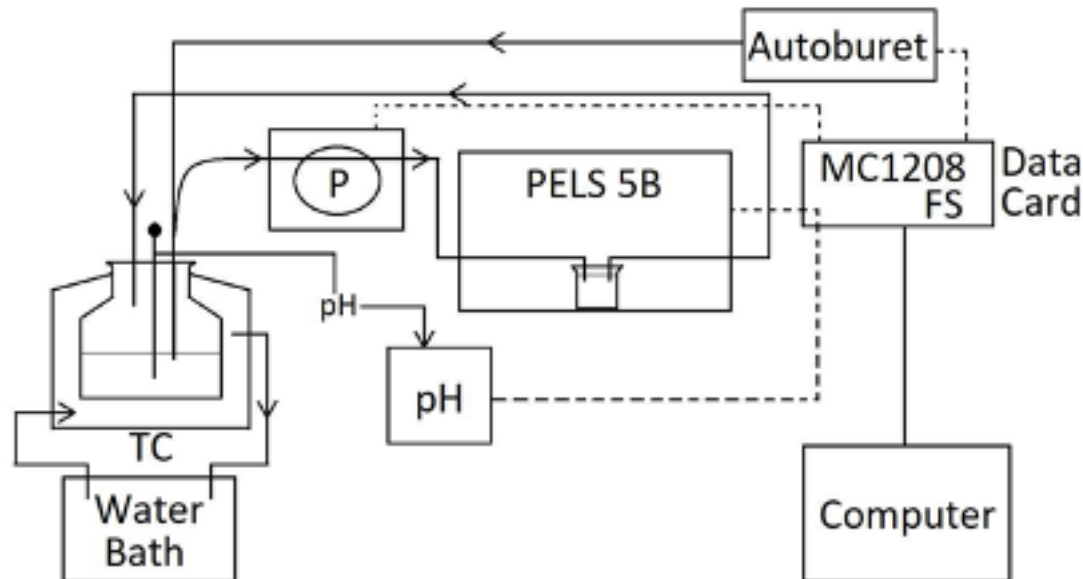


Figure 3.1.1 Schematic of a Continuous Flow Closed Loop System (CFCLS). TC: Thermo-stated mixing cell (35.0 mL), PH- pH probe, T- thermostat, PELS5B: Perkin-Elmer Mode 5B spectrofluorometer, Autoburet: RAZEL precision syringe pump, P: Peristaltic pump controlled by computer, MC 1208 FS-Plus: Measurement Computing data acquisition card (PMD 1208, Measurement Computing Inc., USA)

3.1.3 The operation of the CFCLS

The measurement protocol for the CFCLS was the following: The Perkin-Elmer LS-5B fluorometer was turned on and warmed up for 15 minutes. The tubing connected to the thermo-stated mixing cell was attached to the water bath. The thermo-stated mixing cell was filled with water from the water bath and the temperature was regulated for 15 minutes. The peristaltic pump was turned on for 10 minutes to remove residual liquid in the Teflon tubing. The Teflon tubing attached to the peristaltic pump was changed when surfactants or other solutes were changed. The Teflon tubing was flushed with 30 mL of water mixed with 1-2 mL of acetone and the peristaltic pump ran for five minutes. The thermo-stated mixing cell was filled with 30 mL of the desired solution. The solution was flushed with either Ar or N₂ gas for 10 minutes and then continuously flushed throughout

the experiment in order to ensure the removal of possible O₂ radical quenchers. The peristaltic pump was turned on to fill the cuvette inside the fluorometer. Then the pump was turned off and the required parameters were entered into the Delphi program and the experiment was run. The Teflon tubing was changed when different surfactants or compounds were introduced into the thermo-stated cell in order to prevent any possible contamination. Delphi 6 (Embarcadero, Austin TX) was used to establish the data collection and processing of CFCLS.

A typical CFCLS data acquisition cycle was established with the following parameters (Figure 3.1.2): (a) 50 auto-buret (AB) additions of surfactant to the thermo-stated mixing cell; (b) delay time of 30 seconds between additions from the AB to the thermo-stated mixing cell; and (c) AB add time of surfactant of 10 seconds to the thermo-stated mixing cell. The average number of readings for each recorded data point was 85. The interval between individual fluorescence intensity readings was 100 milliseconds. The ADC full scale was the voltage (± 2.0 V) in the fluorometer that determined the total fluorescence intensity emitted. The fixed scale (0.250 – 1) was the capacity of allowed fluorescence intensity.

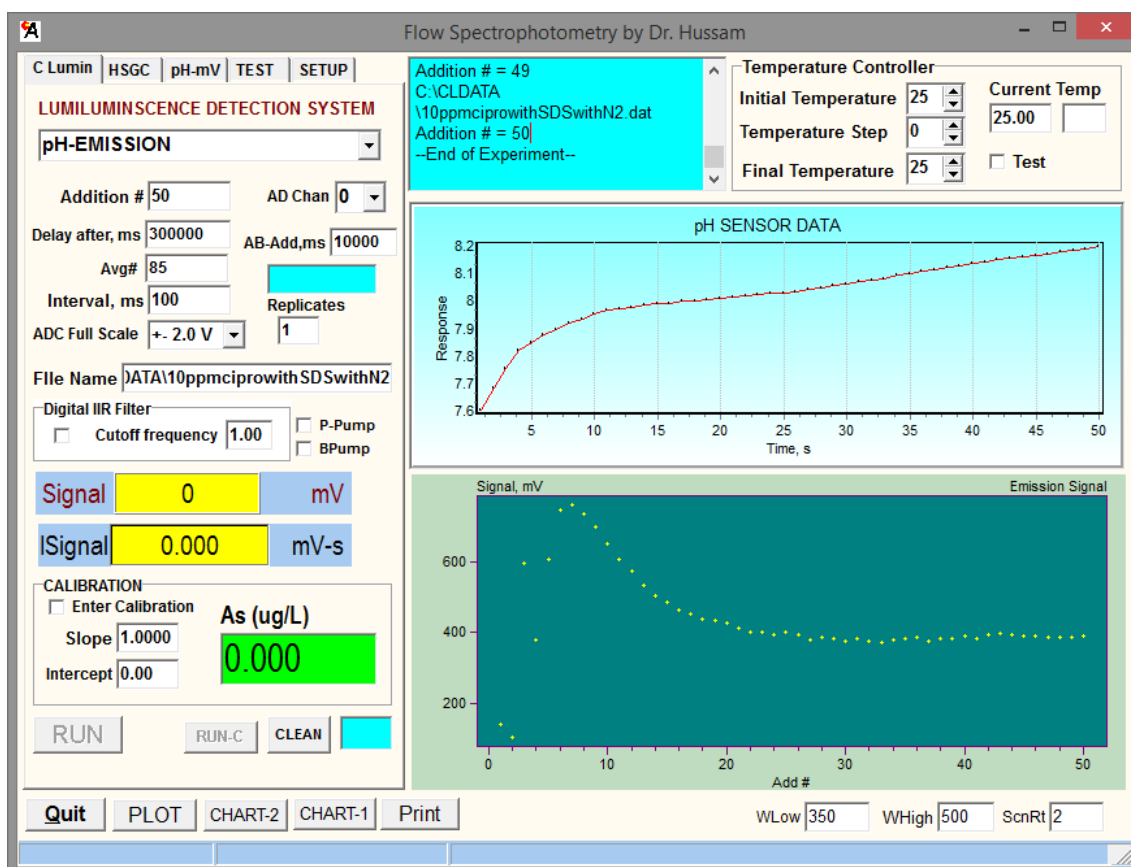


Figure 3.1.2 An example of CFCLS program

The greatest advantage of the CFCLS were the precise addition of reagents, mixing of the reagents, and the delivery to the cuvette without manual manipulation, with all steps under automated computer control. The CFCLS system allowed the measurement of pH and emission intensity simultaneously at any time for as many times as desired. Thus, all pH and emission data reported here is the average of 85 measurements after sample addition and mixing. The measurement precision was less than 1% RSD for pH and fluorescence intensity.

In order to ensure the pH values in the CFCLS were accurate, the probe was calibrated using 4.00, 7.00 and 10.00 pH buffers. The pH calibration is shown in Figure 3.1.3. The maximum error within the probe was ± 5 mV (Figure 3.1.3).

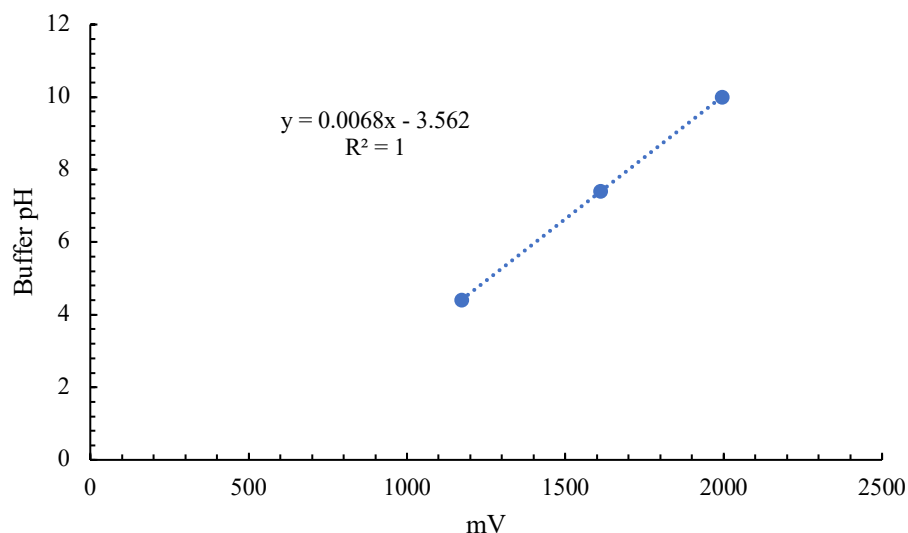


Figure 3.1.3 The calibration of the pH probe used in CFCLS using buffer pH 4.00, 7.00, and 10.00

3.1.4 Measurement of equilibrium mixing time

To measure the equilibrium mixing time a 12 mM of CPF stock solution was loaded in clean cuvette prerinsed with acetone and water. Then thermostated mixing cell was filled with water. The flow rate of the peristaltic pump was 1.28 mL/min. The volume flow (mL/s) was determined by multiplying the flowrate of the pump by the time. As the water in the thermo-stated mixing cell flows into the cuvette filled with CPF and dilutes it, the decrease in fluorescence intensity was measured vs. time. From the volume

flow as shown in Figure 3.1.4, until there is no change in signal is the equilibrium mixing time, which is 300 s or 5 mins.

Table 3.1.1 The experimental parameters of CFCLS to determine the ideal mixing time

Number of additions	500	AB-add (ms)	0
Delay After (ms)	300000	ADC Full Scale (V)	± 2.0
Average Number	10	Interval (ms)	100
Fixed Scale		1	

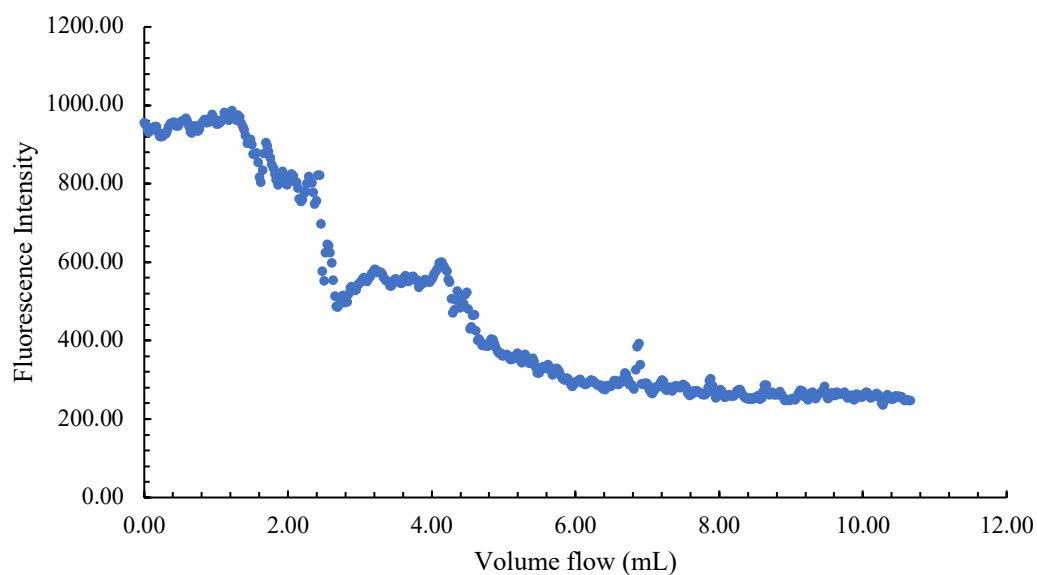


Figure 3.1.4 The fluorescence intensity versus volume flow to determine the ideal mixing time of reagents in the whole flow system in the CFCLS

3.1.5 Fluorophore and surfactant combinations

3.1.5.1 Anthracene and TPGS

Initial proof of concept of the CFCLS was performed using anthracene as the fluorescent probe and TPGS as the surfactant. Anthracene is a neutral substance that is not influenced by solution pH and is a strong fluorophore. This is less complex compared to CPF. TPGS-750M is an amphiphilic surfactant that is environmentally benign. It is overall neutral compared to the overall negatively charged SDS and PFOS and the positively charged MBP. The simplistic factors of these two compounds allowed both to validate the theory and the methodology.

An anthracene stock solution was prepared by mixing 1.0 mg of anthracene in 10.0 μL of methanol as a water-soluble carrier solvent and adding this to distilled water in a 250 mL volumetric flask. The resulting anthracene concentration was 0.023 μM , which was lower than the literature solubility of 0.25 μM .⁶⁴ A total of 30.0 mL of the anthracene stock solution was filtered through a 0.2 micron nylon filter and added directly to the thermo-stated cell in the CFCLS.

A TPGS-750M stock solution was prepared by dissolving 0.5000 g in 25.0 mL of distilled water in a volumetric flask. The stock solution was diluted in distilled water to produce a working concentration of 80.0 mM of TPGS-750 (MW= 1250 g/mol). The working solution was loaded into the autoburet for delivery into the thermo-stated mixing cell in the titration. TPGS-750M was added in 60 μL increments. The titration was performed under the previously optimized settings.

3.1.5.2 pH titrations of CPF

The purpose of the pH titrations was to understand the effect of pH on the structure of CPF as well as the effect on the fluorescent intensity. It was observed that as the pH increased, there was a blue-shift in $\lambda_{\text{emission}}$ from 448nm in acidic conditions to 416 nm in basic conditions. It could then be determined that the effect of pH not only influences the fluorescence of CPF but also the interactions of CPF with surfactants.

To determine the effect of pH on CPF fluorescence properties, batch experiments were initially conducted using the The Shimadzu RF-6000 spectrofluorometer. A total of 15 solutions of CPF including pH 1.00, 2.00, 3.00, 4.00, 5.00, 6.00, 6.50, 7.00, 7.50, 8.00, 8.50, 9.00, 10.00 and 11.00 were created. The concentration of the CPF solution was adjusted to 31.2 μM . CPF was dissolved in 1.0 mL of concentrated HNO_3 instead of

HCl, to prevent possible chloride quenching and adjusted with NaOH to the desired pH values. For pH ranges 1-5, the $\lambda_{\text{emission}}$ was set to 448 nm. For pH ranges 6-11, the $\lambda_{\text{emission}}$ was set to 416 nm. This was to account for the blue shift that occurred with the CPF. The excitation slit was set to 3.0 nm while the emission slit was set to 3.0 nm.

3.1.5.3 CPF and SDS Additions

3.1.5.3.1 CPF and SDS batch experiments with Shimadzu RF-6000

Batch Experiments were conducted using the Shimadzu RF-6000 spectrofluorometer. A 500 mg/L stock solution of CPF was prepared by dissolving 25 mg

of CPF in 2.0 mL 0.1M HCl and 50 mL of ultra-pure distilled water. All solutions were adjusted to pH 8.33, 7.00 and 4.00 in 0.1M phosphate buffer. A stock solution of 0.200 M SDS was prepared in ultra-pure distilled water. The concentrations of SDS ranged from 0-50 mM for a total of 12 solutions. The stock solution of SDS was prepared by dissolving xxx g in mL of distilled water.

To prepare the 12 solutions, the appropriate volume of the SDS stock solution was delivered with a 1000 μ L micropipet. The concentration of CPF was held constant at 31.2 μ M. All of the solutions were stored in amber bottles and in the dark. The $\lambda_{\text{emission}}$ was set to 446 nm and $\lambda_{\text{excitation}}$ was set to 270 nm. The excitation and emission slits were 2.5 nm and 3.0 nm, respectively. The emission scans were collected in triplicate and the intensities were averaged.

3.1.5.3.2 CPF and SDS titration experiments with CFCLS

CFCLS Experiments were conducted with CPF and SDS. The first set of experiments were to observe the interactions when SDS and CPF were dissolved in distilled water. The concentration of SDS was 0.3 M in the AB was titrated in increments of 10 μ L to the thermo-stated mixing cell filled with 30 mL of 31.2 μ M CPF. CPF was thoroughly mixed for five minutes before each addition. A total of 30 - 50 additions were completed for each experiment. The $\lambda_{\text{excitation}}$ was set to 270 nm and the $\lambda_{\text{emission}}$ was set to 448 nm. The excitation and emission slits were set at 3 nm.

The experiment was then repeated where the thermo-stated mixing cell was filled with 15 mL of 600 mM of CPF and 15 mL of 0.1M phosphate buffer to observe the effects of binding with and without a salt buffer.

3.1.5.4 CPF and PFOS additions

3.1.5.4.1 CPF and PFOS batch experiments with Shimadzu RF-6000

Batch Experiments were performed with CPF and PFOS using the Shimadzu RF-6000. A total of 13 solutions of 0.00 mM, 1.60 mM, 3.10 mM, 4.20 mM, 5.00 mM, 8.20 mM, 10.00 mM, 14.00 mM, 20.00 mM, 25.00 mM, 33.00 mM, 40.00 mM and 50 mM of added PFOS to CPF and 0.1 M phosphate buffer were created.

CPF was initially dissolved in 0.1 M HCl, and diluted in 0.1M phosphate buffer pH adjusted to 7.00 to equal a concentration of 31.2 μ M. PFOS was purchased from Sigma-Aldrich as a solution of 41% v/v in water, which converts to 2.279 M. To prepare the range of solutions at the desired PFOS concentrations, a 1000 μ L micropipet was used to deliver calculated amounts of PFOS into 13 amber bottles containing CPF and 0.1 M phosphate buffer. Fluorescence was recorded in triplicate after each PFOS addition. The experiments were repeated in duplicate, and an excitation spectrum was recorded. The $\lambda_{\text{excitation}} = 270$ nm and $\lambda_{\text{emission}} = 448$ nm and the excitation and emission slits were at 3.0 nm.

3.1.5.4.2 CPF and PFOS titration experiments with CFCLS

CFCLS experiments with CPF and PFOS were conducted in pure water, and the presence of phosphate buffer to test the effects of pH and ionic strength on fluorescence.

In pure water titrations either 1 mM or 2.279 M PFOS dissolved in water was added to the AB. The titration was performed in 0.1 mL increments with the AB. The thermo-stated mixing cell contained 30 mL of CPF at concentrations ranging from 100 mM - 600 mM in ultra-pure distilled water.

In the case of phosphate buffer, the thermo-stated mixing cell was filled with 15 mL of 0.1 M phosphate buffer at pH 7.00 and 15 mL of 600 mM CPF. Subsequently, 10 μ L aliquots of PFOS were auto-titrated to thermo-stated mixing cell. The solution was thoroughly mixed for five minutes before additions. A total of 30 additions were completed for each experiment.

Fluorescence measurements were conducted in each case under the optimized CFLCS conditions of $\lambda_{\text{excitation}} = 270$ nm and $\lambda_{\text{emission}} = 448$ nm. The excitation and emission slits were at 3.0 nm.

3.1.5.5 CPF and TPGS-750M titration experiments with CFCLS

The CPF and TPGS-750M experiments were completed using the CFCLS. To prepare the TPGS-750M stock solution, 0.5000 g was dissolved in 25 mL of distilled water. Then, 12.5 mL of TPGS was diluted with water to 25 mL in a volumetric flask and diluted to yield 80 mM. The TPGS-750M 80 mM solution was then added in 6.0 mL to the AB. The CPF solution was prepared in distilled water to yield a concentration of 100 μ M, and 30.0 mL of the CPF solution was added to the thermo-stated mixing cell.

Fluorescence measurements was conducted with $\lambda_{\text{excitation}} = 270$ nm and $\lambda_{\text{emission}} = 448$ nm and the excitation and emission slits were 3.0 nm.

3.1.5.6 CPF and MBP titration experiments with CFCLS

CFCLS experiments were conducted to observe the interaction between CPF and MBP.

The phosphate buffer was prepared by diluting 25 mL of 0.1 M phosphate buffer and diluting it to 250 mL with distilled water to equal 0.01M. The buffer was then filtered through a 0.45 micron Nylon filter in order to further purify it. The phosphate buffer was used to maintain the pH of the CPF solution at pH 7.70. The MBP was dissolved in 0.9% NaCl to yield a concentration of 90.6 mM MBP, where 3.0 mL was added to the AB of the CFCLS. The CPF solution was prepared to be 100 mM in 0.01 M phosphate buffer. A total of 30.0 mL of the CPF solution was added to the thermo-stated mixing cell. Fluorescence measurements was conducted with $\lambda_{\text{excitation}} = 270 \text{ nm}$ and $\lambda_{\text{emission}} = 448 \text{ nm}$ and the excitation and emission slits were 3.0 nm.

Unfortunately, the error within the fluorescence intensity measurements of CPF with MBP were ± 1.93 and the trend displays large error. Therefore the data could not be used for binding analysis.

3.1.6 Data Analysis

Microsoft Excel (Redmond, WA) was used to analyze the all of the data obtained using the Shimadzu RF-6000 and the CFCLS. Excel was used to generate the plots and calculate the binding constants, K_{11} and K_{n1}/n from the slope and intercept of the graphs using simple liner regression. The regression tool in Excel was used to determine the error in binding constants obtained.

The equation used for the data analysis was $F_0/F_T = 1 + K_{11}S + (K_{n1}/n)(S_T - \text{cac})$ to account for fluorescence quenching like behavior (FQ). The experimental cac was determined for each pseudophase compound by plotting F_0/F_T in the y-axis and the concentration of the aggregate added in the x-axis. F_0 represented the initial fluorescence intensity of each individual CPF species without added surfactant. F_T was the total fluorescence for the specific CPF species at the experimental pH, which was derived by multiplying total measured fluorescence (F_T) by alpha for each species (i.e., $F_T = F \cdot \alpha_i$). Finally, the ratio F_0/F_T was obtained at each incremental addition of surfactant. The values K_{11} and K_{n1}/n were obtained from the regression intercept and slope values, respectively. A positive slope was indicative of binding. The aggregation number, n , could not be determined experimentally which is why the values are listed as K_{n1}/n .

Once the slope and intercept were obtained for both equations, the data analysis tool in Excel linear regression analysis was used to determine the standard deviation of the estimated slopes and intercepts, which along with the R^2 values from the plots provided the binding constant errors and goodness of fit of the models, respectively. If a binding constant obtained was negative, or if the error in the binding constant was greater than the binding constant itself, these values were considered to be 0 and no binding between CPF and the aggregate of interest.

To account for the fluorescence enhancement (FE), a straight line was plotted where the y-axis is $(F_T - F_0)/(C_T \cdot \alpha)$ and x-axis is $S_T - \text{cac}$. The intercept is $(k_C + k_{11} \cdot K_{11} \cdot S)$ and a slope is $(k_{n1} \cdot K_{n1}/n)$. The emission constants, k , can be obtained from F in absence of surfactant, k_{11} from the highest F in the premicellar region, and k_{n1} from the

region of complete complexation in the post-micellar region. To a first approximation k , k_{11} , and k_{n1} can be assumed to be constant throughout the experiment if surfactant does not change the conformation of the solute, C , significantly.

DETERMINATION OF ANTHRACENE AND DL- α - TOCOPHEROL SUCCINATE (TPGS-750M) COMPLEXATION

4.1 Anthracene and TPGS-750M complexation

Anthracene, a 3-ring polycyclic aromatic hydrocarbon (PAH) whose binding properties do not depend on solution pH, was the first fluorescent probe to be tested in combination with the biosurfactant DL- α -tocopherol methoxy-polyethylene glycol succinate (TPGS-750M). Anthracene was selected to conduct a first-order evaluation of the binding models.

4.1.1 *The fluorescence spectrum of anthracene*

The emission spectrum of anthracene was obtained using 270 nm as the excitation wavelength. The literature had an excitation wavelength of 253 nm for anthracene.⁶⁵ However, the sensitivity of the Perkin-Elmer LS 5B could not go lower than 270 nm. Therefore, while the emission spectrum was taken with the Shimadzu RF-6000, this was to ensure consistency with the CFCLS. Figure 4.1.1 shows two maxima at 405 and 415 nm in the fluorescence emission spectrum of anthracene. For quenching experiments 405 nm was selected as maximum emission wavelength (λ_{max}), which corresponded with the λ_{max} most often reported in the literature^{65–68} for anthracene. It is important to note that TPGS-750M is fluorescent with an emission maximum of 315 nm.²⁸ From the emission spectrum of Puig-Rigall et al. it was observed that there was no fluorescence emission past 375 nm. Therefore, it was assumed there was no emission overlap existed between TPGS and anthracene.

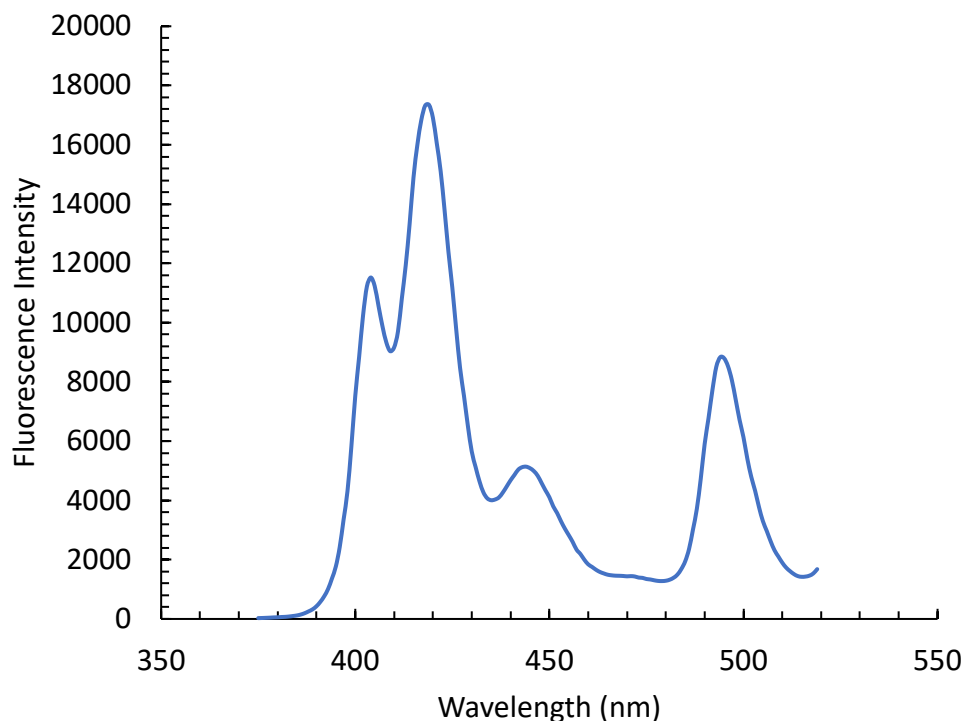


Figure 4.1.1 An emission spectrum of 0.023 μM anthracene in distilled water + 300 μL of methanol without TPGS – 750 M at 25°C. The excitation wavelength = 270 nm

4.1.2 *The effect of TPGS-750M on anthracene fluorescence*

A strong quenching of anthracene fluorescence was observed through a TPGS-750M concentration range of 0 to 7,000 μM (Figure 4.1.2). As the concentration of TPGS-750M increased the total fluorescence intensity decreased. The error within the fluorescence intensity was ± 5 . The pH of the system was 6.26 ± 0.03 and showed a minimal change through the complete range of the titration. The overall resolution from the CFCLS appears to be good. It was observed that past 4000 μM of TPGS added, the fluorescence intensity becomes stagnant. This could be due to saturation of anthracene

within the TPGS pseudophase, or self-quenching from the anthracene fluorophore.

Therefore, 0 – 4000 μM of TPGS added was considered for analysis.

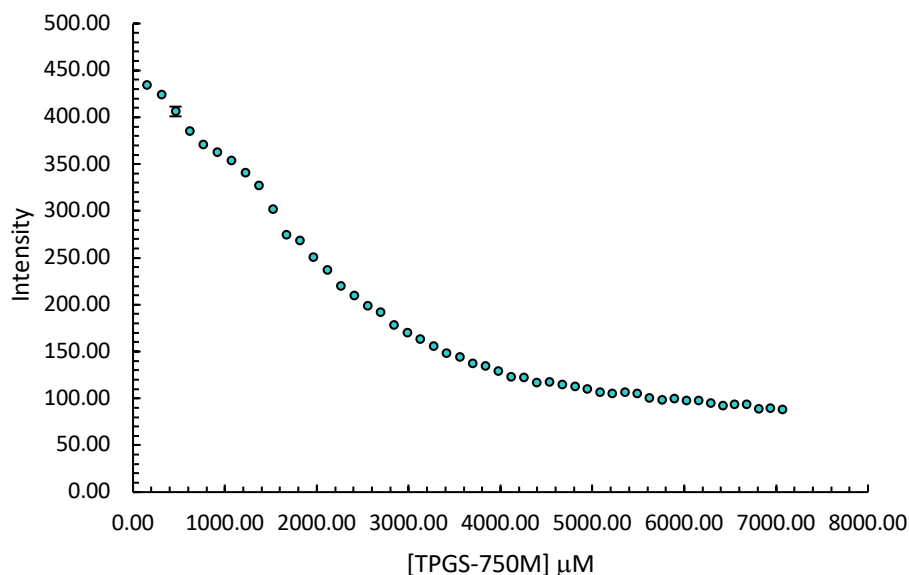


Figure 4.1.2 Fluorescence Intensity ± 5 of anthracene versus the concentration of TPGS – 750M at 25°C.

4.1.3 Determination of the critical aggregation concentration of TPGS-750 M

The cac of surfactants can be determined in spectrometric titrations that conducted above and below the cac. The cac for TPGS-750M was determined from the fluorescence ratio (F_0/F_i) to be 1.51 mM (Figure 4.1.3). The literature values of the cac of TPGS have ranged from 0.02 to 1.51 mM.³⁰ One factor of the varying cac is due to the varying molecular weight. For TPGS-100M it was observed to start at 0.02 mM and 1.51 for TPGS-400M. The molecular weight of TPGS-750M ranges from 1250-1340 g/mol. From Figure 4.1.3, it appears that the cac resembles that of TPGS-400M.

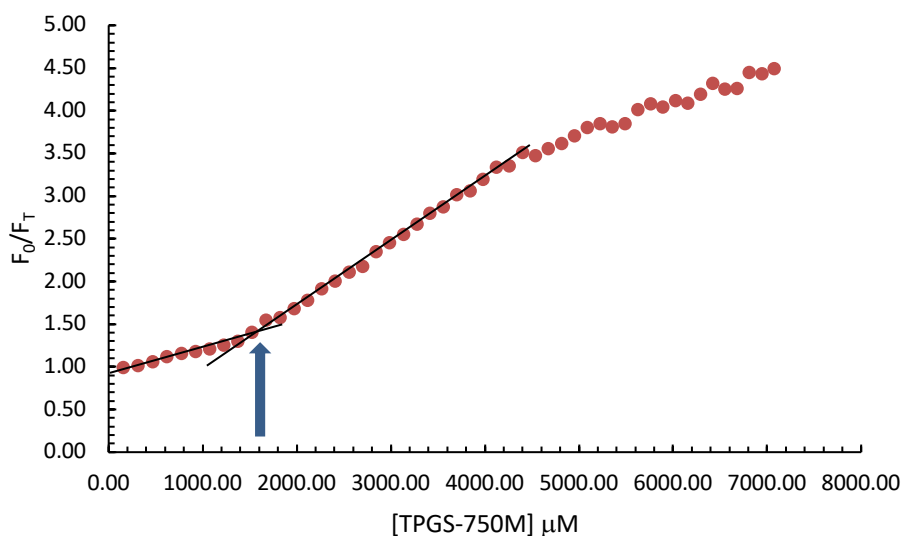


Figure 4.1.3 The figure shows an emission ratio vs. [TPGS] μM added. The critical aggregation concentration, 1512 μM , is found from the intersection of initial slopes as shown.

Compared with other surfactants (Table 4.1.1) the cac for TPGS was smaller than SDS but larger than CTAB and Triton 100X. Knowing the cac of pseudophase compounds is critical as it determines the point at which the monomer becomes an aggregate. The cac also determines the exact point of when the fluorophore partitions within the pseudophase or if no interactions occur. Therefore, by understanding the properties of various pseudophase compounds, and when they aggregate, this aids in the determination of the interactions that occur with the fluorophore.

Table 4.1.1 The literature critical aggregation concentration of other surfactants

Compound	CAC
----------	-----

SDS ⁶⁹	8.0 mM
CTAB ⁶⁹	0.25 mM
Triton 100X ⁶⁹	0.8 mM
Humic Acid ⁷⁰ (HA)	7.0 g/L
Fulvic Acid ⁷⁰ (FA)	6.8 g/L

4.1.4 Binding Constants

The K_{11} and K_{n1} values for anthracene binding in the TPGS preaggregate and postaggregate phases were obtained using the derived model discussed in the Theory section of this dissertation.

A plot of F_0/F_T versus $S_T\text{-cac}$ is shown in Figure 4.1.4 below. The binding constant K_{11} was determined to be $292 \pm 8.2 \text{ M}^{-1}$. The binding in the postaggregate phase greater compared to the binding in the preaggregate phase, and this does not account for the aggregation number, n , of the surfactant. Therefore, if the literature aggregation number of 41 is used, then the K_{n1} would be $(2.77 \pm 0.05) \times 10^4 \text{ M}^{-1}$. This would show that there is significant binding between anthracene and TPGS-750M.

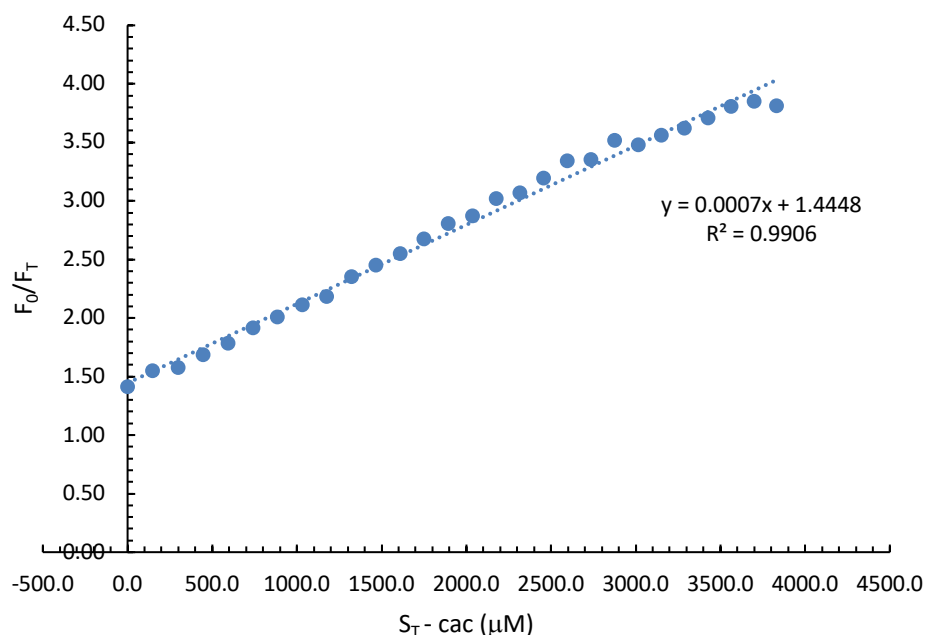


Figure 4.1.4 Figure shows a portion of the emission ratio when $S_T - \text{cac}$ is greater than or equal to 0. The intercept and the slope were used to calculate K_{11} and K_{n1}/n .

Table 4.1.2 The binding of anthracene and TPGS-750M at 25°C. The literature aggregation number of 41 was used to determine K_{n1} .

Slope (μM^{-1})	$(6.75 \pm 0.1) \times 10^{-4}$
Intercept (μM^{-1})	1.44 ± 0.03
R^2	0.9906
K_{11} (M^{-1})	292 ± 8.2
K_{n1}/n (M^{-1})	676 ± 13
K_{n1} (M^{-1})	$(2.77 \pm 0.05) \times 10^4$

Notes: The equation $(F_0/F_T) = 1 + K_{11}[S] + (K_{n1}/n)(S_T - \text{cac})$ was used to extract the K_{11} and K_{n1} binding constants from the intercept and slope of Figure 4.1.4.

Because of the simplicity of anthracene and TPGS used, the data obtained provides a basis for the binding model. This is due to that there is no influence of pH and salt on the compounds.

4.1.1.1 A literature survey of anthracene binding with other pseudophase aggregates

In order to properly understand the experimental binding between anthracene and TPGS-750M it is first important to observe and compare the different binding constants used in previous literature studies. This is shown in (Table 4.1.3) below. There have not been any studies conducted to determine the binding between anthracene and TPGS-750M.

Table 4.1.3 Literature binding constants of anthracene with other pseudophase aggregates. cmc- critical micelle concentration, n- aggregation number of the surfactant not the quencher, K₁₁ is the 1:1 binding constant, K_b - binding constant (water), K_{sv} - Stern-Volmer constant. a. listed in Table 4.1.4, b. N/L = not listed, c. detection limit in nM not a binding constant, d intensity ratio between sodium taurocholate (NaTC)-metal to NaTC alone.

Probe molecule (Eq used), pH, Temp ^a	Quencher-Surfactant or Reactant	CMC (mM)	n	K ₁₁ (M ⁻¹)	K _b	K _{sv} (M ⁻¹)	λ _{ex} /λ _{em} (nm)
Anthracene (1) pH= 8.0 ± 0.1 Temp 20 °C	Cetylpyridinium chloride (CPC) - SDS	N/L	60	N/L ^b	N/L	474 ± 13 ⁷¹	355 / 402
2-Anthracene Sulfonate (2,4) pH= N/L Temp 25 °C	CPC-Triton X-100	0.25	134	N/L	260,000 ⁶⁹	4,800 9,200, 46,000	337 / 412
	CPC-SDS	8.0	50	N/L	70,000	900, 2,300, 6,400	
	CPC-CTAB	0.8	55	N/L	96,000	900, 2,100, 15,000	
	CPC-Tween-80	0.01	124	N/L	250,000	4,000, 8,700, 40,000	
	CPC-Tween-60	0.021	112	N/L	220,000	3,800, 7,600, 37,000	
	CPC-Tween-40	0.023	92	N/L	180,000	3,400, 7,200, 35,000	
	CPC-Tween-20	0.05	86	N/L	160,000	3,300, 7,100, 33,300	
Anthracene (2) pH= N/L Temp 25 °C	CPC -ethanol	N/L	N/L	N/L	N/L	45 ± 0.5 ⁷²	365 / 400
	KI - ethanol	N/L	N/L	N/L	N/L	17 ± 0.5	
	Pyridinium chloride, PC - ethanol	N/L	N/L	N/L	N/L	42 ± 1	
	PC - SDS	N/L	N/L	N/L	N/L	520 ± 20	
	KI- SDS	N/L	N/L	N/L	N/L	< 1.0	

	Quinolinuim-SDS	N/L	N/L	N/L	N/L	1575 ± 50	
	KI - CTAB	N/L	N/L	N/L	N/L	418 ± 15	
	CPC - CTAB	N/L	N/L	N/L	N/L	348 ±12	
	PC - CTAB	N/L	N/L	N/L	N/L	< 1.0	
	NaTC	N/L	4	4.4 ^{64c}	N/L	N/L	
	NaTC-Tb ³⁺	N/L	N/L	1.3 ^d	N/L	N/L	
	NaTC-Eu ³⁺	N/L	N/L	1.2 ^d	N/L	N/L	
	NaTC-Al ³⁺	N/L	N/L	1.2 ^d	N/L	N/L	
	SDS	N/L	N/L	0.46 ^c	N/L	N/L	N/L

From the table, it can be observed that there are three binding constants. K_{11} accounts for the preaggregate binding, K_b is the binding constant in water, and K_{SV} is the Stern-Volmer constant. Often, K_{SV} has been used as a binding constant, however, it is actually a rate constant. This was determined through the derivation where K_{SV} is composed of the rate of disappearance, rate of fluorescence quenching and rate of fluorescence emission. None of the rate constants which compose K_{SV} account for binding. The K_b is the closest to the K_{n1} binding constant, due to the noncovalent interactions which occur between the fluorophore and the pseudophase. They cannot be listed as K_{n1} due to the binding not being exclusive to the micelle or pseudophase compound. The binding determined in the literature values are between the fluorophore and the quencher.

The equations used to determine the binding constants were referenced in Table 4.1.3, are shown in Table 4.1.4.

Table 4.1.4 Equations used to determine the binding constants in Table 4.1.3

No.	Equation
-----	----------

1	$F_0/F = (1 + K_D[Q])(1 + K_S[Q]) = 1 + (K_D + K_S)[Q] + K_D K_S [Q]^2$
2	$F_0/F = 1 + K_{SV}[Q]$
3	$K_b = ([Q]_{\text{micelle}}/([Q]_{\text{water}})[M])$
4	$[Q]_T = \tilde{n}/K + \tilde{n}[M]$
5	$[M] = ([S] - [\text{free monomer}])/n$
6	$\ln (F_0/F) = [Q]n/[S]$

Notes: F_0 = initial fluorescence intensity without quencher, F = total fluorescence intensity, K_D = dynamic quenching constant, K_S = static quenching constant, K_b - Binding or association constant, $[Q]$ = concentration of quencher, $[Q]_T$ = Total quencher, \tilde{n} = average occupancy number of Q per micelle, $[M]$ = concentration of micelle, $[S]$ = total or stoichiometric concentration of surfactant

The literature binding constants obtained in Table 4.1.3 are difficult to compare to the experimental due to the nature of the experiments conducted. The experiments conducted were three-constituent systems as expressed prior. The three-constituent systems consist of the fluorescent probe, the solvent and the quencher. The K_b values obtained with anthracene sulfonate are the closest to the K_{n1} binding constant. However, the addition of the sulfonate ion on the anthracene while increases the solubility in water, could also minimize the binding between the aggregate past the cac, encouraging the fluorophore to interact more with the water soluble quencher, cetylpyridinium chloride (CPC)

However, from the results determined, past the cac, interactions between anthracene and TPGS-750M pseudophase display overall fluorescence quenching like behavior, where the fluorescence intensity decreased as the concentration of TPGS-750M increased. Therefore, the precision in the binding constants obtained in Table 4.1.3 was

affected due to multiple quencher compounds within the solutions. TPGS is unique with the ability to be soluble in both polar and nonpolar solvents. Therefore, the interactions with anthracene are plausible with anthracene's low solubility in water. Anthracene will migrate to interact with the pseudophase aggregate until it is saturated. This is why there is a high binding observed in the preaggregate and postaggregate phase.

THE EFFECT OF PH ON CIPROFLOXACIN (CPF) SPECIATION AND FLUORESCENT PROPERTIES

5.1 The effect of pH on CPF speciation and fluorescent properties

CPF is known to be a strongly fluorescent compound. Because CPF is a multiprotic acid its fluorescent properties are strongly pH dependent. There has been variation among the pK_a values and associated speciation of CPF reported in the literature (Table 5.1.1). Previous studies have regarded CPF as a diprotic, triprotic, or more recently as a tetraprotic acid. It is critically important to express CPF dissociation accurately because fluorescence in relation to pH speciation (acid-base forms) can substantially impact the determination of binding constants.

Table 5.1.1 The literature protonation and pK_a values reported for ciprofloxacin using various experimental methods.

CPF as	pK_{a1}	pK_{a2}	pK_{a3}	pK_{a4}	Method
Tetraprotic acid ^{11,73–76}	3.64,	5.05,	6.95,	8.95,	Electrophoresis and spectrometric titration
	3.32,	5.59,	6.14,	8.85,	
	3.01	6.14	8.70	10.58	
Triprotic acid ^{6,8}	-021	5.05	6.30	8.61	Potentiometric and spectrometric titration
			6.35	8.95	
Diprotic acid ^{7,77,78}	3.01	6.09, 6.10, 6.14	7.41	8.62, 8.70	Spectrometric titration

CPF has four measurable pK_a values, but the assignment of each pK_a to a position on the molecule has varied. A proposed CPF proton dissociation scheme is illustrated in Figure 5.1.1. Qiang et al.⁷⁶ stated the proton on the carboxylic acid is the first to dissociate because the pK_a of 1-naphthoic acid (3.69) is similar to the measured pK_{a1} of CPF, correlating with the structural similarity between naphthoic acid and fluoroquinolones. The authors further state that the remaining pK_a values were assigned to the three reactive nitrogen atoms based on electron density, in order of the quinolone nitrogen (N1, pK_{a2}), first piperazine nitrogen (N1', pK_{a3}) and second piperazine nitrogen (N4', pK_{a4}). However, De Bel et al.⁷⁵, Salma et al.¹¹ and Van Doorslaer et al.⁷³ assigned pK_{a1} to the quinolone nitrogen N1, pK_{a2} to N1', pK_{a3} to the carboxylic acid and pK_{a4} to N4'. Van Doorslaer et al.⁷³ declared data for pK_{a1} and pK_{a2} were scarce with contradictory results making it difficult to unequivocally assign these proton dissociation sites, but they confidently assigned pK_{a3} and pK_{a4} to the carboxylic acid and the N4' nitrogen on the piperazinyl ring, respectively. Yang et al.⁴² and Khan et al.⁴⁸ also associated pK_{a1} with the quinolone nitrogen. Yang et al.⁴² stated the relationship between pH and the luminescent species is complicated, but the authors assumed CPF was triprotic and stated that pK_{a2} and pK_{a3} occurred N1' and carboxylic acid, respectively. The authors proposed that in acidic solution CPF produces a tautomerism between ketone and enol-forms. Therefore, according to the authors the tautomerism is what influences the shift of proton of N1 to N1' and carboxylic acid dissociation. However, because Yang et al. does not account for CPF as a tetraprotic acid, there is greater stability at N1' due to the additional hydrogen at N4'.

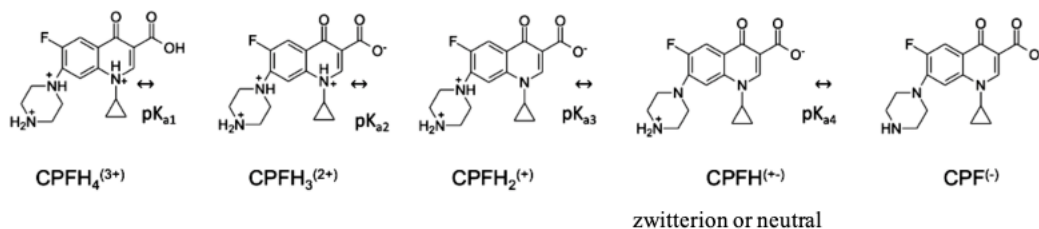


Figure 5.1.1 CPF dissociation and the corresponding species (left to right) with designated fractions α_0 , α_1 , α_2 , α_3 , and α_4 for CPF as a tetraprotic acid.

The chemical structures presented in Figure 5.1.1 were adopted from Salma et al.¹¹ along with the corresponding pK_a values (Table 5.1.1). The order of dissociation presented in Figure 5.1.1 represents that displayed by Qiang et. al. The corresponding mechanism in Figure 5.1.1 was established due to the nature of the corresponding functional groups with their nature and literature acid dissociation constants.

The carboxylic acid and the quinolone (N1) nitrogen pK_a values are 4.20⁷⁹ and 4.92⁸⁰ having similar pK_a values to benzoic acid and quinolone-H⁺, respectively. The determination of pK_{a1} and pK_{a2} are not as important to resolve because, as stated by Doorslaer et al., these values do not impact speciation in conditions near neutral pH where CPFH₄³⁺ and CPFH₃²⁺ do not exist. However, pK_{a3} and pK_{a4} appear to be critical to accurately defining speciation. This is due to the zwitterionic nature of CPFH^{+/-} and CPF⁻ which are the predominate species of CPF present at neutral pH.

The dissociation constant for the first proton (i.e., pK_{a1}) could be either the carboxylic acid or the quinolone nitrogen (N1) depending on CPF's solvent environment.

In theory, if the solvent is acidic (e.g., aqueous HCl), then the proton on the quinolone, N1, would be the first to dissociate because the carboxylic acid would be more stable due to the lower pK_a of the corresponding functional group in the acidic solution. However, if the solvent is water then the polarity of the solvent would influence the proton on the carboxylic acid to dissociate first. Therefore, for the purpose of the experiments conducted, pK_{a1} was associated with the carboxylic acid due to the solvent being water. The two piperazinyl nitrogen atoms, N1' and N4', would be the last to dissociate due to the literature pK_a value for a quinolone ring functional group.⁸¹ This would correspond to pK_{a4} and pK_{a3} when looking at the nitrogen atoms in the structure from left to right.

In Figure 5.1.2, the species distribution is shown as the fractional concentration of the species versus pH. It is interesting to note that two species of CPF, $CPFH_2^+$ and $CPFH^{+-}$ exist at almost equal concentrations near pH 7. Clearly, the assumption of only one species at this pH would be erroneous upon consideration of the binding constants. Most importantly, Figure 5.1.2 shows that the species distribution is very sensitive to the change in pH even at pH 7. However, if only three pK_a values are used for CPF speciation the pH distribution profiles are significantly different (Figure 5.1.3). At pH 7, the diprotic acid, $CPFH_3^{2+}$, (α_1), the monoprotic $CPFH_2^+$ (α_2), and the deprotonated $CPFH^{+-}$ (α_3) fractions are 16, 82, and 2 percent, respectively. All these have a significant impact on the activity of the drug CPF in various biological compartments having different pH values. Consequently, the binding of these species is also pH dependent. Therefore, reliable pK_a measurement is of paramount importance. Also, continuous pH

measurement during binding constant experiments is necessary even in the presence of a buffer.

By knowing the fractional distribution of all forms of CPF (α_{0-4}) the contribution of any particular species towards the observed emission intensity can be calculated at any pH. A precise pH measurement will help determine the fluorescence intensity contribution from each species. Species present at a given pH will contribute to the total fluorescence intensity independently and each species of CPF will have a unique fluorescence efficiency. This can be calculated from the measured emission through a wide pH range. Therefore, it is imperative to understand the total number of dissociating protons and the precise pK_a values. Species concentrations are only determined by the pH and the ionic strength, the error in the binding constants are reflected by these parameters. By measuring the pH and fluorescence intensity simultaneously in the binding equilibria, the error can be minimized.

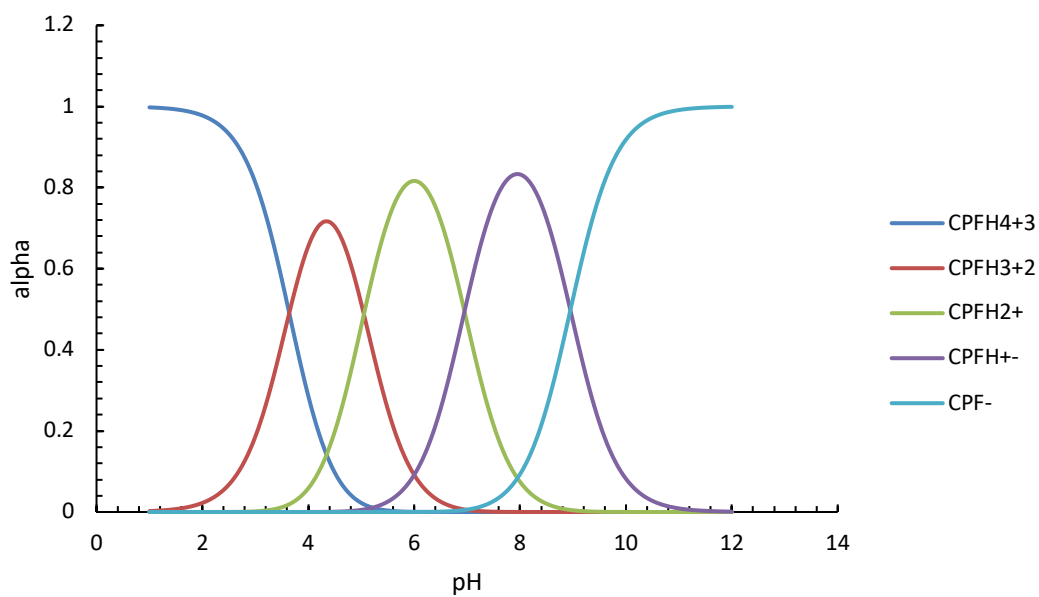


Figure 5.1.2 Fractional distribution (α) of CPF species as a function of pH for a tetraprotic acid. The pK_a values used were 3.64, 5.05, 6.95 and 8.95

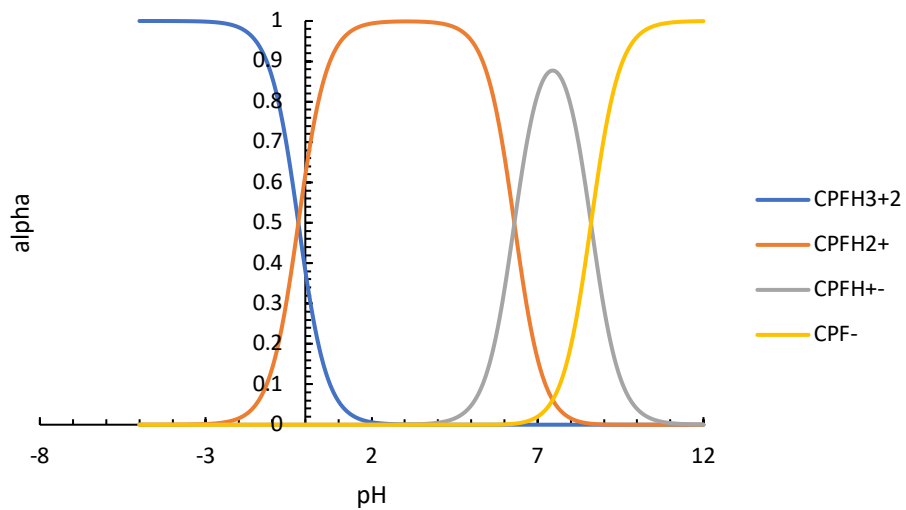


Figure 5.1.3 Distribution of CPF species (α) as a function of pH for a triprotic acid. The pK_a values used were -0.21, 6.30 and 8.61.

5.1.1 *The effect of pH on the fluorescence spectra of CPF species*

The excitation and emission spectra of CPF were measured in the range of pH 1 to 11 at increments of 1 for pH 1-5 and 9-11 as well as increments of 0.5 from pH 6.00 - 8.50 (Figure 5.1.4). In Figure 5.1.4(a), the excitation maximum was determined to be 270 nm. While the fluorescence intensity appeared to have intensity maximums at pH 4.00, 6.00, 7.00 and 8.50, there was no shift in the excitation maximum.

The fluorescence emission intensity increased from pH 1.00-4.00 at $\lambda_{\text{emission}} = 448$ nm (Figure 5.1.4). At pH 5, the fluorescence intensity decreased at $\lambda_{\text{emission}} = 448$ nm. This is indicative of the shift of species CPFH_4^{3+} to CPFH_3^{2+} . At pH 6, the $\lambda_{\text{emission}}$ maximum shifted from 448 nm to 416 nm. This shift indicates a major change in the deprotonation of CPFH_3^{2+} to CPFH_2^+ . The fluorescence intensity maximums appeared at pH 6.00, 7.00 and at pH 8.50 at 416 nm. From pH 9.00-11.00, the fluorescence intensity decreased.

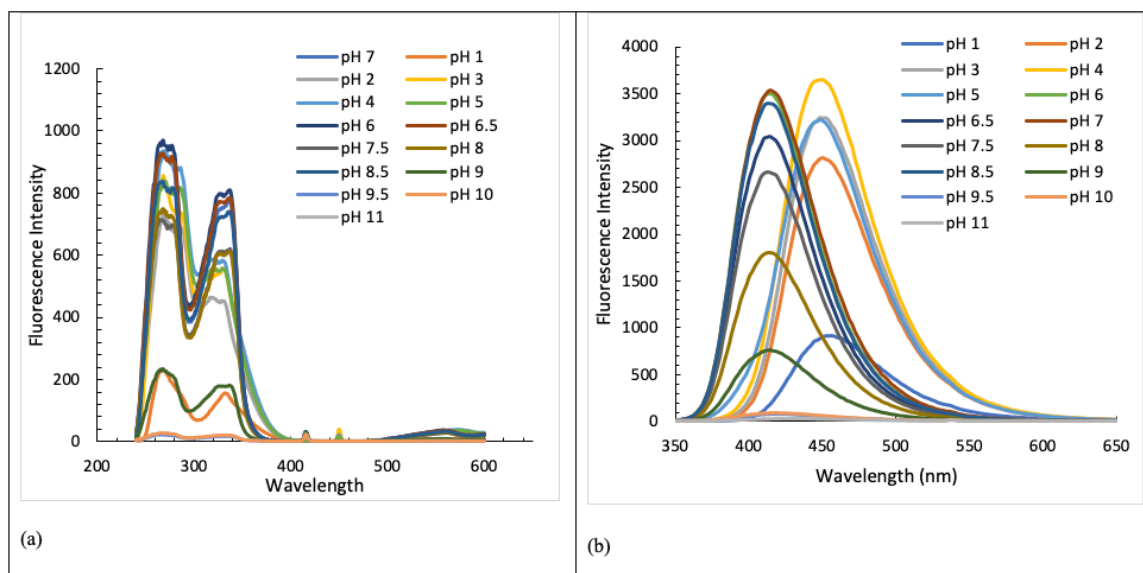


Figure 5.1.4 The excitation (a) and emission (b) spectra of 31.2 μM CPF from pH 1-11 using Shimadzu RF-6000 at 25°C. $\lambda_{\text{excitation}} = 270 \text{ nm}$, excitation slit = 3.0 nm; emission slit = 3.0 nm

The predominant fluorescing CPF species varies depending on the pH. The maximum fluorescence emission also varies with the change of pH. It was experimentally determined that in acidic pH (1.00-5.00) the emission wavelength maximum was 448 nm. In more basic pH solutions (6.00-11.00) the emission wavelength maximum was 416 nm. Therefore, this can influence literature experimental results if the pH is not consistent with the choice of the emission wavelengths.

When fluorescence intensity was plotted against pH at a particular $\lambda_{\text{emission}}$, the maximums represent pK_{a} s (Figure 5.1.5). Therefore, it was determined that $\text{pK}_{\text{a}1}$, $\text{pK}_{\text{a}2}$, $\text{pK}_{\text{a}3}$, and $\text{pK}_{\text{a}4}$ were 4.00, 6.00, 7.00 and 8.50, respectively, at 416 nm, confirming that CPF is tetraprotic. The literature pK_{a} values of 3.64, 5.05, 6.95, and 8.95 (Table 5.1.1, Figure 5.1.2) provided by Salma et. al.¹¹ were used in the model calculations for K_{11} and K_{n1} . This was to ensure consistency in the determined speciation of the upcoming CPF

and pseudophase measurements. While at 448 nm, the pK_{a1} , pK_{a2} , pK_{a3} values were 4.00, 7.00 and 8.50, respectively. It appears at this wavelength, the two species at pH 6.00 and 7.00 were not resolved spectroscopically.

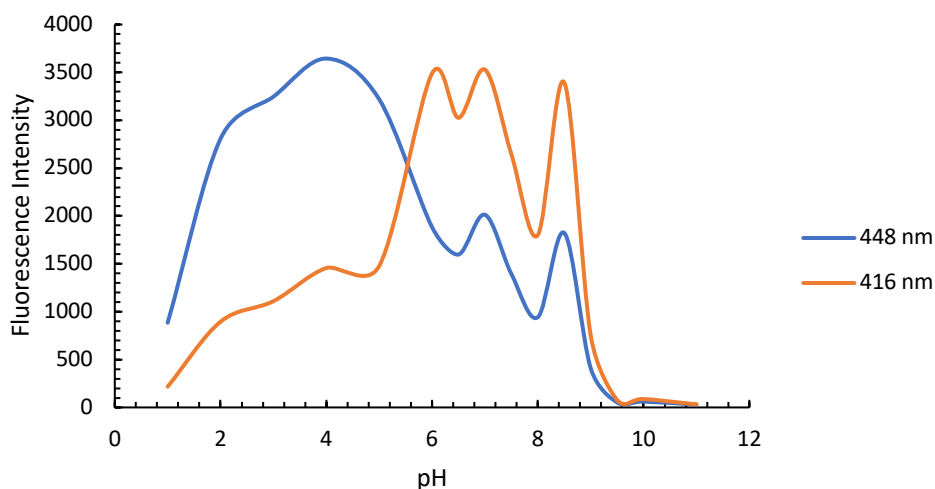


Figure 5.1.5 The experimental fluorescence intensity vs pH of CPF at $\lambda_{\text{emission}}$ of 448 nm and 416 nm. The fluorescence intensity maximums between the two wavelengths correspond to the experimental pK_a values.

5.1.2 Concentration calibration of CPF: Effect of speciation

In order to check for the linearity of CPF calibration, the CFCLS was used to measure pH and fluorescence intensity data simultaneously without removing the cuvette from the spectrometer to minimize systematic error. Figure 5.1.6 shows the concentration calibration of CPF where the total fluorescence intensity was recorded. Since the pH was measured for each data point, the fluorescence intensity for the two predominant species present in the respective pH ranges was accounted for as CPFH_2^+ and CPFH^{+-} concentrations in Figure 5.1.6 from pH 7.60 through 8.00. For the calculation of

fluorescence intensity and speciation, CPF was considered to be a tetraprotic acid. To calculate the fluorescence intensity for the species of tetraprotic CPF present in solution the observed fluorescence intensity was multiplied by the fraction obtained from the distribution diagram at the measured pH (Figure 5.1.2). Clearly, the emission sensitivity was different for each species and can, therefore, affect the overall binding constants determined between CPF and various surfactants or proteins.

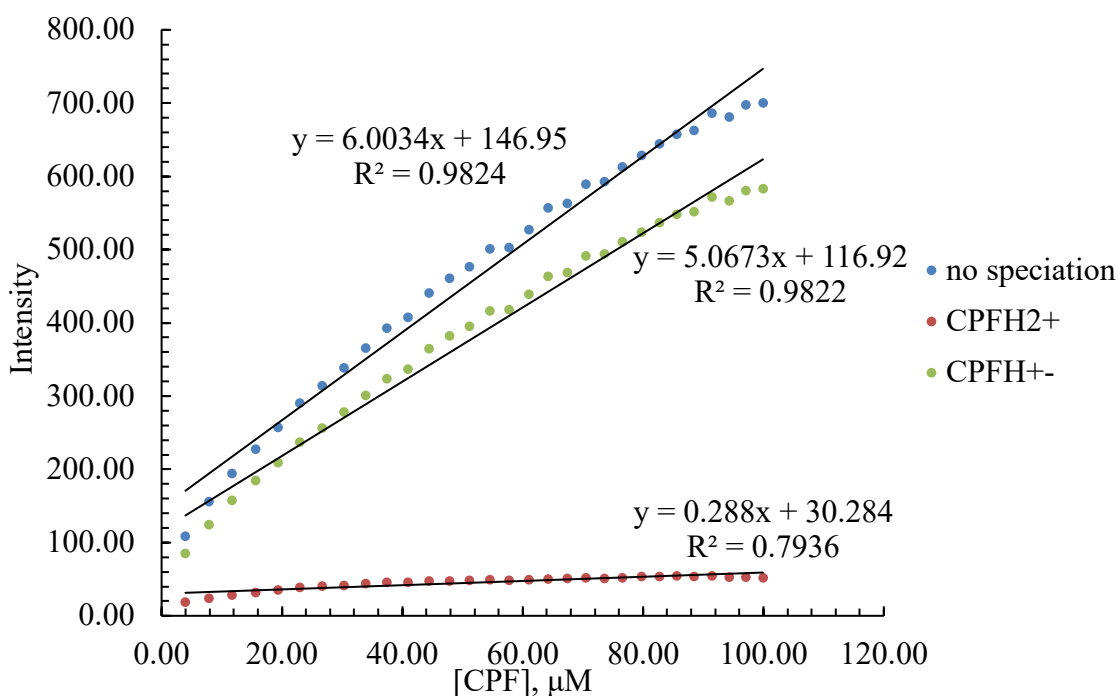


Figure 5.1.6 Calibration of CPF in water. The measured fluorescence intensity is shown in blue. The tetraprotic CPF distribution curve (Figure 5.1.2) was used to calculate the contribution of the species to the measured fluorescence e.g., CPFH₂⁺ (alpha-2) (grey) and CPFH⁺⁻ (alpha-3) (orange).

DETERMINATION OF CIPROFLOXACIN (CPF) AND SODIUM DODECYL SULFATE (SDS) PSEUDOPHASE INTERACTIONS

6.1 The determination of CPF and SDS pseudophase interactions

Anionic surfactant compounds such as SDS share many of the same properties as phospholipids in cell membranes,^{41,48} making SDS a biologically relevant pseudophase at concentrations above the cac. Because CPF and SDS binding constants have been previously studied, it provides an opportunity to compare the present model with published values, as well as analyze the difference in binding constants depending on the protonation of CPF is considered to be. Binding constants between these compounds are listed in Table 6.1.1. The binding constants range across approximately nine orders of magnitude, due in part, to the nature of the experimental conditions and the variety of models used to generate the constants. With CPF increasing its predominance in the environment⁸², it will also aid in developing methods in removing it and affecting other biological systems.

Table 6.1.1 The literature binding constants of SDS and SLS with CPF using various experimental methods and parameters.

Solute	Compound	K_{11} , (M^{-1})	K_{n1}/n , (M^{-1})	n	Temp (°C)	pH	Method	$\lambda_{ex}/\lambda_{em}$ (nm)	Ex/em slits (nm)
CPF	SDS	57.5 ⁽⁴¹⁾	-	N/A ^a	N/A	N/A (triprotic)	Fluorescence	270/445	2.5/30
		19.048	-			0.5-1.0 (triprotic)	UV-Vis and FTIR	200/400	N/A
		-	6.08 ⁽⁴⁸⁾			0.5-1 (triprotic)			
		26.2	-			9.2 (triprotic)			

		-	8.51			9.2 (triprotic)			
		-	0.77 ⁽⁵⁹⁾		25	N/A (triprotic)	UV-Vis, NMR, Conductivity and Isothermal titration calorimetry	190/400	
		2660 ⁽⁴²⁾	-		N/A	N/A (triprotic)	Fluorescence	290/440	
	SLS	-	154			3.6 (triprotic)		N/A	

- a. N/A = not applicable
- b. n = binding affinity
- c. K_{SV}

From Table 6.1.1, it can be observed that the literature varies in terms of considering the protonation of CPF, along with the experimental conditions and the equations to calculate the binding constants.

CPF was studied where SDS, and sodium lauryl sulfonate (SLS) were the solutes added. It can be observed that all of the studies in Table 6.1.1 considered CPF to be a triprotic acid, which overall minimizes the binding that occurs with the pseudophase compounds. The experimental conditions varied with the use of fluorescence spectroscopy, UV-vis, FTIR and NMR.

Khan et. al.⁴¹ studied the binding between CPF and SDS using fluorescence. When determining the binding with fluorescence spectroscopy, a variation of the Stern-Volmer (SV) equation was used, however, the authors accounted for the fluorescence efficiency ratio when CPF was bound with SDS and free in solution. They were able to determine the binding constant in the preaggregate phase with a value of 57.5 M^{-1} .

However, in their experimental, CPF was dissolved in HCl, in which case Cl^- interfered with the total fluorescence intensity measured because of the known Cl^- quenching.

When Khan et. al.⁴⁸ analyzed the CPF and SDS interactions using UV-vis and FTIR, the analysis was more critical as they account for the effect of pH of CPF on the binding with SDS. They used Equation 1.3.27 and accounted for the critical micelle concentration. Using UV-vis and FTIR, the authors were able to determine the binding in the postaggregate phase of SDS.

Banipal et. al.⁵⁹ specifically focused on the effect of NaCl on the binding of CPF and SDS using Equation 1.3.27. However, the authors did not account for the speciation of CPF or the effect of pH which also influences the binding with SDS.

Yang et. al.⁴² went in depth to understand the effects of binding under different conditions such as pH and surfactant. The authors were only able to determine the preaggregate binding between CPF and SDS, but determined the postaggregate binding with SLS. The binding in the preaggregate phase appeared to be the greatest compared to the literature values obtained in Table 6.1.1. Yang et. al.⁴² used the SV equation to determine the binding constants of CPF with SDS and SLS. However, it was explained that while the SV equation is widely used to determine binding constants, the value itself is a rate constant which does not accurately portray the binding between CPF and the compounds studied.

All of the values obtained in Table 6.1.1 displayed the variation in binding depending on the conditions of the experimental and data analysis.

6.1.1 CPF and SDS monomer and pseudophase interactions in the presence of phosphate buffer

The Shimadzu RF- 6000 was used to observe the effects of SDS on the fluorescence of CPF. The corresponding pH values were used for these experiments in order to observe the effects of acidic, neutral and basic environments. CPF was considered tetraprotic in the analysis.

6.1.1.1 CPF and SDS monomer and pseudophase interactions at pH 7.00

The fluorescence emission spectrum of CPF during the addition of SDS is shown in Figure 6.1.1. As the concentration of SDS increased, a fluorescence enhancement (FE) effect was observed. Fluorescence effects can be quenching, as was found with the anthracene and TPGS-750M additions or enhancing as was found for CPF and SDS.

Fluorescence enhancement is defined as the amplification of the fluorescence signal of the fluorophore with the addition of a binding compound. This technique has been used to enhance fluorophore signals with the addition of compounds like noble metal nanoparticles⁸³.

Emission spectra were taken for CPF as the concentration of SDS increased. In Figure 6.1.1 it was determined that the emission maximum was 448 nm.

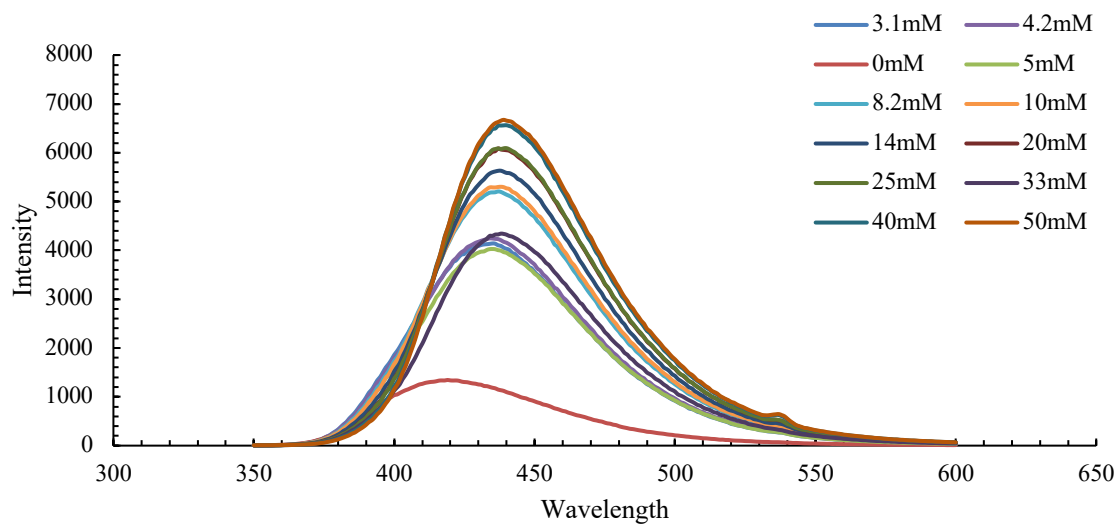


Figure 6.1.1 Emission spectrum of SDS additions into 31.2 μM of CPF at pH 7.00. The excitation wavelength = 270 nm and the excitation and emission slits were 3.0 nm.

From the emission maximum, the fluorescence intensity at 448 nm was plotted against the concentration of SDS added in Figure 6.1.2.

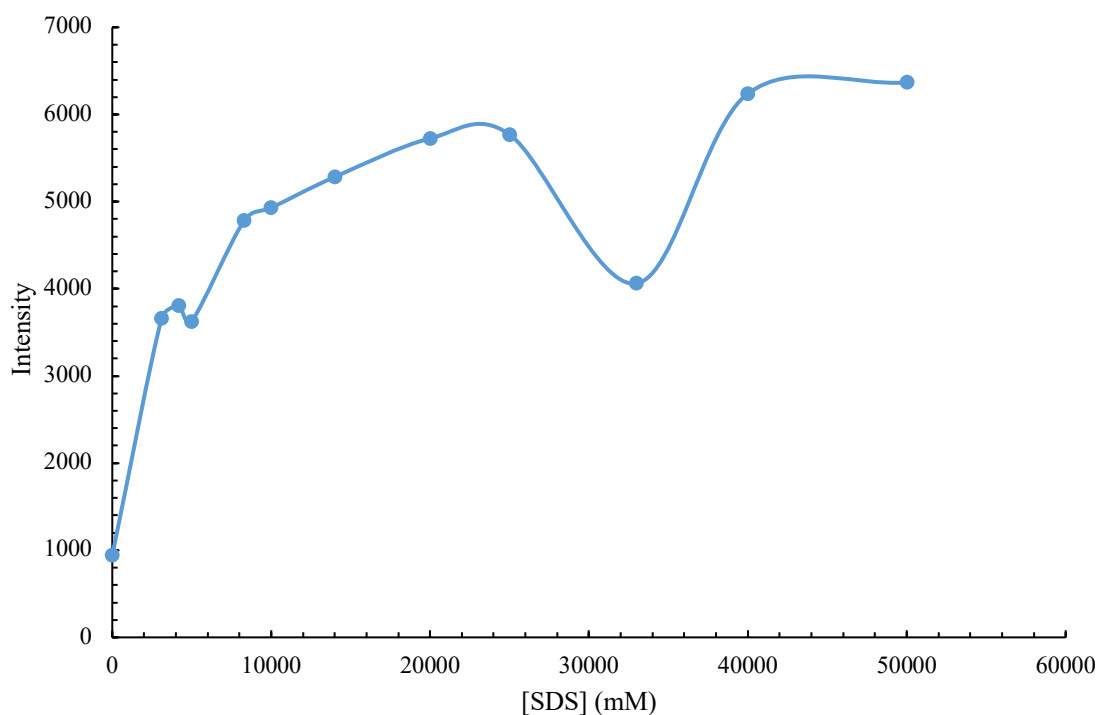


Figure 6.1.2 The fluorescence intensity versus concentration of SDS added to 31.2 μM CPF at pH 7.00 and $\lambda_{\text{emission}} = 448 \text{ nm}$

Another perspective of FE is shown in Figure 6.1.2 at the emission maximum of 448 nm. It was observed that the plot shows regions of FE and FQ, and the overall interactions do not display a linear relationship. To better describe the binding interactions between CPF and SDS, the predominate speciation was determined using Table 6.1.2.

Table 6.1.2 The fraction of CPF speciation present in solution at pH 7.00

	CPFH_4^{+3}	CPFH_3^{+2}	CPFH_2^{+}	CPFH^{+-}	CPF^{-}
Fraction	2.28×10^{-6}	0.00523	0.466	0.522	0.00587

It can be observed from Table 6.1.2 that the predominant species of CPF present at pH 7.00 were CPFH^{+-} and CPFH_2^+ .

To determine the K_{11} and K_{n1}/n binding constants, the fluorescence efficiencies of k_C , k_{11} and k_{n1} were determined by dividing the fluorescence intensity by the concentration of CPF when no SDS was added, at the cac of SDS and after the cac. The fluorescence efficiencies are expressed in Table 6.1.3.

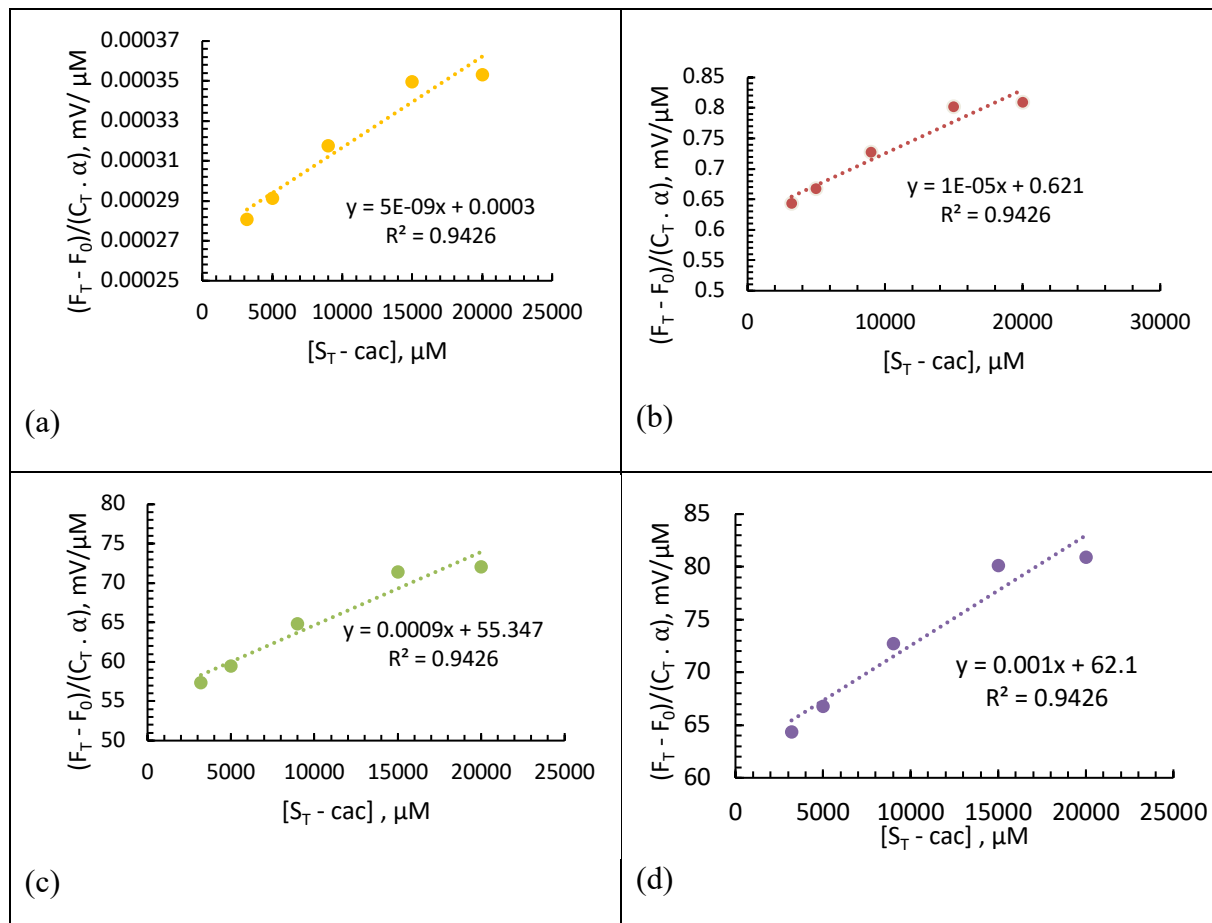
Table 6.1.3 The fluorescence efficiency of free CPF, CPF-monomer (CS) and CPF-pseudophase (CS_n) complexes at pH 7.00 and 25°C.

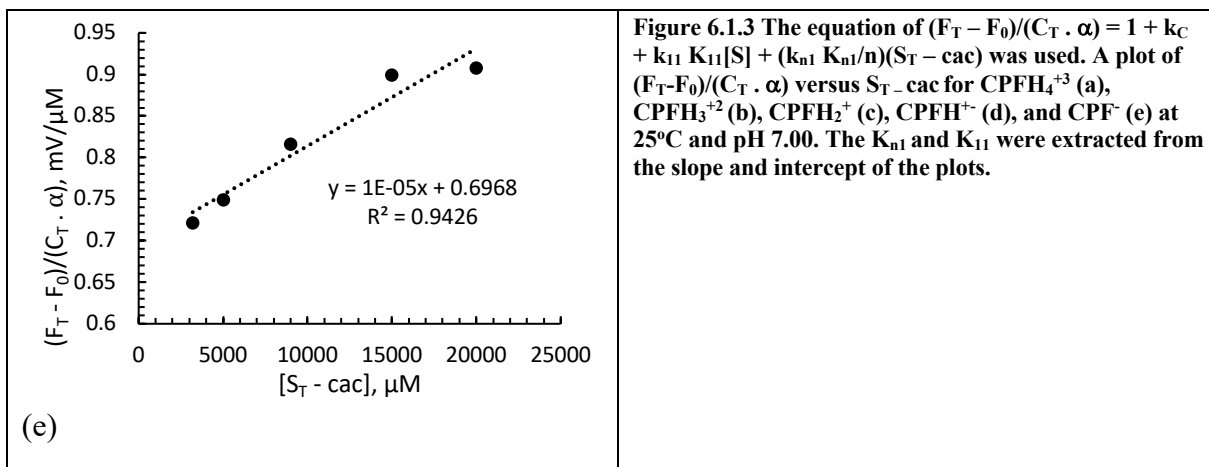
	Fluorescence efficiency (mV/μM)	Fluorescence intensity (mV)	[CPF] (μM)
k_C	30.2	941.8	31.2
k_{11}	116.2	3627	
k_{n1}	172.9	5395	

Notes: k_C , k_{11} and k_{n1} were determined by dividing the fluorescence intensity by the concentration of CPF.

From Table 6.1.3, it can be observed that the fluorescence efficiency increased as the concentration of SDS increased. It was observed the fluorescence was amplified once CPF forms a preaggregate and postaggregate complex with SDS pseudophase compared to unbound CPF. The fluorescence efficiencies obtained were multiplied by α to account for each species of CPF.

Figure 6.1.3 (a) - Figure 6.1.3 (e) from the 12 fluorescence intensities obtained, five were plotted. The values obtained when $S_T - \text{cac}$ was greater than zero were used in order to determine the K_{11} and K_{n1}/n binding constants for each species of CPF.





In Figure 6.1.3 (a), it can be observed that the R^2 value is 0.9426, The positive slope is indicative of postaggregate binding of $CPFH_4^{+3}$ with SDS.

The R^2 value of Figure 6.1.3 (b) is the same as the value in Figure 6.1.3 (a). The positive slope observed corresponds to binding in the postaggregate phase.

The slope (Figure 6.1.3 (c)) is higher for $CPFH_2^{+}$ compared to the other species of CPF. This is due to this fraction of CPF being higher at pH 7.00 compared to $CPFH_4^{+3}$ and $CPFH_3^{+2}$. The R^2 value is the same as the values in Figure 6.1.3 (a) and Figure 6.1.3 (b).

In Figure 6.1.3 (d) the binding in the postaggregate phase is the greatest compared to $CPFH_4^{+3}$, $CPFH_3^{+2}$ and $CPFH_2^{+}$. It is the most abundant species in solution. CPF^- appears to have less binding in the postaggregate phase compared to $CPFH^{+-}$. The R^2 values matches the values obtained in Figure 6.1.3 (a) - Figure 6.1.3 (d) . A summary of the determined binding constants in the preaggregate and postaggregate phase of CPF with SDS is shown in Table 6.1.4.

Table 6.1.4 Summary of preaggregate and postaggregate binding constants for CPF and SDS complexation extracted from the slope and intercept of Figure 6.1.3 (a-e) at pH 7.00. The literature aggregation number of 60 was used to determine K_{n1} .

	CPFH_4^{+3}	CPFH_3^{+2}	CPFH_2^{+}	CPFH^{+-}	CPF^{-}
Slope (μM^{-1})	$(4.6 \pm 0.6) \times 10^{-9}$	$(1.0 \pm 0.1) \times 10^{-5}$	$(9.3 \pm 1) \times 10^{-4}$	$(1.0 \pm 0.1) \times 10^{-3}$	$(1.2 \pm 0.1) \times 10^{-5}$
Intercept (μM^{-1})	$(2.7 \pm 0.08) \times 10^{-4}$	0.62 ± 0.02	55 ± 2	62 ± 2	0.70 ± 0.02
R²	0.9426	0.9426	0.9426	0.9426	0.9426
K₁₁ (M^{-1})	0*	0*	43 ± 49	55 ± 49	0*
K_{n1}/n (M^{-1})	$(2.6 \pm 0.4) \times 10^{-5}$	0.06 ± 0.009	5.4 ± 0.8	6.04 ± 0.9	0.07 ± 0.009
K_{n1} (M^{-1})	$(1.6 \pm 0.2) \times 10^{-3}$	3.6 ± 0.5	323 ± 46	362 ± 52	4.1 ± 0.6

Notes: The equation $(F_T - F_0)/(C_T \cdot \alpha) = 1 + k_C + k_{11} K_{11}[S] + (k_{n1} K_{n1}/n)(S_T - \text{cac})$ was used to extract the K_{11} and K_{n1} binding constants from the intercept and slope of Figure 6.1.4 (a) – (e). * K_{11} was negative for CPFH_4^{+3} (-52), CPFH_3^{+2} (-50), and CPF^{-} (-51).

Binding was observed in the preaggregate phase with CPFH^{+-} followed by CPFH_2 . These two species are the most abundant in solution. However the error is greater in comparison to the K_{n1} binding constants.

The K_{n1} binding constants were determined with the literature aggregation number of 60. All species of CPF appeared to bind with SDS in the postaggregate phase. It was observed that the greatest binding occurred with the most abundant CPF species, CPFH^{+-} followed by CPFH_2^{+} . Therefore, these species are the majority that reside within the hydrophobic core of the pseudophase aggregate.

6.1.1.2 CPF and SDS monomer and pseudophase interactions at pH 8.33

Similarly to section 6.1.1, the next set of experiments were at pH 8.33. Figure 6.1.5 is the emission spectrum of CPF as the concentration of SDS increased. The emission maximum was observed to be 448 nm, same as what was observed at pH 7.00.

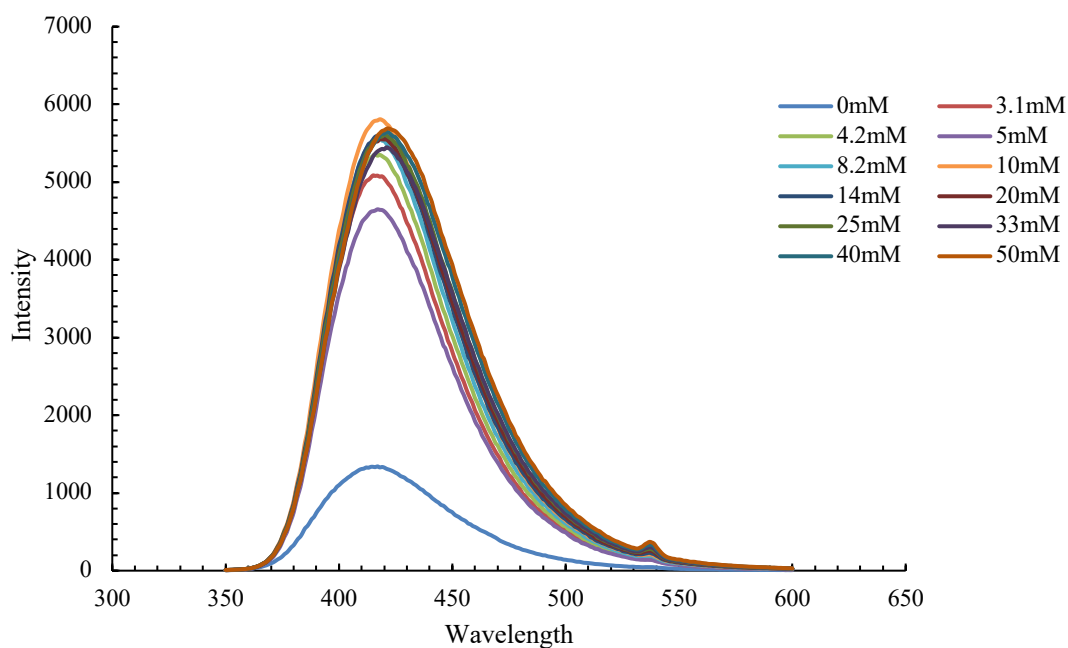


Figure 6.1.5 Emission spectrum of SDS additions into 31.2 μ M of CPF at pH 8.33. The excitation and emission slits were 3.0 nm.

It was observed there was an overall FE as the concentration of SDS increased. Figure 6.1.6 was a plot of fluorescence intensity versus concentration of SDS added at the emission maximum of 448 nm. It displayed an overall FE and the fluorescence intensity became stagnant after 10 mM of SDS was added.

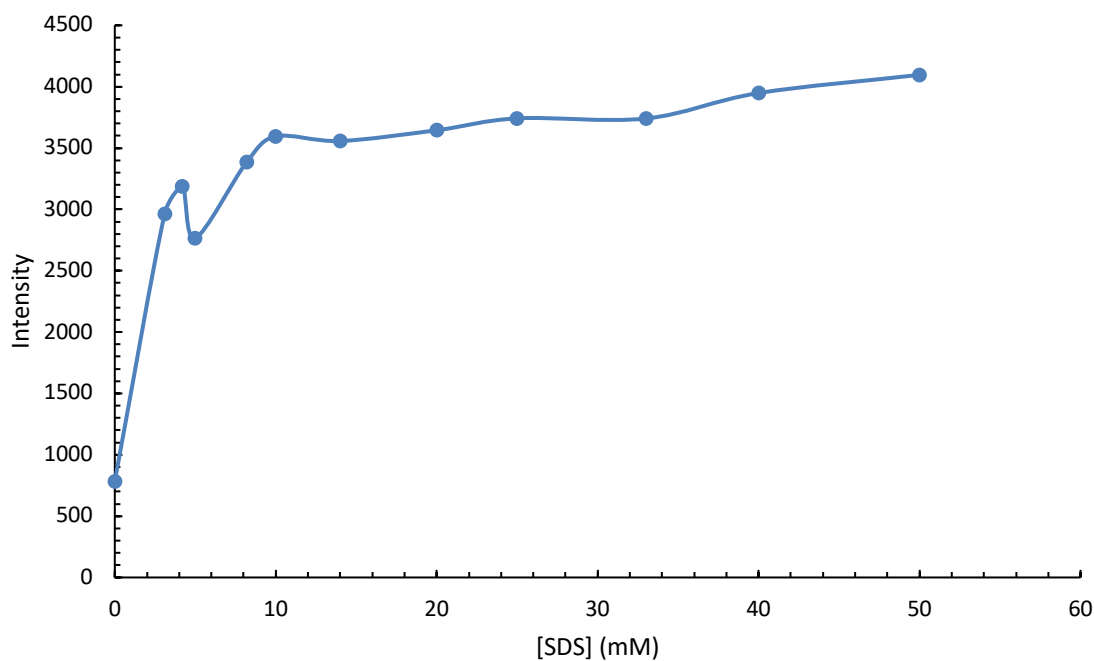


Figure 6.1.6 The fluorescence intensity versus concentration of SDS added to 31.2 μ M CPF at pH 8.33 and $\lambda_{\text{emission}} = 448 \text{ nm}$

To account for the speciation of CPF at the corresponding pH, Table 6.1.5 below accounts for the fractions present within solution.

Table 6.1.5 The fraction of CPF speciation present in solution at pH 8.33

	CPFH_4^{+3}	CPFH_3^{+2}	CPFH_2^{+}	CPFH^{+-}	CPF^-
Fraction	4.33×10^{-10}	1.98×10^{-5}	0.0352	0.788	0.176

It can be observed that the greatest speciations of CPF present in solution were zwitterionic CPFH^{+-} and CPF^- respectively. The fluorescence efficiencies of k_C , k_{11} and

k_{n1} were determined by dividing the fluorescence intensity by the concentration of CPF when no SDS was added, at the cac and after the cac. The values used are expressed in Table 6.1.6.

Table 6.1.6 The fluorescence efficiency of free CPF, CPF-monomer (CS) and CPF-pseudophase (CS_n) complexes at pH 8.33 and 25°C

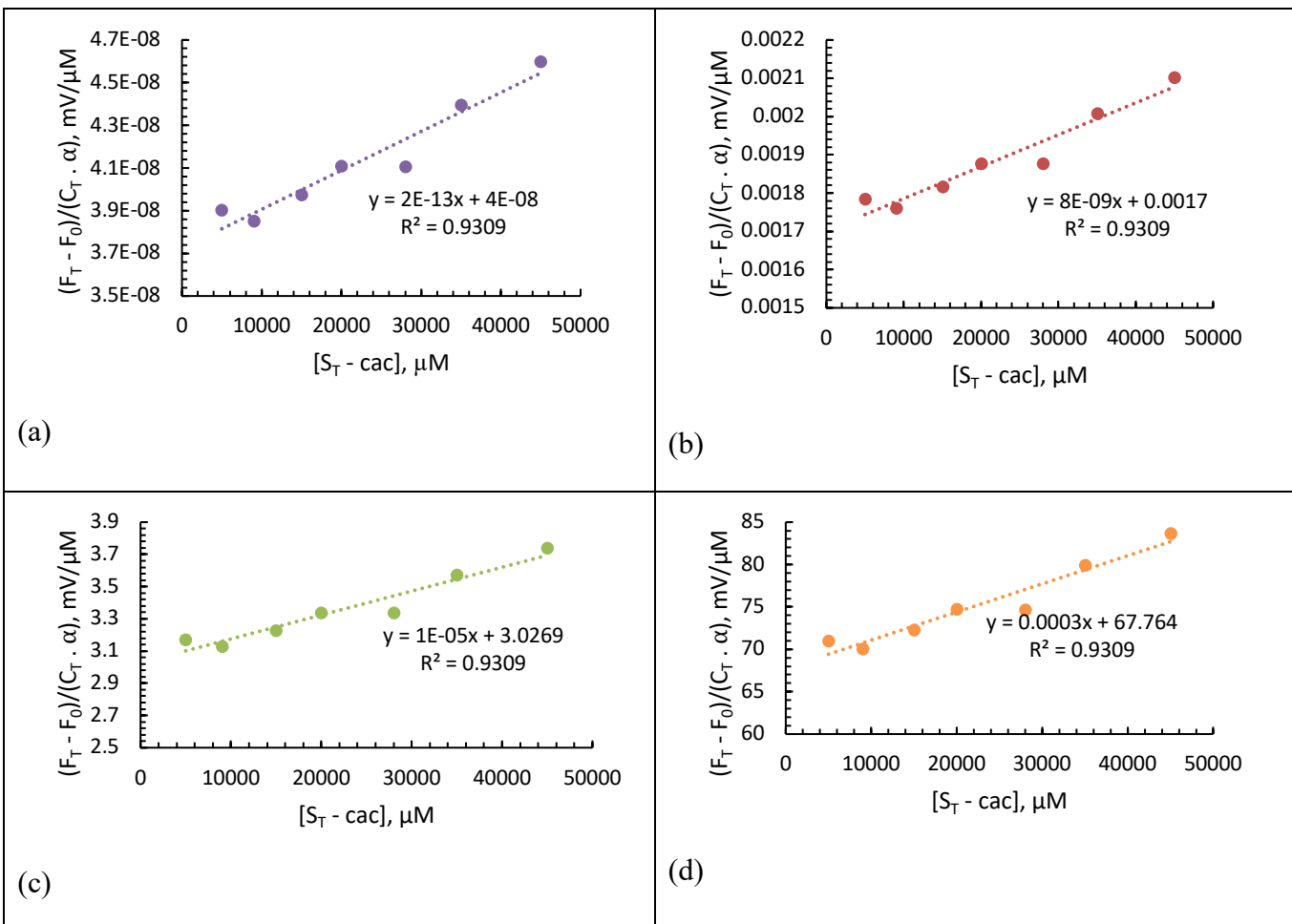
	Fluorescence efficiency (mV/μM)	Fluorescence intensity (mV)	[CPF] (μM)
k_C	25.1	783.8	31.2
k_{11}	88.7	2766	
k_{n1}	119	3714	

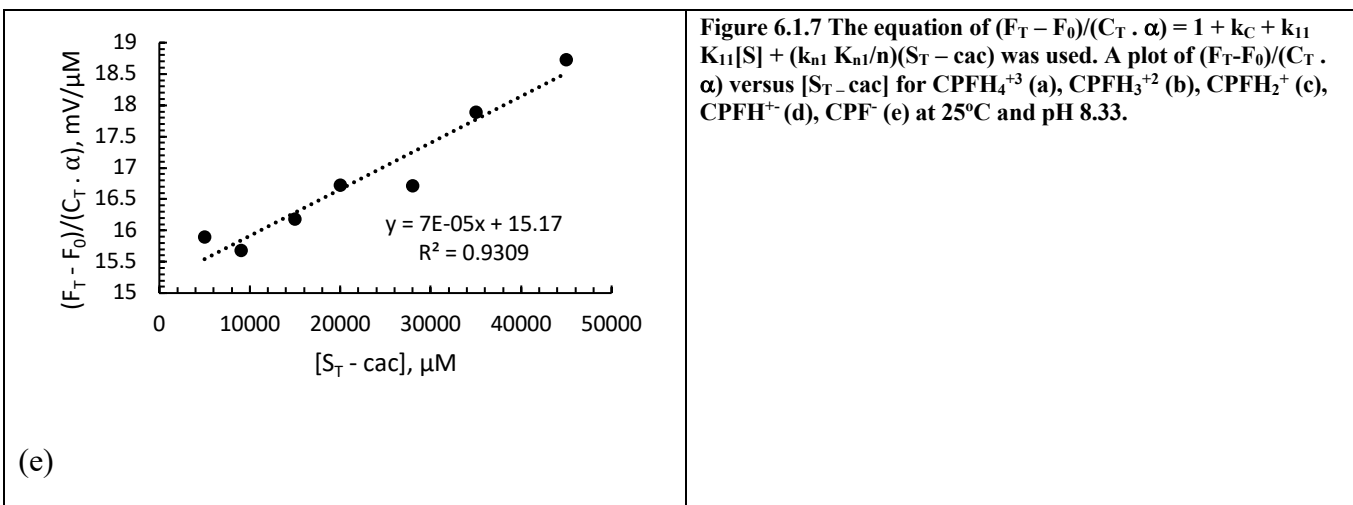
Notes: k_C , k_{11} and k_{n1} were determined by dividing the fluorescence intensity by the concentration of CPF.

It can be observed that at pH 8.33 the fluorescence efficiency is less than the values determined at pH 7.00. The fluorescence efficiencies obtained at pH 7.00 were about 1.2 times greater than the values in Table 6.1.6.

However, the trend observed at pH 7.00 is also observed at pH 8.33 where as the concentration of SDS increased the overall fluorescence efficiency of CPF also increased. Since the fluorescence efficiency of CS_n is the greatest, this confirms the observed FE interactions within the SDS pseudophase compound. In order to determine the binding

constants K_{11} and K_{n1}/n , plots $F_T - F_0 / C_T \cdot \alpha$ versus $S_T - \text{cac}$ were created for all five species of CPF. This is shown in Figure 6.1.7 (a) - Figure 6.1.7 (e).





Compared to the data obtained for $CPFH_4^{+3}$ at pH 7.00, it can be observed that the slope is significantly smaller at pH 8.33. The R^2 was determined to be 0.9309. The slope of Figure 6.1.7 (b) is greater than the slope for $CPFH_4^{+3}$. The R^2 value is the same in Figure 6.1.7 (a), this could be due to the minimal change in the pH. The positive slope is indicative of binding in the postaggregate phase.

In Figure 6.1.7 (c), it can be observed that the binding in the postaggregate is greater compared to the data in Figure 6.1.7 (a) - Figure 6.1.7 (b).

$CPFH^{+-}$ is the most predominant species at the corresponding pH. The slope is greater compared to the more positively charged species $CPFH_4^{+3}$, $CPFH_3^{+2}$ and $CPFH_2^{+}$.

CPF^- is the second most abundant species of CPF present within solution at pH 8.33. The positive slope is indicative of binding in the postaggregate phase of SDS. The data in Figure 6.1.7 (a) - Figure 6.1.7 (e) was used to calculate the K_{11} and K_{n1}/n binding constants. The results obtained are shown in Table 6.1.7.

Table 6.1.7 Summary of preaggregate and postaggregate binding constants for CPF and SDS complexation extracted from the slope and intercept of Figure 6.1.7 (a-e) at pH 8.33. The literature aggregation number of 60 was used to determine K_{n1}

	CPFH₄⁺³	CPFH₃⁺²	CPFH₂⁺	CPFH⁺⁻	CPF⁻
slope (μM^{-1})	$(1.8 \pm 0.2) \times 10^{-13}$	$(8.3 \pm 1) \times 10^{-9}$	$(1.5 \pm 0.2) \times 10^{-5}$	$(3.3 \pm 0.4) \times 10^{-4}$	$(7.4 \pm 0.9) \times 10^{-5}$
intercept (μM^{-1})	$(3.7 \pm 0.05) \times 10^{-8}$	$(1.7 \pm 0.02) \times 10^{-3}$	3.0 ± 0.05	68 ± 1	15 ± 0.2
R²	0.9309	0.9309	0.9309	0.9309	0.9309
K₁₁ (M⁻¹)	0*	0*	0*	96 ± 54	0*
K_{n1}/n (M⁻¹)	$(1.5 \pm 0.2) \times 10^{-9}$	$(7.0 \pm 0.8) \times 10^{-5}$	0.12 ± 0.02	2.8 ± 0.3	0.62 ± 0.08
K_{n1} (M⁻¹)	$(9.2 \pm 1) \times 10^{-8}$	$(4.2 \pm 0.5) \times 10^{-3}$	7.5 ± 0.9	167 ± 20	37 ± 5

Notes: The equation $(F_T - F_0)/(C_T \cdot \alpha) = 1 + k_C + k_{11} K_{11}[S] + (k_{n1} K_{n1}/n)(S_T - \text{cac})$ was used to extract the K_{11} and K_{n1} binding constants from the intercept and slope of Figure 6.1.7 (a-e). * K_{11} binding was negative for CPFH₄⁺³ (-57), CPFH₃⁺² (-57), CPFH₂⁺ (-50) and CPF⁻ (-22).

At pH 8.33, CPFH⁺⁻ exhibits the greatest binding in the postaggregate phase.

Interestingly, while it is more abundant at the corresponding pH, the binding is less in

comparison to pH 7.00 with K_{n1} being $167 \pm 20 \text{ M}^{-1}$ and $362 \pm 52 \text{ M}^{-1}$ respectively. It is

also the only species to exhibit binding in the preaggregate phase. However, the K_{n1}

increased for CPF⁻ as its fraction in solution increased as the pH increased. K_{n1} went from

4.1 ± 0.6 at pH 7.00 to $37 \pm 5 \text{ M}^{-1}$ at pH 8.33. However, the binding is still weaker in

comparison to the binding that occurred with CPFH^{+-} . With SDS being an overall anionic compound, more repulsions would be experienced with CPF^- in comparison to CPFH^{+-} . The change in pH is indicative of the effect pH has on the binding between CPF and SDS.

6.1.1.3 CPF and SDS monomer and pseudophase interactions at pH 4.00

The final experiments conducted with the Shimadzu RF-6000 were the SDS additions with CPF at pH 4.00. Figure 6.1.8 accounts for the emission spectrum from 350 nm – 600 nm as the concentration of SDS added increased.

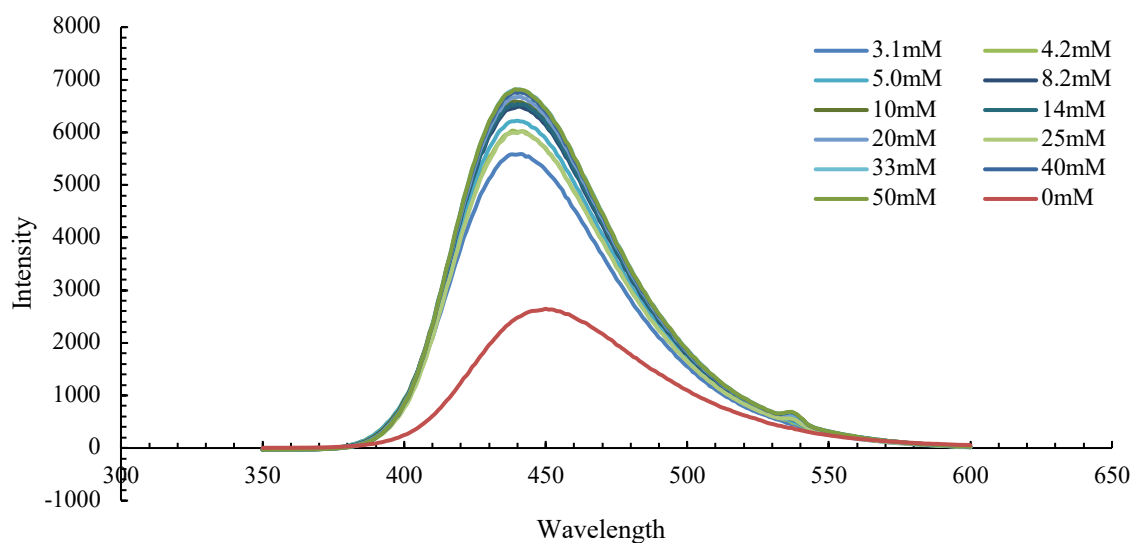


Figure 6.1.8 Emission spectrum of SDS additions into 31.2 μM of CPF at pH 4.00. The excitation and emission slits were 3.0 nm.

To observe the overall change in fluorescence intensity versus the concentration of SDS added, Figure 6.1.9 was plotted at the emission maximum of 448 nm.

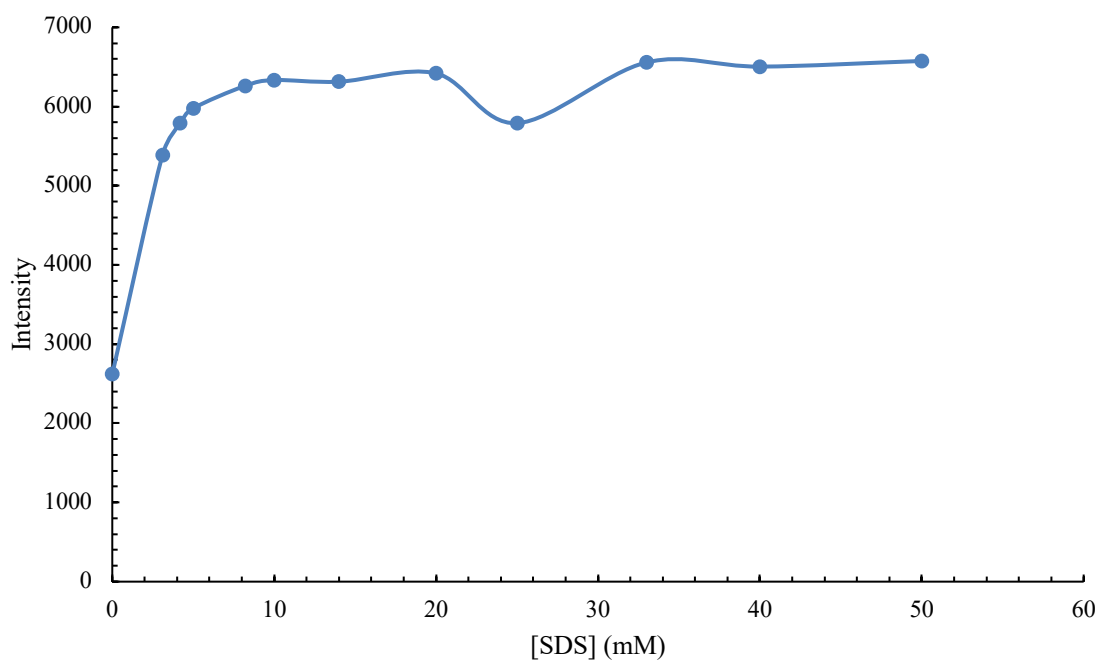


Figure 6.1.9 Fluorescence intensity versus concentration of SDS added to CPF at pH 4.00 and $\lambda_{\text{emission}} = 448 \text{ nm}$

It was observed that as the concentration of SDS increased in solution, the overall fluorescence intensity increased and reached a plateau after 10 mM of SDS was added.

The specific speciation of CPF present within the solution can be observed in Table 6.1.8.

Table 6.1.8 The fraction of CPF speciation present in solution at pH 4.00

	CPFH_4^{+3}	CPFH_3^{+2}	CPFH_2^{+}	CPFH^{+-}	CPF^{-}
Fraction	0.286	0.655	0.0584	6.55×10^{-5}	7.36×10^{-10}

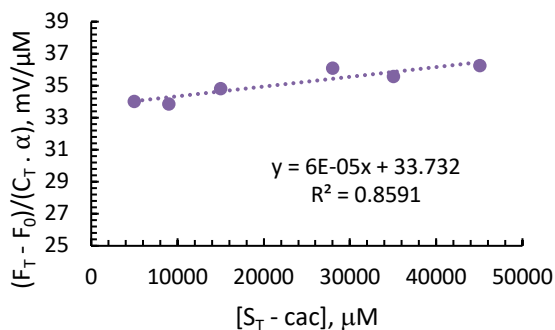
From Table 6.1.8, it can be determined that the most abundant species of CPF within solution was CPFH_3^{+2} and CPFH_2^+ respectively. The fluorescence efficiencies of k_C , k_{11} , and k_{n1} were calculated and expressed in Table 6.1.9.

Table 6.1.9 The fluorescence efficiency of free CPF, CPF-monomer (CS) and CPF-pseudophase (CS_n) complexes at pH 4.00 and 25°C

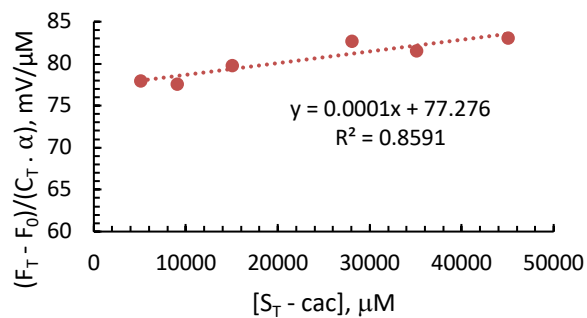
	Fluorescence efficiency (mV/μM)	Fluorescence intensity (mV)	[CPF] (μM)
k_C	84.0	2620	31.2
k_{11}	191.6	5977	
k_{n1}	203.3	6344	

Notes: k_C , k_{11} and k_{n1} were determined by dividing the fluorescence intensity by the concentration of CPF.

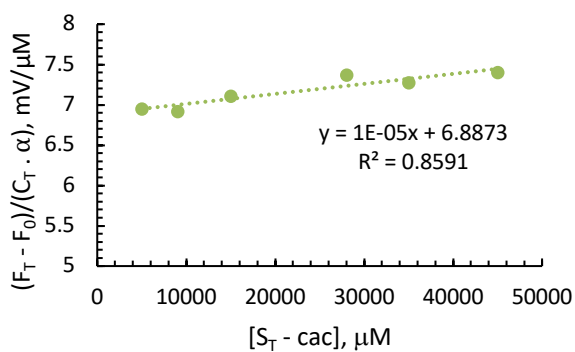
In Table 6.1.9, the greatest fluorescence efficiencies of CPF were at pH 4.00. It can be determined that the unbound CPFH_3^{+2} and CPFH_4^{+3} provide the greatest fluorescence emission compared to other species of CPF in solution as they are the most predominant in solution. This is shown in Table 6.1.8. In order to determine the binding constants K_{11} and K_{n1}/n , Error! Reference source not found. (a) - Error! Reference source not found. (e) were created and plotted below.



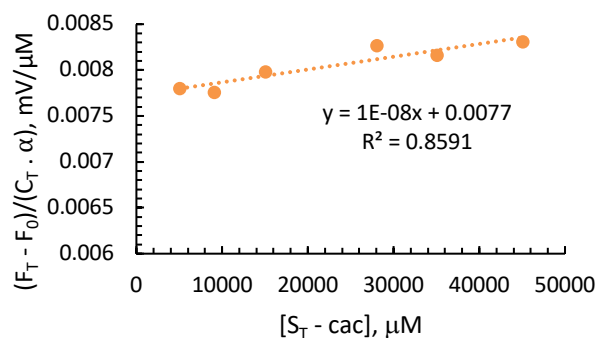
(a)



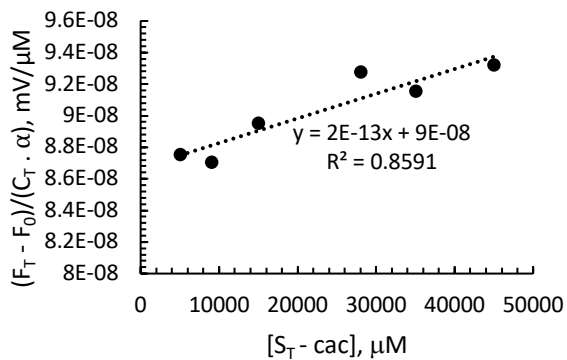
(b)



(c)



(d)



(e)

Figure 6.1.10 The equation of $(F_T - F_0)/(C_T \cdot \alpha) = 1 + k_C + k_{11} K_{11}[S] + (k_{n1} K_{n1}/n)(S_T - \text{cac})$ was used. Aplot of $(F_T - F_0)/(C_T \cdot \alpha)$ versus $S_T - \text{cac}$ for CPFH_4^{+3} (a), CPFH_3^{+2} (b), CPFH_2^+ (c), CPFH^+ (d) and CPF^- at 25°C and pH 4.00.

CPFH₄⁺³ is the second highest species of CPF in solution. The data in Figure 6.1.10 (a) shows binding in the postaggregate phase of SDS. CPFH₃⁺² is the most abundant in solution. The slope in Figure 6.1.10 (b) is greater compared to the slope in Figure 6.1.10 (a).

In Figure 6.1.10 (c), the positive slope is associated with binding in the postaggregate phase of SDS. The R² values matches the values in Figure 6.1.10 (a) and Figure 6.1.10 (b).

The slope is lower in Figure 6.1.10 (d) compared to Figure 6.1.10 (a) - Figure 6.1.10 (c) because of CPFH⁺⁻ being one of the least predominant species in solution at pH 4.00.

CPF⁻ is the least abundant species in solution. Figure 6.1.10 (e) displays positive binding in the postaggregate phase based on the positive slope. The slope is the smallest compared to the other species of CPF. The binding constants obtained from Figure 6.1.10 (a) through Figure 6.1.10 (e) are expressed in Table 6.1.10.

Table 6.1.10 Summary of preaggregate and postaggregate binding constants for CPF and SDS complexation extracted from the slope and intercept of Figure 6.1.10 (a-e) at pH 4.00. The literature aggregation number of 60 was used to determine K_{n1}.

	CPFH ₄ ⁺³	CPFH ₃ ⁺²	CPFH ₂ ⁺	CPFH ⁺⁻	CPF ⁻
Slope (μM⁻¹)	(6.08 ± 1) x 10 ⁻⁵	(1.4 ± 0.3) x 10 ⁻⁴	(1.2 ± 0.3) x 10 ⁻⁵	(1.4 ± 0.3) x 10 ⁻⁸	(1.6 ± 0.3) x 10 ⁻¹³
Intercept (μM⁻¹)	34 ± 0.3	77 ± 0.8	6.9 ± 0.07	(7.7 ± 0.08) x 10 ⁻³	(8.7 ± 0.09) x 10 ⁻⁸
R²	0.8591	0.8591	0.8591	0.8591	0.8591

K₁₁ (M⁻¹)	0*	0*	0*	0*	0*
K_{n1}/n (M⁻¹)	0.30 ± 0.06	0.69 ± 0.1	0.061 ± 0.01	(6.9 ± 1) x 10 ⁻⁵	(7.69 ± 2) x 10 ⁻¹⁰
K_{n1} (M⁻¹)	18 ± 4	41 ± 8	3.7 ± 0.7	(4.1 ± 0.8) x 10 ⁻³	(4.6 ± 0.9) x 10 ⁻⁸

Notes: The equation $(F_T - F_0)/(C_T \cdot \alpha) = 1 + k_C + k_{11} K_{11}[S] + (k_{n1} K_{n1}/n)(S_T - \text{cac})$ was used to extract the K_{11} and K_{n1} binding constants from the intercept and slope of Figure 6.1.11 (a) – (e). * K_{11} binding was negative for CPFH_4^{+3} (-52), CPFH_3^{+2} (-7.0), CPFH_2^{+} (-80), CPFH^{+-} (-87) and CPF^- (-87).

At pH 4.00, it can be observed that there is no binding between CPF and SDS in the preaggregate phase, as all the K_{11} binding constants were negative. The greatest binding was observed in the postaggregate phase of SDS.

Interestingly, the K_{n1} values were overall weaker compared to the data obtained at pH 7.00 and pH 8.33. This is due to the fluorescence efficiency of CPF being weaker at pH 4.00 compared to pH 7.00. CPFH_3^{+2} exhibits the greatest binding in the postaggregate phase, as it is the most predominant in solution followed by CPFH_4^{+3} . If the K_{n1} of CPFH^{+-} in Table 6.1.4 was compared it is 8.8 times greater compared to the binding at pH 4.00 with CPFH_3^{+2} . Khan et al. determined K_{n1}/n to be 6.08 M⁻¹ at pH 0.5 – 1 for CPF and SDS interactions. This can be observed in Table 6.1.1. If the literature aggregation number of SDS was accounted for, the corresponding values would be 364.8 M⁻¹. If the closest K_{n1} values were compared this would be at pH 4.00, 41 ± 8 for CPFH_3^{+2} and 18 ± 4 for CPFH_4^{+} .

6.1.2 CPF and SDS monomer and pseudophase interactions in the absence of phosphate buffer

The following experiments were conducted using the CFCLS instead of the Shimadzu RF-6000. The upcoming experiments were completed in order to observe the effect of buffer on the fluorescence intensity and the binding between SDS and CPF. The experiment was first conducted where the fixed scale of the monomer was 1000 mV. This means that any fluorescence intensity value greater than 1000 mV is cut off. Therefore, the experiment was repeated, and the fixed scale was adjusted to 500 mV in order to prevent the fluorescence intensity cut off in the instrument. The repeated experiment is shown in Figure 6.1.12.

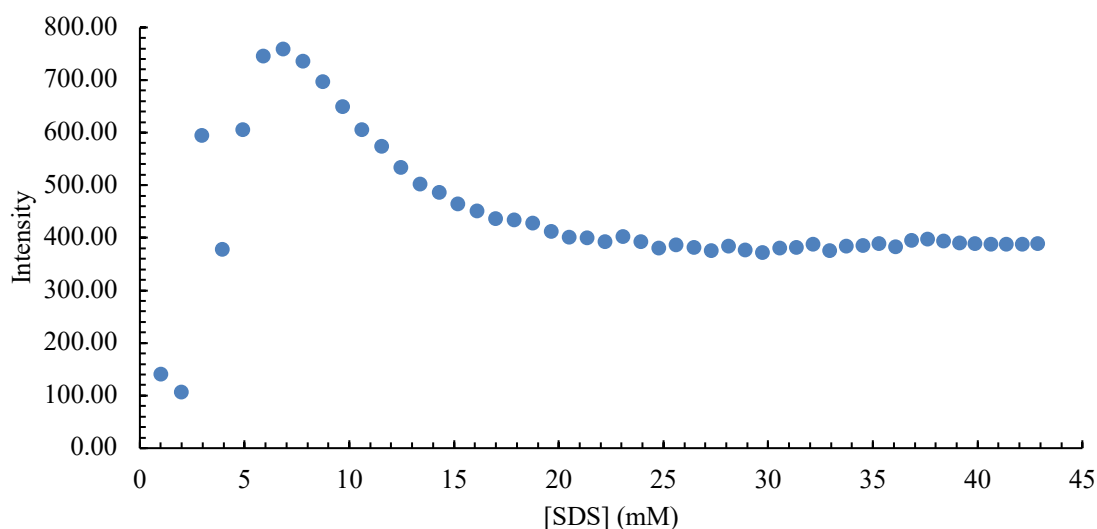


Figure 6.1.12 The fluorescence intensity versus concentration of SDS added with 31.2 μ M of CPF flushed with N_2 (g) without added phosphate buffer

The speciation of CPF at experimental pH was determined using Figure 6.1.13. It can be observed that there is a shift in pH as the concentration of SDS increased because of the lack of buffer to maintain the pH. The experimental pH ranged from 7.60 – 8.20.

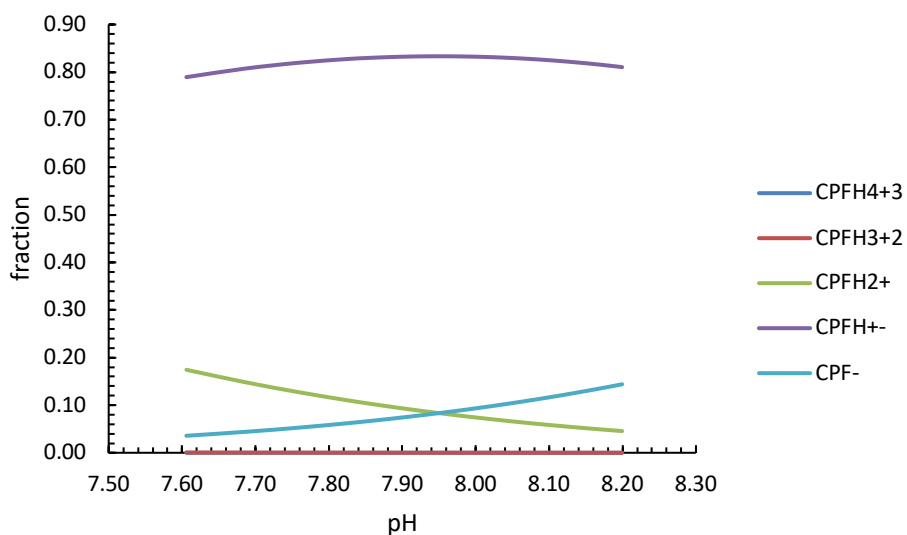


Figure 6.1.13 The distribution of CPF speciation from pH 7.60 – 8.20 \pm 0.01.

It was observed from Figure 6.1.13 that the greatest speciation of CPF present in solution was the zwitterionic CPFH^{+-} followed by the positively charged CPFH_2^+ . This will aid in the determination of the complexation of CPF and SDS under the corresponding experimental conditions.

Table 6.1.11 The fluorescence efficiency of free CPF, CPF-monomer (CS) and CPF-pseudophase (CS_n) complexes at 25°C

	Fluorescence efficiency (mV/μM)	Fluorescence intensity (mV)	[CPF] (μM)
k _C	4.54	141	31.2
k ₁₁	25.7	759	29.5
k _{n1}	43.7	1131	25.9

Notes: k_C, k₁₁ and k_{n1} were determined by dividing the fluorescence intensity by the concentration of CPF.

The fluorescence efficiencies obtained from the CFCLS were smaller compared from the data from the Shimadzu RF-6000. It appears that the FE was greater in the CS complex compared to the CS_n complex.

To determine the binding with CPF and SDS, Equation 1.3.22 can be rewritten as:

Equation 23.3.23 Determination of K₁₁ and K_{n1} to account for FE, a revision of Equation 1.3.22

$$\frac{F_T}{F_0 \cdot \alpha} - 1 = \left[\left(\frac{k_{11}}{k_C} \right) \cdot K_{11}S + \left(\frac{k_{n1}}{k_C} \right) \cdot \frac{K_{n1}}{n} (S_{T-cac}) \right]$$

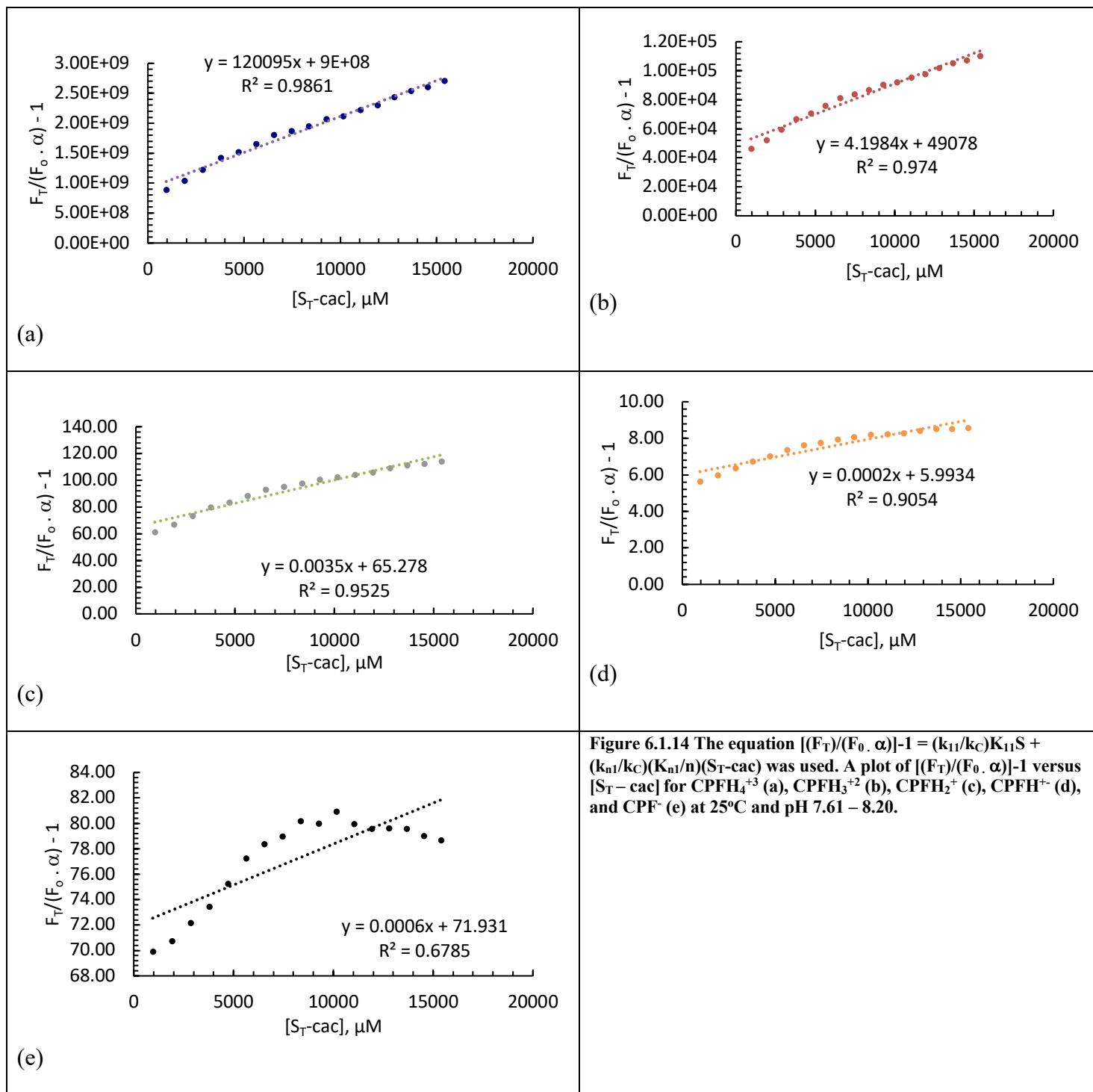
Here, α is the fractional concentration of the specific acid-base species (ie., α₀, α₁, α₂, α₃ and α₄). Here, α₀ is the completely protonated and most positively charged species, while α₄ is the least protonated and most negatively charged species. The above equation can be used to calculate the K₁₁ and K_{n1} for the specific species from the plot of $\frac{F_T}{F_0 \cdot \alpha}$ versus (S_{T-cac}). The slope, $\left(\frac{k_{n1}}{k_C} \right) \cdot \frac{K_{n1}}{n}$ and the intercept $\left(\frac{k_{11}}{k_C} \right) \cdot K_{11}S$ are used to

calculate K_{n1} and K_{11} respectively. The equation above is valid in the postaggregate region where S is equal to the cac .

The fluorescence efficiency ratios were adjusted to account for each CPF species by multiplying each ratio by the corresponding α . This is shown in Table 12. The ratios were used to extract K_{11} and K_{n1}/n from the intercept and slope of Figure 6.1.14 (a) - Figure 6.1.14 (e).

Table 12 The fluorescence efficiency ratios obtained from the data in Table 6.1.11

k_{n1}/k_C	9.32
k_{11}/k_C	5.48



CPFH₄⁺³ is the smallest species of CPF present within solution Figure 6.1.14 (a). However, the slope is the highest out of all the other species of CPF. The R² in this model is 0.9861

The binding in the postaggregate phase in Figure 6.1.14 (b) is less compared to Figure 6.1.14 (a) with a slope of 4.2. There is a high agreement in the binding due to the R² value of 0.9740. In Figure 6.1.14 (c) the R² value of 0.9525 displays a high agreement to the binding model. While the slope is less than the other positive species of CPF, there still appears to be binding in the postaggregate phase. While CPFH⁺⁻ is the most predominant species in solution, the slope is smaller compared to the positively charged species of CPF in Figure 6.1.14 (d). The R² of Figure 6.1.14 (d) is also smaller in comparison with a value of 0.9054.

The R² of Figure 6.1.14 (e) is higher with a value of 0.6785. The data in the figure does not display an overall linear relationship. The binding constants of K₁₁ and K_{n1/n} obtained from Figure 6.1.14 (a) - Figure 6.1.14 (e) are expressed in Table 6.1.13.

Table 6.1.13 The determination of preaggregate and postaggregate binding constants for CPF and SDS complexation using the CFCLS extracted from the slope and intercept Figure 6.1.14 (a) – (e). The literature aggregation number of 60 was used to determine K_{n1}.

	CPFH ₄ ⁺³	CPFH ₃ ⁺²	CPFH ₂ ⁺	CPFH ⁺⁻	CPF ⁻
slope (μM ⁻¹)	(1.2 ± 0.04) x 10 ⁵	4.2 ± 0.2	(3.5 ± 0.2) x 10 ⁻³	(2.0 ± 0.2) x 10 ⁻⁴	(6.0 ± 1) x 10 ⁻⁴
intercept (μM ⁻¹)	(9.0 ± 0.3) x 10 ⁸	(4.9 ± 0.2) x 10 ⁴	65 ± 2	6.0 ± 0.2	72 ± 1

R²	0.9861	0.9740	0.9525	0.9054	0.6785
K₁₁ (M⁻¹)	(4.08 ± 0.1) x 10 ¹⁰	(1.85 ± 0.08) x 10 ⁶	2050 ± 63	156 ± 5	1560 ± 22
K_{n1}/n (M⁻¹)	(3.57 ± 0.1) x 10 ¹⁰	(8.77 ± 0.4) x 10 ⁵	514 ± 29	20.7 ± 2	43.6 ± 7
K_{n1} (M⁻¹)	(2.14 ± 0.07) x 10 ¹²	(5.26 ± 0.3) x 10 ⁷	(3.08 ± 0.2) x 10 ⁴	1240 ± 124	2620 ± 44

Note: $[(F_T)/(F_0 \cdot \alpha)] - 1 = (k_{11}/k_C)K_{11}S + (k_{n1}/k_C)(K_{n1}/n)(S_T - \text{cac})$ was used to determine K_{11} and K_{n1} .

There are several important observations made from this study. The binding constants K_{11} and K_{n1} decrease from the most protonated species, CPFH_4^{+3} , to the least protonated species CPF^- . There are about 10 orders of magnitude difference in the binding constants. CPFH_4^{+3} appears to interact with the anionic micelles through a strong electrostatic attraction, thus having the largest binding constants. The better correlation coefficients for these species indicate the validity of the model. However, the concentrations of such species are small due to the extremely low concentrations of the protonated species as evident from the species distribution in Figure 6.1.13.

The less protonated species, CPFH^{+2} and CPF^- , have lower binding constants due to weaker electrostatic attractions. These species are generally distributed near the micelles due to the hydrophobic interactions. However, these species constitute the majority (80 – 90%) of the bound species.

The pH change over the entire experiment is significant. Therefore, species distribution and their nature are important in binding.

6.1.2 Conclusion of CPF and SDS binding

The interactions between CPF and SDS were the most studied in the literature compared to the other systems in this dissertation. Khan et al studied CPF and SDS interactions using fluorescence spectroscopy⁴¹, UV-vis spectroscopy,⁴⁸ and FTIR. They observed FE interactions when the concentration of SDS added was greater than 30 mM. However, the authors considered CPF as a triprotic acid instead of tetraprotic and did not specify the binding mechanism or structures involved with the interactions. They used HCl which lowered the experimental fluorescence intensity. Therefore, their binding constants are less accurate.

Khan et al. determined K_{n1}/n to be 6.08 M^{-1} and 8.51 M^{-1} at pH 0.5 – 1 and 9.2 respectively for CPF and SDS interactions. This can be observed in Table 6.1.1. If the literature aggregation number of SDS was accounted for, the corresponding values would be 364.8 M^{-1} and 510.6 M^{-1} . If the closest K_{n1} values were compared this would be at pH 8.33, where the greatest binding was observed with CPFH^{+-} and K_{n1} was 167 ± 20 .

However, binding constants Khan et al. obtained are not exclusive to particular CPF species. The authors do not state the type of buffer in solution as well as the concentration. This influences the binding that occurs between these compounds. The binding between CPF and SDS significantly increased in the absence of buffer which was observed in Table 6.1.13.

Anger et al.⁸⁴ observed that FE and FQ can occur within a single molecule depending on the distance between molecules and the excitation wavelength. If time

resolved fluorescence (TRF) was available, the interactions between CPF and SDS could be further determined as the interactions occur rapidly.

Hua et al.⁸⁵ observed that FE with CPF was based on the strong hydrogen bond interactions and charge transfer. This is possible with SDS as the overall charge on the exterior of the pseudophase is negative. Wang et al.⁸⁶ determined that the energy (ΔG) of aggregation for SDS is minimally affected when there is a change in pH. Therefore, the biggest effect of pH on the interactions with the pseudophase is with the CPF species. While little to no binding occurred in the preaggregate phase, the interactions between CPF and SDS in the postaggregate phase were significant. Most of the CPF will reside within the hydrophobic core in the pseudophase. Water molecules will also hydrogen bond with the SDS pseudophase which will limit the interactions with CPF.

Due to SDS being an overall anionic compound, therefore, the greatest interactions should be between the positively charged species of CPF. This was observed overall in the K_{n1}/n binding constants. The precision of the binding constants was improved greatly when data was collected with the CFCLS compared to the Shimadzu RF-6000, which was shown in the obtained R^2 values of the linear plots. This was due to the CFCLS' ability to take a significantly greater amount of data points comparatively.

DETERMINATION OF CIPROFLOXACIN (CPF) AND PERFLUOROOCTANESULFONIC ACID (PFOS) PSEUDOPHASE INTERACTIONS

7.1 Determination of CPF and PFOS pseudophase interactions

7.1.1 *Acid dissociation properties of PFOS*

PFOS is strongly acidic and behaves as an anionic surfactant. The pK_a values reported for PFOS are summarized in Table 7.1.1. It has been observed to have different reported pK_a values.

Table 7.1.1 The literature pK_a values of PFOS.

Literature pK_a values of PFOS	-3.3 ²²	+3.27 ²⁰	>1 ⁸⁷	-3.27 ⁸⁸
---	--------------------	---------------------	------------------	---------------------

To account for the acidity and species of PFOS, a distribution diagram is shown in Figure 7.1.1. The pK_a of -3.3 was chosen because most of the literature shows the acid dissociation constant being less than 1.

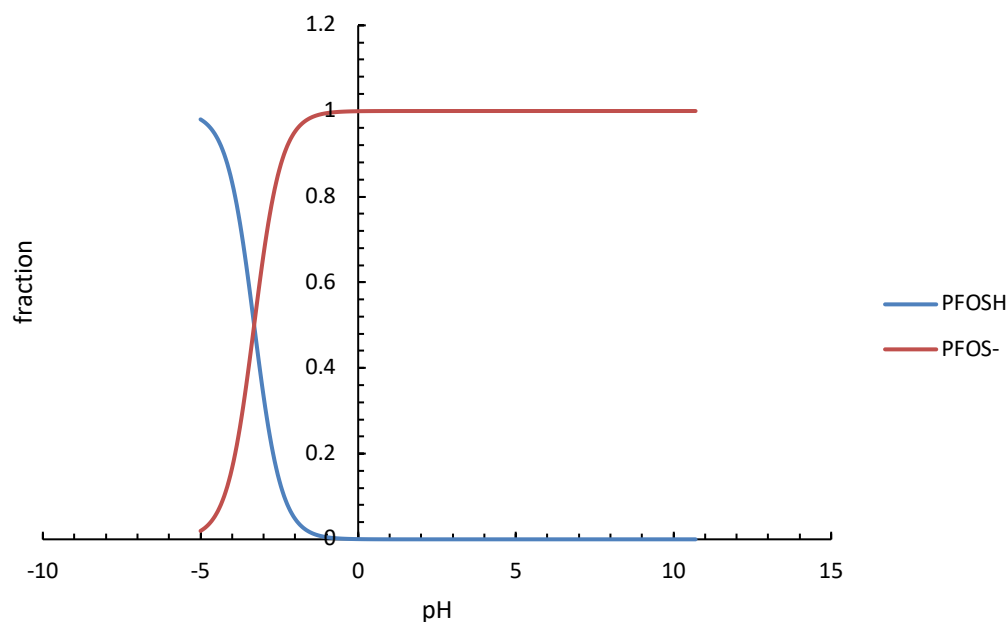


Figure 7.1.1 The fractional distribution of PFOS when the pKa is -3.3

From the distribution diagram, it is clear the only relevant PFOS species interacting with CPF within the pH range 1-10 is PFOS⁻. This simplifies the analysis because PFOS is consistently in the negatively charged conjugate base form.

7.1.2 Effect of PFOS on CPF Fluorescence

7.1.2.1 Determination of CPF and PFOS interactions in the presence of phosphate buffer

The Shimadzu RF – 6000 was used to observe the effects of phosphate buffer on the PFOS and CPF interactions. In Table 7.1.2 that as the concentration of PFOS in the sample increased, the overall fluorescence intensity at the maximum wavelength decreased following the trend of fluorescence quenching. For basic pH ranges (6.00-

11.00) 416 nm is the maximum emission while 448 nm the maximum emission for acidic pH ranges (1.00-5.00). This trend was observed in the Effect of pH section.

As stated earlier, PFOS is strongly acidic. While the CPF was dissolved in phosphate buffer to help provide a constant pH at 7.00, the pH dropped to 6.27 as the concentration of PFOS increased during the titration. There also appeared to be a effect of the phosphate buffer on PFOS. An observation made during the experiment was that the fluorometer displayed a saturation value at 50 mM of PFOS. A white solid precipitated when the 50 mM solution was mixed and settled. This could explain the increase of error in fluorescence intensity as the concentration of PFOS increased passed the critical aggregation concentration (cac). The white precipitate is assumed to be the $\text{PFOS}^- \text{Na}^+$ salt.

The changes in CPF excitation and emission intensities upon the addition of PFOS during the titration are shown in Figure 7.1.2.

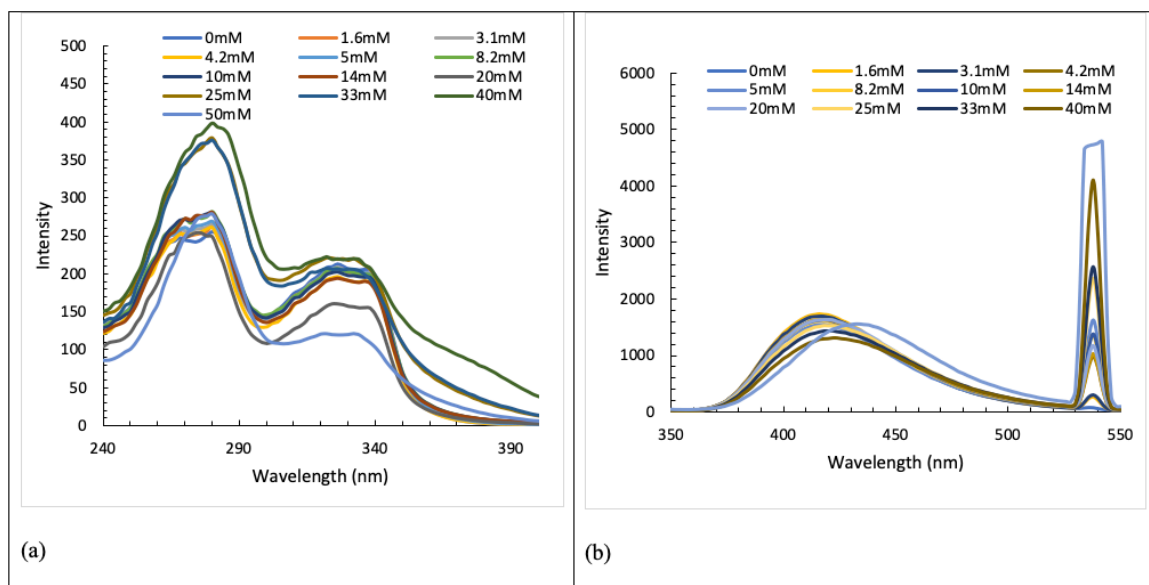


Figure 7.1.2 The excitation (a) and emission (b) spectra for 31.2 μ M of CPF upon addition of PFOS. $\lambda_{\text{excitation}} = 270 \text{ nm}$ and $\lambda_{\text{emission}} = 416 \text{ nm}$ and excitation and emission slits were 3.0 nm, respectively.

Table 7.1.2 Data obtained for CPF with PFOS additions using Shimadazu RF-6000 and pH measurement

pH	[PFOS] (mM)	Fluorescence Intensity
7.00	0.0 ± 0.00	1721.7 ± 6.1
6.93	1.6 ± 0.02	1737.7 ± 7.6
6.90	3.1 ± 0.03	1696.9 ± 7.6
6.91	4.2 ± 0.04	1612.7 ± 5.0
6.86	5.0 ± 0.05	1543.6 ± 4.2
6.86	8.2 ± 0.08	1618.4 ± 7.2
6.79	10 ± 0.1	1614.9 ± 9.0
6.76	14 ± 0.1	1630.8 ± 2.0
6.70	20 ± 0.2	1620.8 ± 6.9
6.61	25 ± 0.3	1512.6 ± 13.8
6.51	33 ± 0.3	1417.2 ± 18.7
6.51	40 ± 0.4	1292.8 ± 21.7
6.27	50 ± 0.5	1313.7 ± 70.4

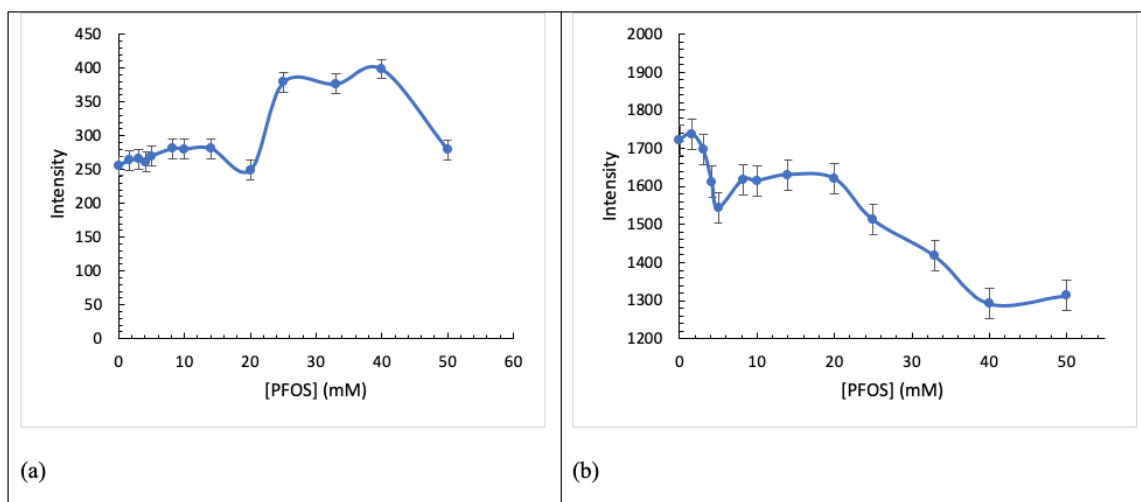


Figure 7.1.3 Plot of intensity vs concentration of PFOS added into 31.2μM of CPF at excitation maximum $\lambda_{\text{excitation}} = 270 \text{ nm}$ (a) and emission maximum $\lambda_{\text{emission}} = 416 \text{ nm}$ (b)

From Figure 7.1.3 Plot of intensity vs concentration of PFOS added into 31.2μM of CPF at excitation maximum $\lambda_{\text{excitation}} = 270 \text{ nm}$ (a) and emission maximum $\lambda_{\text{emission}} = 416 \text{ nm}$ (b), the data obtained from the excitation (a) and emission (b) maxima displays an overall fluorescence decreased as the concentration of PFOS increased. The exact concentrations of PFOS added to solution are observed in Table 7.1.2.

7.1.2.2 Comparison of binding when CPF is tetraprotic versus triprotic

Because CPF speciation is critically important to binding processes, a comparison of the tetraprotic and triprotic dissociation of CPF is necessary because the pH effects complexation and binding with compounds like PFOS. A distribution diagram (Figure

7.1.4) was created for CPF when it was considered a tetraprotic (a) and triprotic acid (b) at the experimental pH.

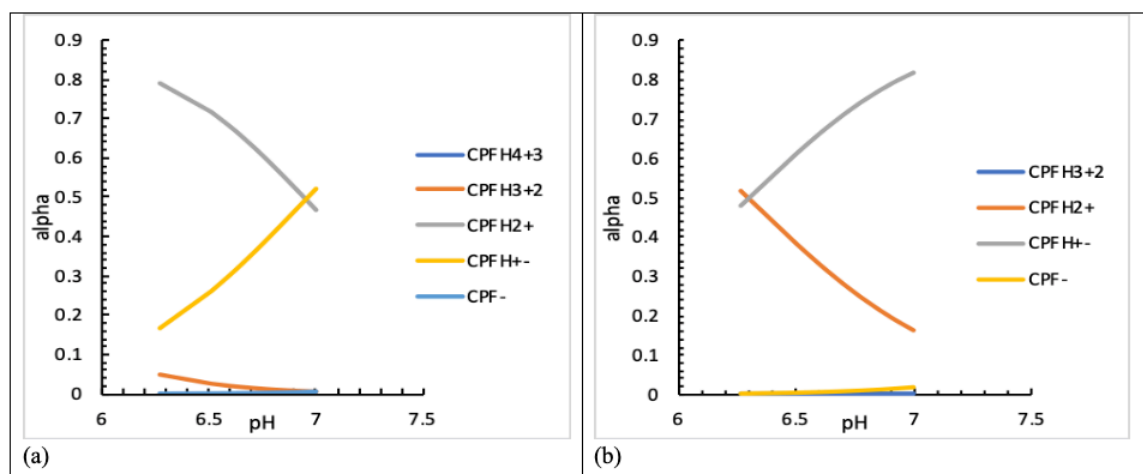


Figure 7.1.4 Fractional distribution of CPF species as (a) tetraprotic acid and (b) triprotic acid

Although CPFH_2^+ and CPFH^{+-} predominate between pH 6.00 to 7.50, the fractions of each at a given pH vary widely depending on whether CPF is considered a triprotic or tetraprotic acid. It was observed from the diagram that the predominant species for both tetraprotic and triprotic CPF are CPFH_2^+ and CPFH^{+-} . This will show which specific species of CPF were interacting with anionic PFOS at the experimental pH as well as which species contribute to the overall fluorescence intensity.

From Figure 7.1.5 the cac of PFOS can be determined from the decrease of fluorescence intensity as the concentration increases from 0 – 5 mM. At 8.2 mM of PFOS, the fluorescence intensity increased. This change in fluorescence intensity is

indicative of the critical aggregation content of PFOS. These changes are not sharp due to small change in fluorescence and weak association of PFOS with CPF species.

7.1.2.2.1 The effect of protonation on fluorescence intensity

It was first necessary to transform total fluorescence intensity into the fluorescence contributions from each individual CPF species. The calculated fluorescence intensity was obtained by multiplying the observed intensity by the associated α_i value at the experimental pH. This is displayed in Figure 7.1.5 for the predominant species.

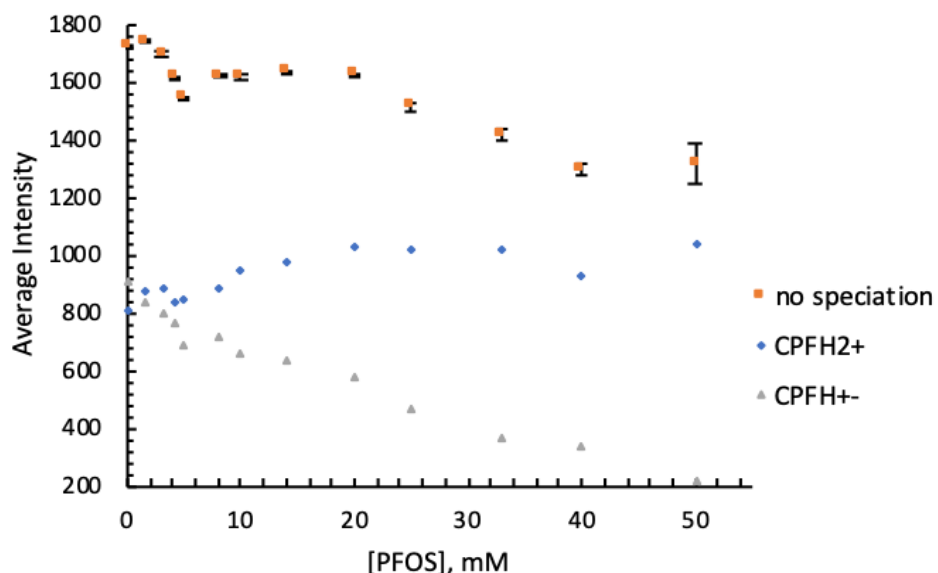


Figure 7.1.5 The observed fluorescence intensity (orange) versus the concentration of PFOS added to CPF. The calculated intensities due to CPFH₂⁺ (blue) and CPFH⁺⁻ (grey) account for CPF being a tetraprotic acid. The error bars in the diagram show the error within the fluorescence measurement. The error is the greatest when 50 mM of PFOS was added because it precipitated out.

From Figure 7.1.5, it can be observed that when CPF is considered tetraprotic the fluorescence intensity contribution was from CPFH₂⁺. For CPFH⁺⁻, total intensity

decreased as the concentration of PFOS increased which is indicative of complexation with PFOS.

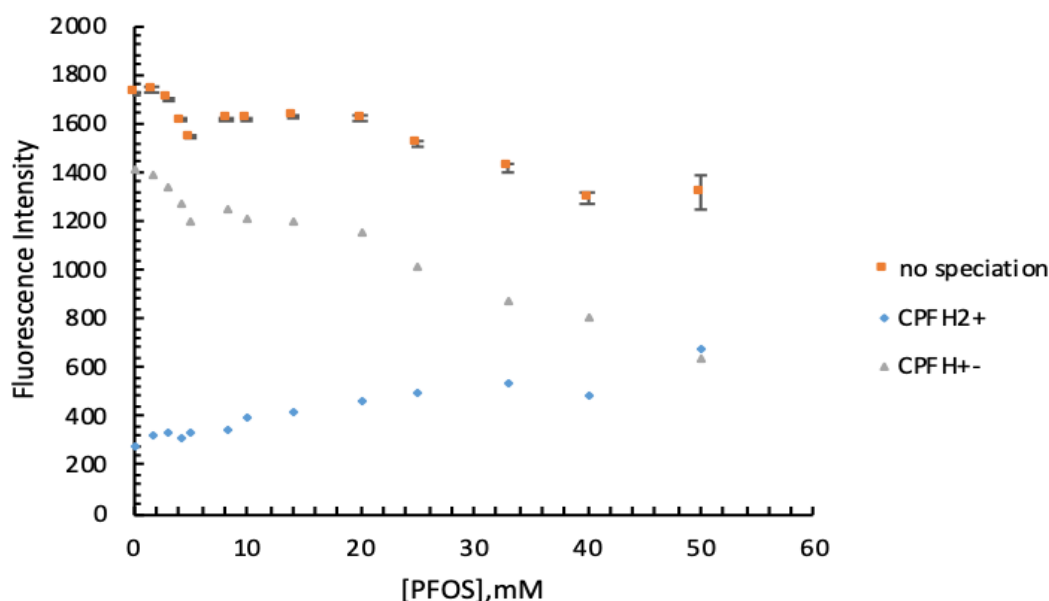


Figure 7.1.6 The observed fluorescence intensity (orange) versus the concentration of PFOS added to CPF. The calculated intensities due to CPFH₂⁺ (blue) and CPFH⁺ (grey) accounts for CPF being a triprotic acid.

In Figure 7.1.6, the same trend can be observed that the overall fluorescence intensity of CPFH⁺ decreased as the concentration of PFOS increased. However, when CPF is considered triprotic, the zwitterionic species appeared to also contribute to the majority of fluorescence in solution.

From the fluorescence intensity versus PFOS added data observed in Figure 7.1.5 and Figure 7.1.6, the difference in protonation can display a difference in calculated fluorescence intensity based on the fractional concentration of predominant species present in the system. For both tetraprotic and triprotic CPF, the majority species that

interact with PFOS were CPFH_2^+ and CPFH^{+-} , which are +1 and neutral (or zwitterionic) chemical forms.

7.1.2.2.2 *The effect of protonation of CPF on the binding with PFOS*

The binding constants, K_{11} and K_{n1}/n and were calculated by plotting (F_0/F_T) versus $(S_T - \text{cac})$ according to the second binding model which is observed in Figure 7.1.7 and Figure 7.1.8. The second binding model is used because of the interactions resembling fluorescence quenching. This means that as the concentration of the PFOS increased, the overall fluorescence intensity decreased. From the current methods used, n could not be determined, therefore, only the value of K_{n1}/n is reported. Figure 7.1.7 shows the data fit assuming CPF as a tetraprotic acid and for CPFH_2^+ and CPFH^{+-} . A similar plot (Figure 7.1.8) is shown assuming CPF as the triprotic acid which also accounts for the predominant species of CPFH_2^+ and CPFH^{+-} .

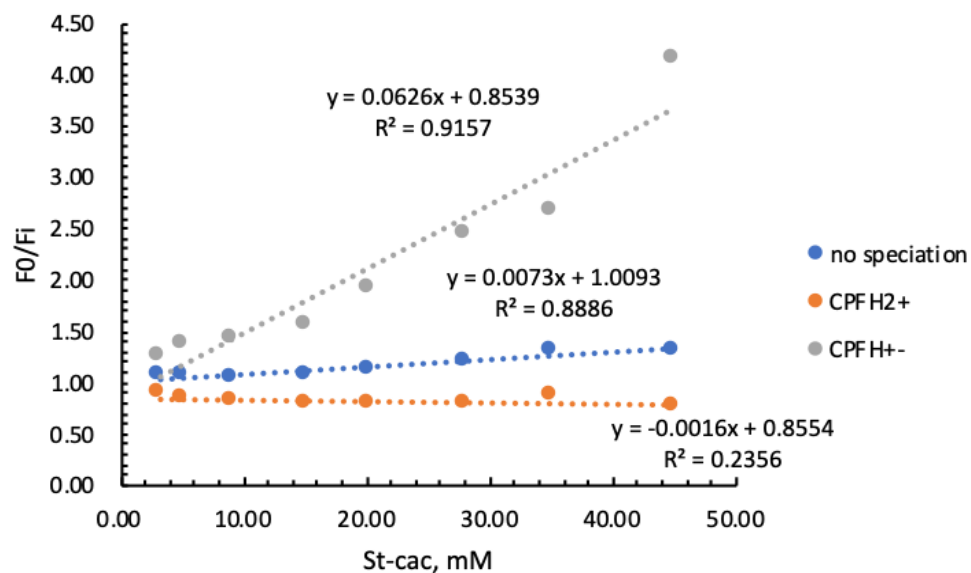


Figure 7.1.7 The equation $F_0/F_T = 1 + K_{11}[S] + (K_{n1}/n)(S_T - cac)$ was used. A plot of (F_0/F_T) versus $[S_T-cac]$ for no speciation, $CPFH_2^+$ and $CPFH^{+-}$ when CPF is tetraprotic, where $CPFH_2^+$ (orange) and $CPFH^{+-}$ (grey)

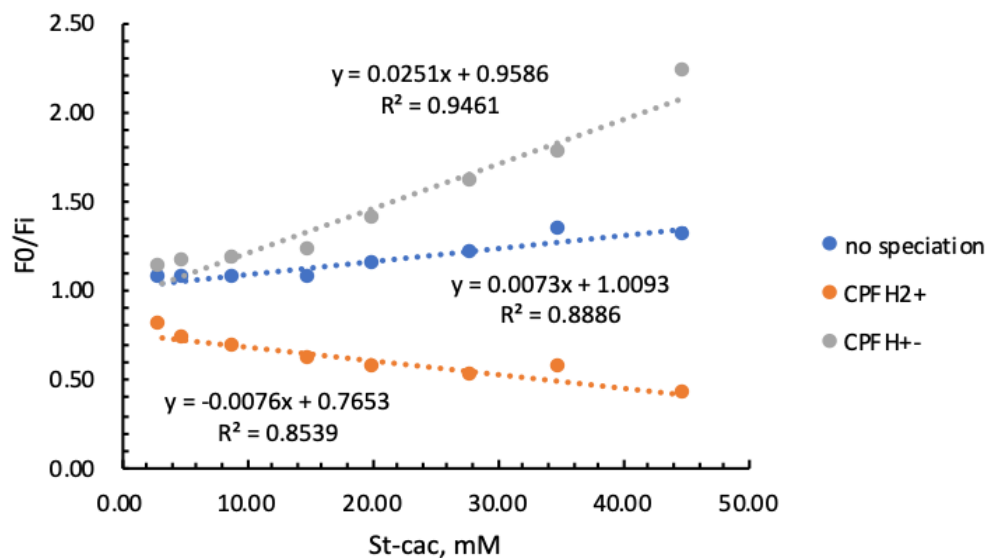


Figure 7.1.8 The equation $F_0/F_T = 1 + K_{11}[S] + (K_{n1}/n)(S_T - cac)$ was used. A plot of (F_0/F_T) versus $[S_T-cac]$ for no speciation, $CPFH_2^+$ and $CPFH^{+-}$ when CPF is triprotic, where species $CPFH_2^+$ (orange) and $CPFH^{+-}$ (grey).

7.1.2.2.3 Determination of CPF and PFOS monomer and pseudophase binding

The calculated binding constants for CPF as a tetraprotic and triprotic acids are shown in Table 7.1.3. It can be observed that there is no binding ($K_{11} = 0$) in the preaggregate phase of PFOS with CPFH_2^+ and CPFH^{+-} species within experimental error. The same is true without speciation. Therefore, there is no noncovalent attraction between PFOS and CPFH_2^+ and CPFH^{+-} species in the preaggregate region within the specified pH range. In the post aggregate pseudophase, the K_{n1}/n values show some binding with neutral CPFH^{+-} (or zwitterionic) but none with CPFH_2^+ species. However, it is important to note that the binding with CPFH^{+-} is 2.5 times larger for CPF being a tetraprotic acid versus a triprotic acid. This shows that the neutral CPFH^{+-} species associates with PFOS pseudophase to the greatest extent. The aggregation number only changes the relative value K_{n1} . Turro et. al³⁸. determined the aggregation number of PFOS to be approximately 7. With this in consideration, experimental K_{n1} values for CPFH^{+-} as a tetraprotic acid and triprotic acid would equal $438.2 \pm 56 \text{ M}^{-1}$ and $175.7 \pm 14 \text{ M}^{-1}$ respectively. CPF binding is relatively low in comparison with other surfactants. For example, Yang et. al.⁴² determined the K_{n1}/n for a similar system of CPF as a triprotic acid with sodium lauryl sulfonate (SLS) to be 154 M^{-1} . This does not include the aggregation number.

Table 7.1.3 Binding constants for tetraprotic and triprotic CPF species with PFOS surfactant and PFOS-pseudophase at 25.0 °C. The literature aggregation number 7 was used to determine K_{n1} .

Tetraprotic CPF	No speciation	CPFH_2^+	CPFH^{+-}
Slope (mM^{-1})	0.0073	-0.0016	0.0626
Intercept (mM^{-1})	1.01	0.855	0.854

R^2	0.8886	0.2356	0.9157
$K_{11} (M^{-1})$	1.86 ± 30	0*	0*
$K_{n1}/n (M^{-1})$	7.3 ± 1	0*	62.6 ± 8
$K_{n1} (M^{-1})$	51.1 ± 7	0*	438.2 ± 56
Tripotric CPF	No speciation	CPFH₂⁺	CPFH⁺⁻
Slope (mM ⁻¹)	0.0073	-0.0076	0.0251
Intercept (mM ⁻¹)	1.01	0.765	0.959
R^2	0.8886	0.8539	0.9461
$K_{11} (M^{-1})$	1.86 ± 30	0*	0*
$K_{n1}/n (M^{-1})$	7.3 ± 1	0*	25.1 ± 2
$K_{n1} (M^{-1})$	51.1 ± 7	0*	175.7 ± 14

Notes: The equation $F_0/F_T = 1 + K_{11}[S] + (K_{n1}/n)(S_T - \text{cac})$ was used to determine K_{11} and K_{n1} binding constants. * K_{11} and K_{n1} binding was negative for CPFH₂⁺

Table 7.1.3 shows greater binding with PFOS pseudophase when CPF is considered tetraprotic. Accounting for the additional proton within CPF increases the precision the determination of the binding in the postaggregate phase.

7.1.3 Determination of CPF and PFOS binding in the absence of phosphate buffer

The next set of experiments account for the addition of PFOS using the CFCLS without the addition of sodium phosphate buffer. This was observed if there was an effect of salt buffer on PFOS pseudophase and the interactions with CPF. With the CFCLS, the number of data points increased, which should add precision and accuracy to the determination of the binding constants.

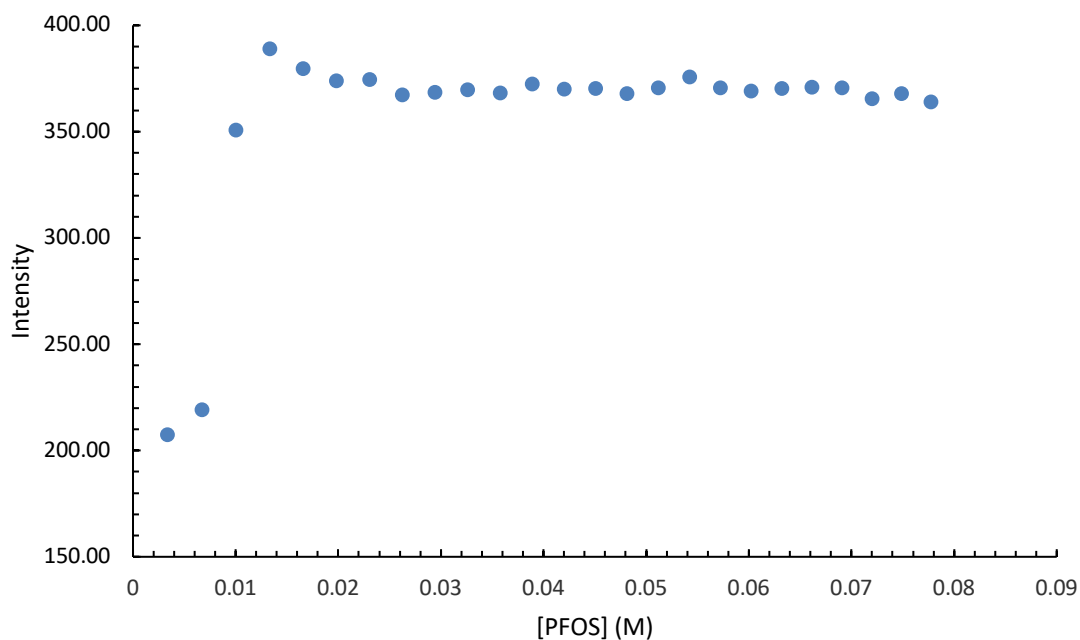


Figure 7.1.9 The fluorescence intensity versus the concentration of PFOS added to 31.2 μM CPF without added phosphate buffer flushed with N_2 (g).

Through the CFLS, additional data points were possible in order to increase precision and the accuracy of the fluorescence intensity measurements. A portion of the experimental data obtained is shown in Table 7.1.4.

Table 7.1.4 The change in pH and concentration of PFOS obtained with the CFCLS at 25°C.

pH	$[\text{H}^+]$, M	[PFOS], mM
2.85	1.40×10^{-3}	6.70
2.63	2.32×10^{-3}	10.01
2.44	3.59×10^{-3}	13.30
2.31	4.90×10^{-3}	16.57

It can be observed that in the absence of a buffer, the pH significantly decreased as the concentration of PFOS in the solution increased. After the first addition of PFOS, the pH dropped from pH 7.00 to 2.85. Therefore the data analyzed started at 2.85. Therefore, a distribution diagram of CPF at the experimental pH was created in order to observe the speciation of CPF as the pH decreased (Figure 7.1.10).

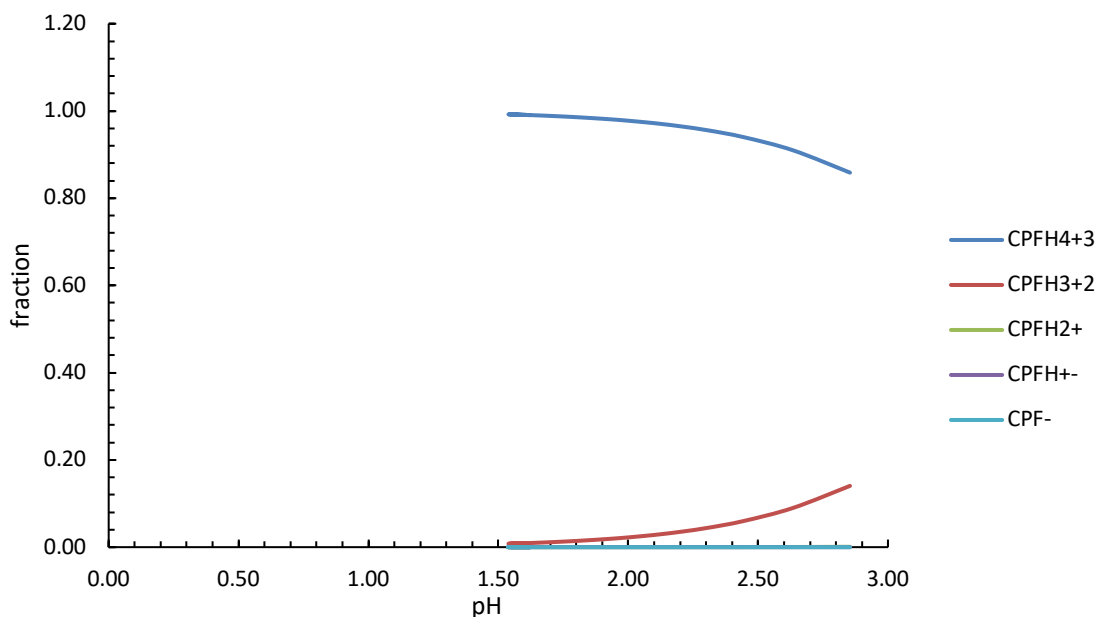


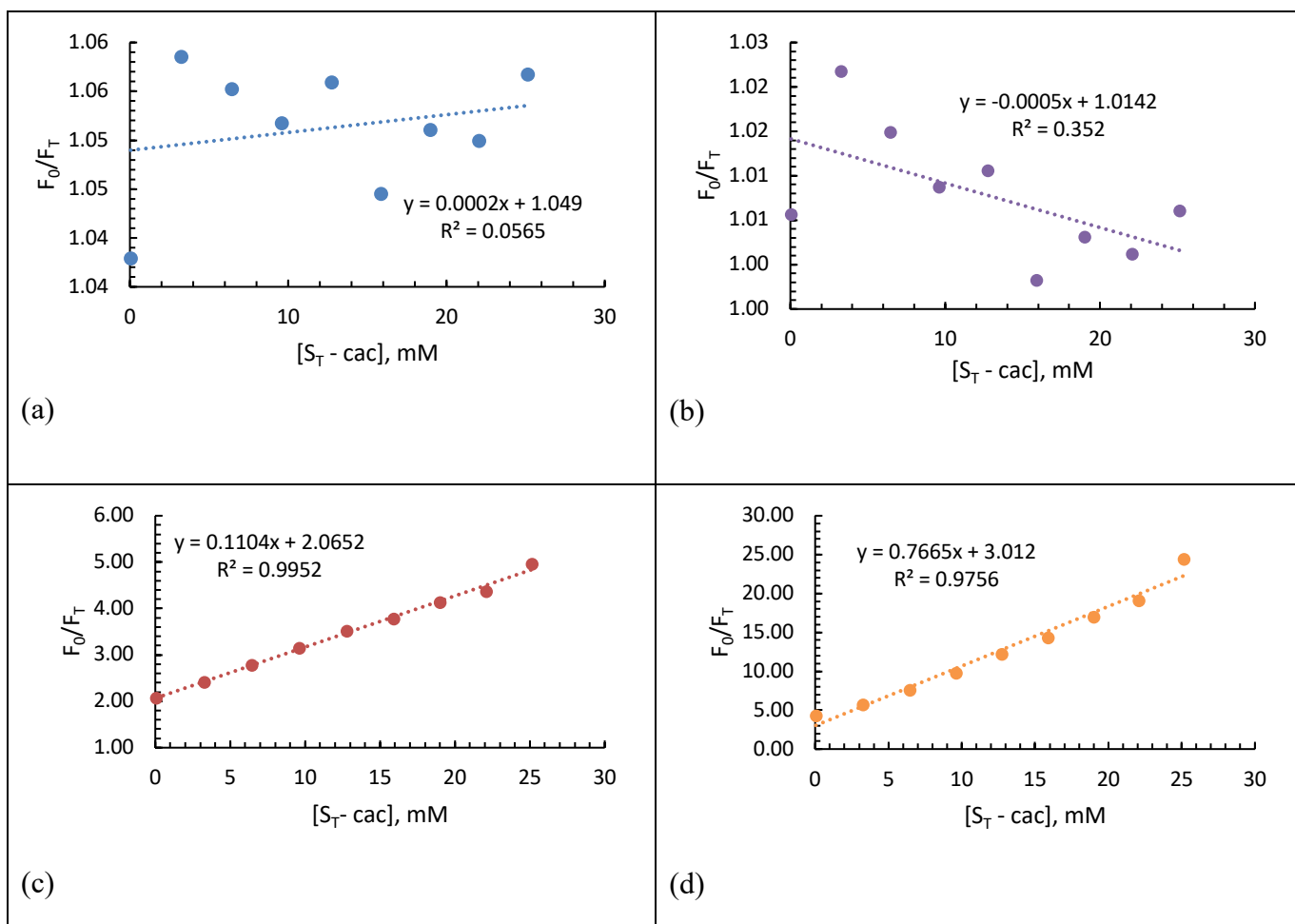
Figure 7.1.10 Distribution diagram of CPF at experimental pH

From Figure 7.1.10, it can be observed that the greatest speciation of CPF present in solution was CPFH_4^{+3} followed by CPFH_3^{+2} .

In order to determine the preaggregate and postaggregate binding constants, K_{11} and K_{n1}/n , Equation 1.3.12 was used. It is shown below. Figure 7.1.11 (a) - Figure 7.1.11 (f)

were plotted to determine the binding. The experimental fluorescence was multiplied by α to account for all CPF species.

$$\frac{F_0}{F_T} = 1 + K_{11}S + \left(\frac{K_{n1}}{n}\right)(S_{T-cac})$$



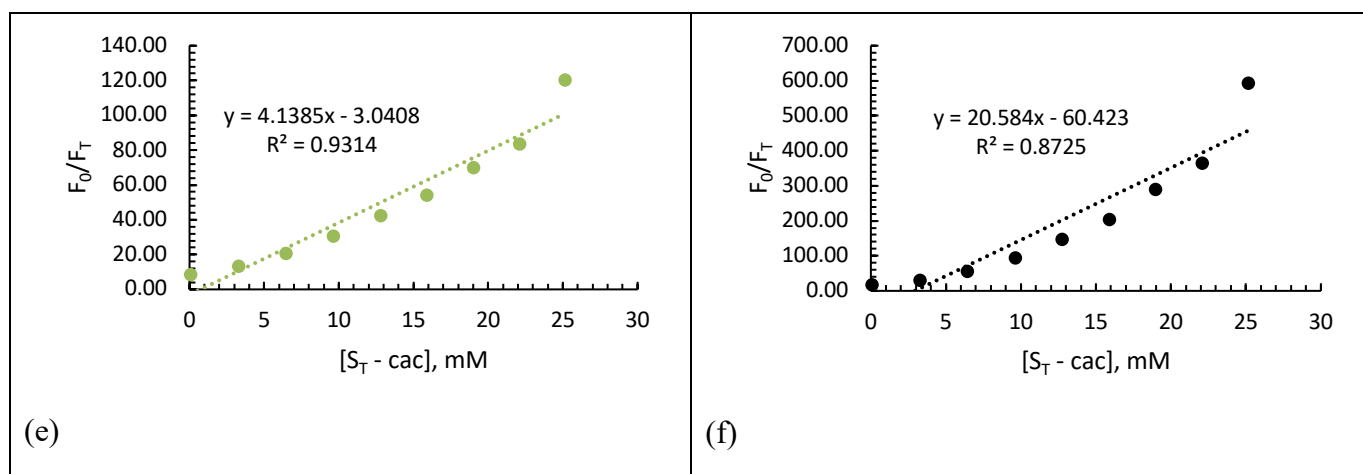


Figure 7.1.11 The equation $F_0/F_T = 1 + K_{11}[S] + (K_{n1}/n)(S_T - \text{cac})$ was used. A plot of (F_0/F_T) versus $[S_T - \text{cac}]$ for no speciation of CPF (a), CPFH_4^{+3} (b), CPFH_3^{+2} (c), CPFH_2^+ (d), CPFH^{+-} (e), and CPF^- (f) at 25°C.

In Figure 7.1.11 (a), it can be observed that there is very weak to no binding observed. CPFH_4^{+3} resembles the data in Figure 7.1.11 (a). Therefore it is the greatest fluorescence contributing species. This is true because it is the most predominant species in solution at the experimental pH.

CPFH_3^{+2} is the second most abundant species in solution. It displays postaggregate binding with the PFOS pseudophase as the slope is positive in Figure 7.1.11 (c). The R^2 value of 0.9952 shows a high agreement to the binding model used.

In Figure 7.1.11 (d), the slope increased compared to the values in Figure 7.1.11 (a) - Figure 7.1.11 (c). The R^2 value is 0.9756 which shows a good fit to the binding theory. For CPFH^{+-} , the binding in the postaggregate phase increased, although it is one of the least abundant species in solution. The greatest fit is observed in Figure 7.1.11 (f) with CPF^- . However, it is the least abundant species in solution. However, it has a lower R^2 value compared to Figure 7.1.11 (c) - Figure 7.1.11 (e).

7.1.3.1.1 Determination of CPF and PFOS monomer and pseudophase binding

It was found that no binding occurred in the preaggregate phase. However, the greatest binding in the postaggregate phase occurs with the zwitterionic and negatively charged species of CPF. The data obtained is shown in Table 7.1.5.

Table 7.1.5 Binding constants K_{11} and K_{n1} for CPF species with PFOS surfactant and PFOS pseudophase at 25°C. The literature aggregation number of 7 was used to determine K_{n1} .

	No Speciation	CPFH_4^{+3}	CPFH_3^{+2}	CPFH_2^{+}	CPFH^{+-}	CPF^{-}
Slope (mM^{-1})	$(2.0 \pm 3) \times 10^{-4}$	$(-5.0 \pm 3) \times 10^{-4}$	0.1 ± 0.003	0.77 ± 0.05	4.1 ± 0.4	21 ± 3
Intercept (mM^{-1})	1.0 ± 0.004	1.01 ± 0.004	2.0 ± 0.04	3.0 ± 0.7	-3.0 ± 6	-60 ± 44
R^2	0.0565	0.352	0.9952	0.9756	0.9314	0.8725
K_{11} (M^{-1})	0*	0*	46 ± 42	87 ± 14	0*	0*
K_{n1}/n (M^{-1})	0.182 ± 0.3	0*	110 ± 3	766 ± 45	4139 ± 424	$(2.06 \pm 0.3) \times 10^4$
K_{n1} (M^{-1})	1.27 ± 2	0*	773 ± 20	5365 ± 320	$(2.90 \pm 0.3) \times 10^4$	$(1.44 \pm 0.2) \times 10^5$

Notes: The equation $F_0/F_T = 1 + K_{11}[S] + (K_{n1}/n)(S_T - \text{cac})$ was used to determine K_{11} and K_{n1} binding constants. * K_{11} binding was negative for no speciation, CPFH_4^{+3} , CPFH^{+-} , and CPF^{-} . K_{n1} binding was negative for CPFH_4^{+3} .

7.1.3.1.2 Analysis of preaggregate and postaggregate binding between CPF and PFOS

It was hypothesized that the greatest interactions would occur with the positively charged species of CPF which were CPFH_4^{+3} , CPFH_3^{+2} and CPFH_2^{+} . This is due to the charge along with species having highest concentrations in solution at the experimental pH. Interestingly, it was observed that the greatest interactions that occurred in the postaggregate phase were the with the zwitterionic and negatively charged species. It is

possible that due to these species of CPF having the lowest presence in solution, to interact with the anionic PFOS first. Also, with the interactions that occur between PFOS and H₂O, that occupies space, unable for the positively charged species of CPF to bind with the PFOS. However, the values obtained can not be valid because of the nonlinear fit to a linear model.

It can be observed that compared to the data obtained when PFOS was dissolved in phosphate buffer, the binding is significantly higher in comparison. Therefore it can be determined that there are salt effects that occur between PFOS that interfere with binding with CPF speciation.

7.1.3.2 Binding of CPF and PFOS in the preaggregate phase in the absence of phosphate buffer

In order to understand the interactions that occur between CPF and PFOS in the preaggregate phase, the solutions were prepped at 1 μ M of PFOS and 100 μ M of CPF. This concentration of PFOS was significantly lower than the cac of PFOS which is 8.0 mM in the literature. The solutions were dissolved in distilled water in order to avoid the influence of salt buffer with PFOS. The experimental results are observed in Figure 7.1.12.

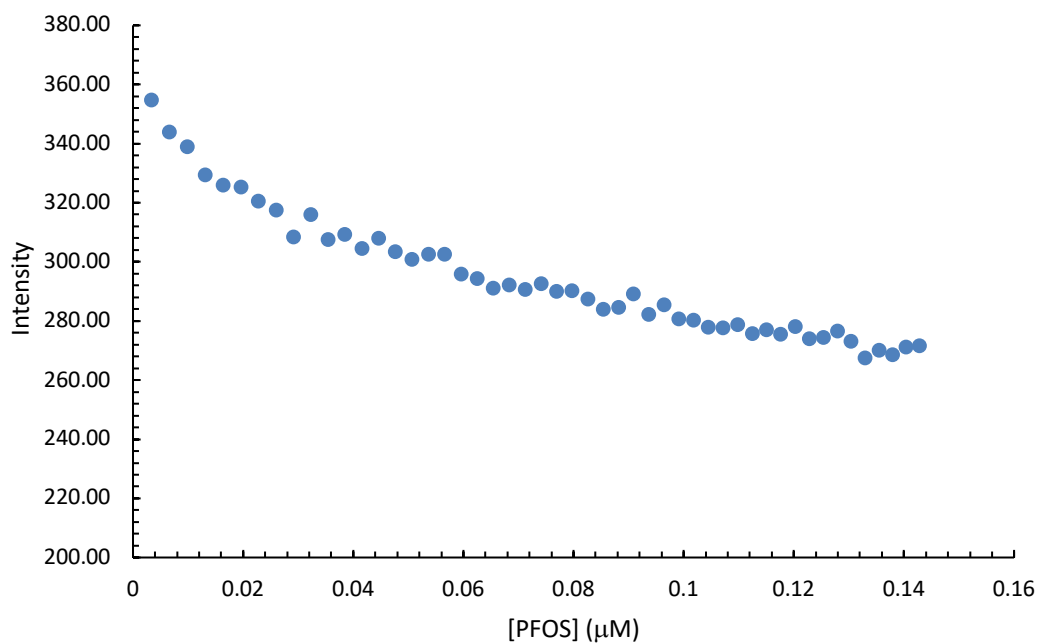


Figure 7.1.12 A plot of fluorescence intensity versus concentration of PFOS added to CPF at 25°C flushed with N₂ (g).

The low concentration of PFOS prevents the significant change in pH of the solution. A distribution of the CPF speciation is shown in Figure 7.1.13.

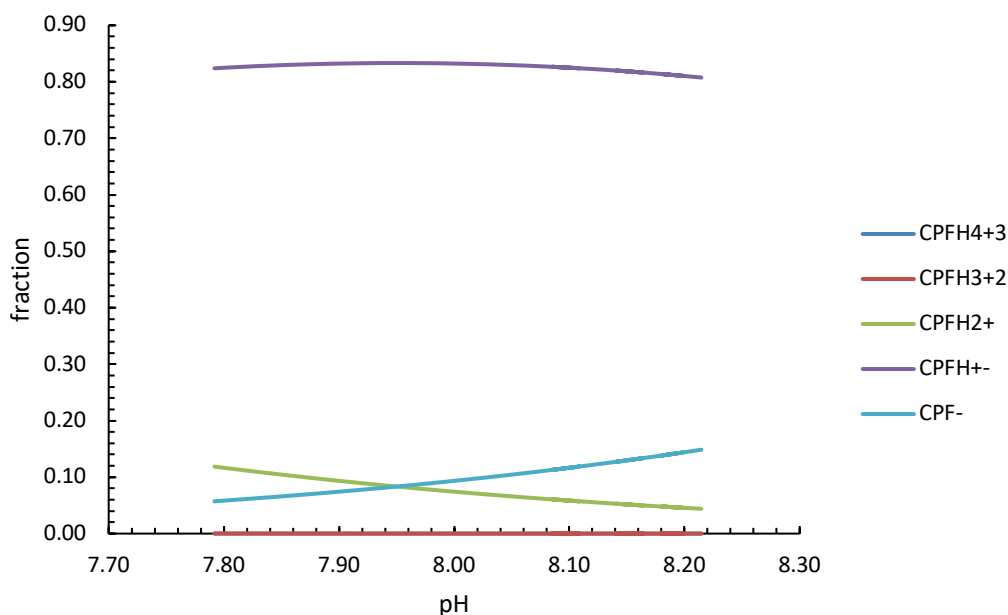


Figure 7.1.13 The distribution of CPF speciation from pH 7.75 – 8.25 \pm 0.01.

From Figure 7.1.13, it can be observed that the predominant species of CPF was CPFH^{+-} , followed by CPFH_2^{+} .

The plots of (F_0/F_T) versus $[S_T]$ were used instead of $S_T - \text{cac}$ due to the concentration of PFOS being significantly lower than the cac. A variation of Equation 1.3.12 was used when the cac is 0 therefore K_{n1}/n is also 0.

$$\frac{F_0}{F_T} = 1 + K_{11}S$$

A positive slope of the line is equal K_{11} binding constant. The fluorescence intensity was adjusted to account for each CPF species by multiplying it by α .

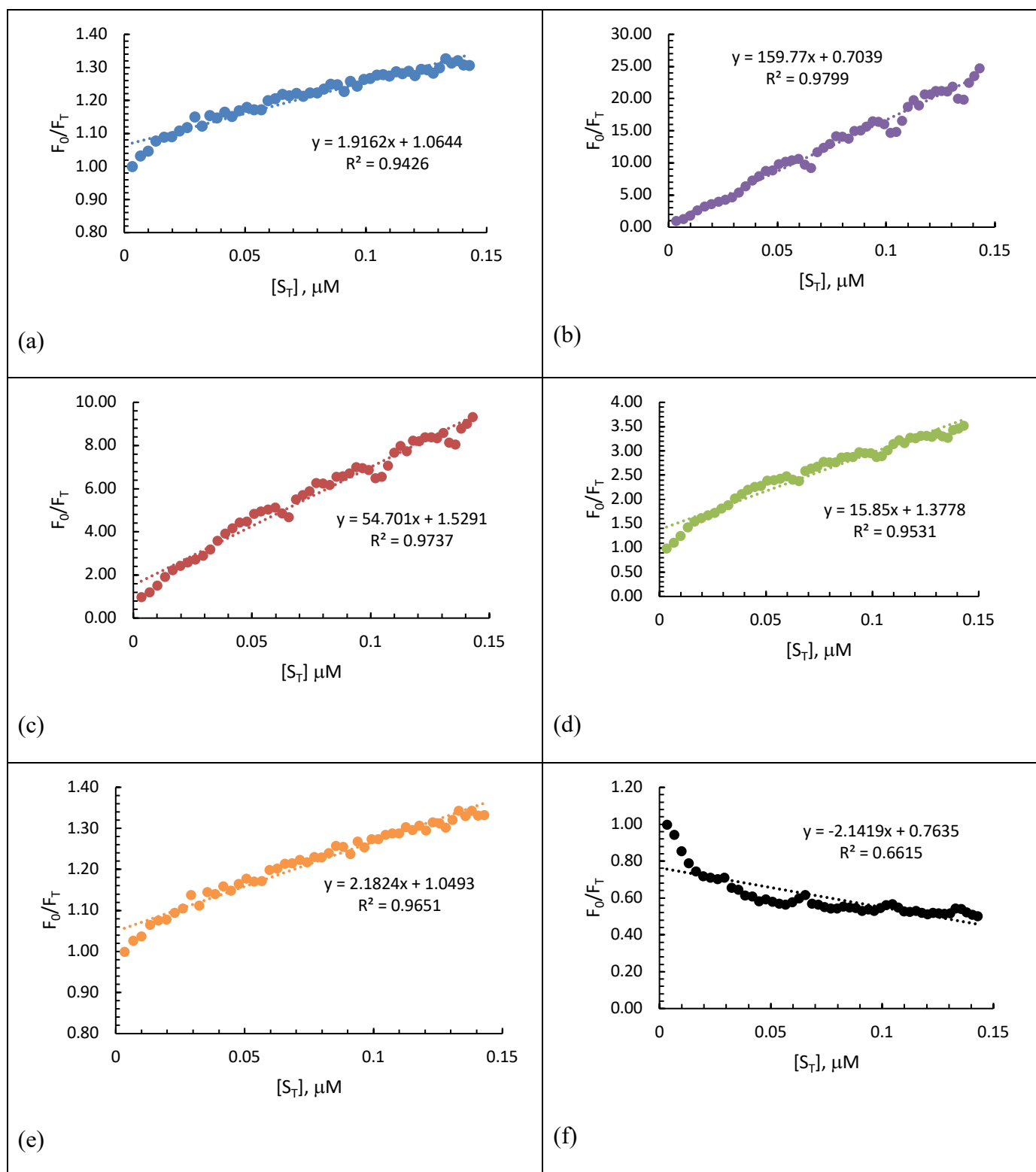


Figure 7.1.14 The equation $(F_0/F_T) = 1 + K_{11}[S]$ was used to determine K_{11} . A plot of (F_0/F_T) versus $[S_T]$ for no speciation of CPF (a), CPFH_4^{+3} (b), CPFH_3^{+2} (c), CPFH_2^{+} (d), CPFH^{+-} (e), CPF^- (f) at 25°C.

When no speciation is accounted for (Figure 7.1.14 (a)), there appears to be positive binding in the preaggregate phase of PFOS. There is a higher agreement to this binding theory due to the R^2 value of 0.9426.

CPFH_4^{+3} to have the greatest binding in the preaggregate phase of PFOS. The R^2 value is also the highest in Figure 7.1.14 (b).

The positive slope for this speciation is indicative of binding in the preaggregate phase with PFOS. The data for Figure 7.1.14 (c) has high agreement to the binding model due to the R^2 value.

In Figure 7.1.14 (d), the CPFH_2^{+} speciation shows to have positive binding in the preaggregate phase of PFOS. However, it is less compared to CPFH_4^{+3} and CPFH_3^{+2} . This speciation also fits the binding model due to the R^2 value of 0.9531.

The data in Figure 7.1.14 (e) it can be observed that there is minor binding with PFOS. The data in this figure similarly resembles the data from Figure 7.1.14 (a) when no speciation of CPF is accounted for. The speciation of CPF^- is the only speciation that does not display binding in the preaggregate phase. The R^2 value in Figure 7.1.14 (f) is indicative of the low agreement to the binding model for this species of CPF.

The binding constants obtained from Figure 7.1.14 (a) - Figure 7.1.14 (f) are summarized in Table 7.1.6. It was determined that the greatest binding from the second model was with CPFH_4^{+3} . While CPFH^{+-} is the greatest concentration present in solution,

it appears to be the greatest fluorescent contributing compound. Interestingly, while CPF⁻ was the second greatest speciation in solution, it did not contribute to any binding in the preaggregate phase of PFOS.

Table 7.1.6 Determination of preaggregate binding constant K_{11} for CPF species with PFOS surfactant extracted from the slope of Figure 7.1.14 (a) - Figure 7.1.14 (f) at 25°C.

	No Speciation	CPFH ₄ ⁺³	CPFH ₃ ⁺²	CPFH ₂ ⁺	CPFH ⁺⁻	CPF ⁻
Slope (μM^{-1})	1.92 ± 0.07	160 ± 3	55 ± 1	15.9 ± 0.5	2.18 ± 0.06	-2.14 ± 0.2
Intercept (μM^{-1})	1.1 ± 0.006	0.7 ± 0.3	1.5 ± 0.1	1.4 ± 0.04	1.1 ± 0.005	0.76 ± 0.02
R²	0.9426	0.9799	0.9737	0.9531	0.9651	0.6615
K₁₁ (μM^{-1})	1.9 ± 0.07	160 ± 3.3	55 ± 1.3	16 ± 0.5	2.2 ± 0.06	0*

Notes: The equation $(F_0/F_T) = 1 + K_{11}[S]$ was used to determine K_{11} . * K_{11} binding was negative for CPF⁻.

Due to PFOS being negatively charged, it is expected that the greatest interactions occur with CPFH₄⁺³, CPFH₃⁺² and CPFH₂⁺. This was confirmed with the K_{11} values obtained. Since the positively charged species of CPF had the lowest presence in solution at the experimental pH, this also confirms that the zwitterionic speciation is the greatest fluorescence contributing while the CPF⁻ species is the most free in solution due to the repulsion of the negative charges.

7.1.4 Conclusion of CPF and PFOS binding

Understanding the physical, non-covalent binding between CPF and PFOS requires several factors to be considered, including buffer and pH. It was observed that

the binding overall was less when a buffer was included in solution and PFOS was observed to precipitate out when the concentration was too high.

It was also determined that salt buffer affects the speciation of CPF as well as the interactions that occur with PFOS. It was observed that if the concentration of PFOS reached 50 mM in the presence of 0.1 M phosphate a precipitate formed. This in turn lowers the binding between CPF and PFOS. Also the buffer helps keeps the presence of the specific CPF species constant, therefore increases the accuracy of the binding constants determined. pH affects which species of CPF binds with PFOS. Due to PFOS acidity, without a buffer in solution, the pH can drastically change if the concentration of PFOS is too high.

There is also binding that occurs in the postaggregate phase with water along with CPF. The water occupies space which minimizes the amount of CPF within the aggregate. The number of aggregates PFOS forms is lower than other pseudophase compounds which is why the binding constants may be lower in comparison.

The interactions that occur in the preaggregate phase versus the postaggregate phase are significantly different. The more positively charged species of CPF displays greater binding in the preaggregate phase while the zwitterionic and negatively charged speciation contribute to more interactions in the pseudophase. This is due to the loss of the proton and overall negatively charged PFOS⁻.

To explain the low binding constant of small molecules like CPF with PFOS, one has to consider the solvation or hydration of fluorine in the perfluorinated chain. The perfluorination of the hydrocarbon chain in PFOS makes it extremely hydrophobic.

However, the F in monomer PFOS is strongly attached to hydrogen bonded water as shown in Figure 7.1.15, thus, reducing its hydrophobicity to some degree. This explains the significant solubility of PFOS in water 680 mg/L²² along with its propensity to form a weak pseudophase aggregate with a low aggregation number. PFOS is also a very strong acid (pK_a -3.3), therefore, the terminal anion is also strongly hydrated. This environment is not conducive to noncovalent binding with CPF species as reflected by the binding constants.

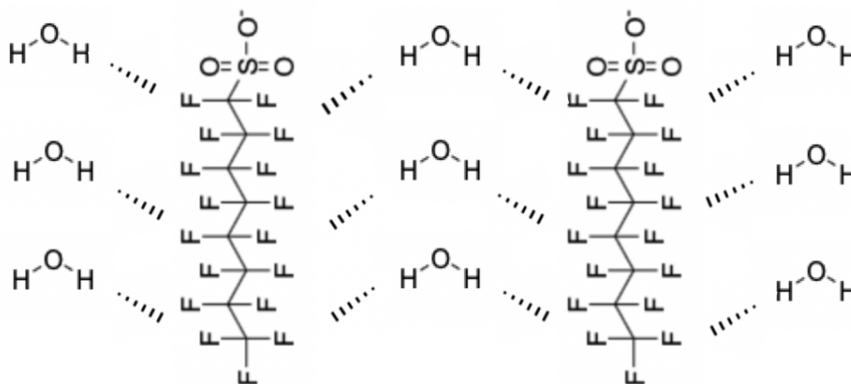


Figure 7.1.15 2:1 complex of water hydrogen binding with nearby PFOS in aqueous solution. The number of water molecules shown are much less for clarity.

As for the structure of the pseudophase, the water hydrogen in the shell could be strongly hydrogen bonded to fluorine and forms a very tight and stable shell structure as shown in Figure 7.1.16. The core size, therefore, could be minimized. With a smaller core with very low water concentration (on mole fraction basis), other guest molecules such as CPF species cannot partition in the core. The protonated $CPFH_2^+$ species are most likely

to stay close to the surface or the shell due to the attraction of fluorine- electron cloud and the protonated species at lower pH (< 7). The zwitterionic (or neutral) species should have some affinity to bind near the shell pseudophase of PFOS. Binding of solutes in these environments requires breaking the hydrogen bonded water to form new hydrogen bonds with molecular functional groups, which is not thermodynamically favorable.

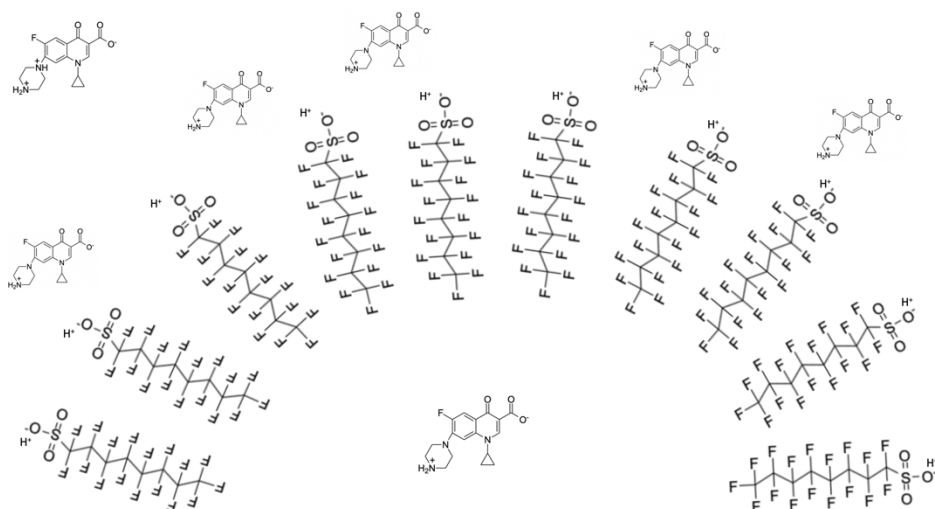


Figure 7.1.16 Figure shows a conceptual depiction of the pseudophase aggregate. A hemispherical part of the PFOS aggregate showing the shell and the core. At low pH (< 7) CPFH₂⁺ species remains in the outer edge while CPFH⁺ is weakly bound in the inside edge. This is speculated from the weak binding constants. The PFOS is shown as completely deprotonated base due to its low pK_a (-3.3)

This shows that the binding constants change depending on whether CPF is regarded as tetraprotic or triprotic acid. It is observed that the binding is greater when CPF is considered tetraprotic with $K_{n1} = 438.2 \pm 56 \text{ M}^{-1}$ and $175.7 \pm 14 \text{ M}^{-1}$ as a triprotic acid. However, the binding constants obtained are low in comparison to other surfactants, as observed in Yang et al.⁴² This could be due to the complex nature of both CPF and PFOS pseudophase and the low aggregation number of PFOS. In order to fully

understand the true binding between CPF and surfactant, it is necessary to understand the pH dependent speciation of CPF. Additional experiments such as NMR and quasielastic light scattering can be used to measure the exact aggregation number and size of the pseudophase microenvironment may provide further insight.

DETERMINATION OF CIPROFLOXACIN (CPF) AND DL- α -TOCOPHEROL SUCCINATE (TPGS-750M) PSEUDOPHASE INTERACTIONS

8.1 The binding of DL- α -tocopherol succinate (TPGS-750M) and Ciprofloxacin (CPF)

The description of the data obtained below is between CPF and TPGS-750M. The results obtained will be compared with the two binding equations as well as compared to other pseudophase aggregates.

8.1.1 Effect of TPGS-750M on CPF fluorescence

8.1.1.1 Concentration of TPGS-750M on fluorescence emission of CPF

A quenching of CPF fluorescence in the presence of TPGS-750M was observed as the concentration was increased up to 4500 μ M. This is observed in Figure 8.1.1. As the concentration of TPGS-750M increased the total fluorescence intensity decreased. This trend follows Stern-Volmer (SV) behavior, where the fluorescence intensity decreases as the concentration of the surfactant increases. This has not been observed for the CPF and SDS interactions as well as the CPF and PFOS interactions.

From the results displayed in Figure 8.1.1, there greatest error is observed in the error bar on the fourth data point.

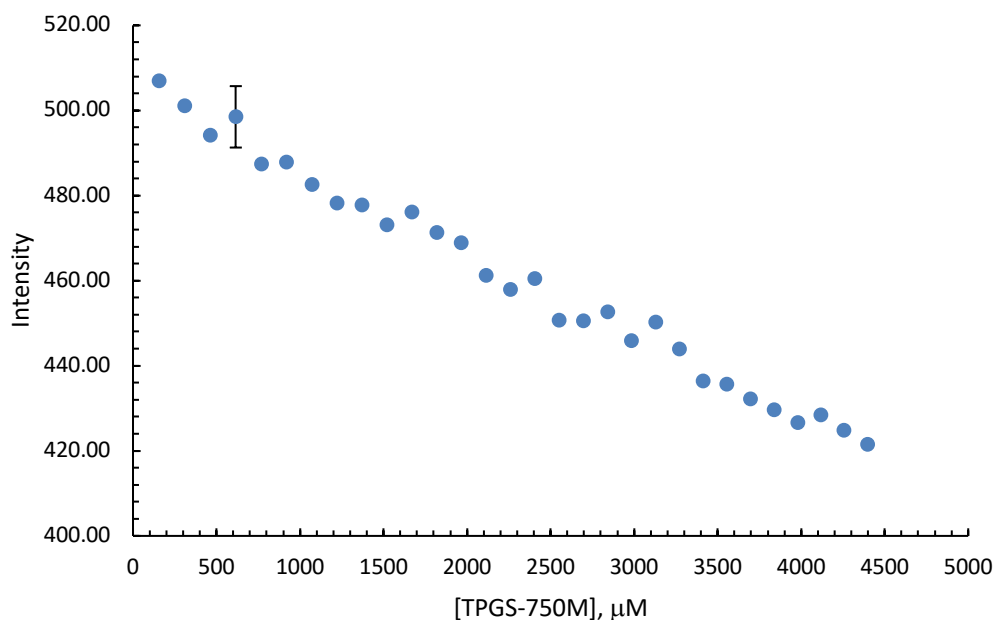


Figure 8.1.1 The fluorescence intensity versus concentration of TPGS-750M added to CPF.

The pH range of the solution was 7.77 through 7.59 ± 0.01 . The pH slightly decreased as the concentration of TPGS-750M increased. This is due to the solutions of this system being dissolved in distilled water instead of a buffer. This was to ensure that there was no salt effect from the buffer on the cac of the TPGS-750M.

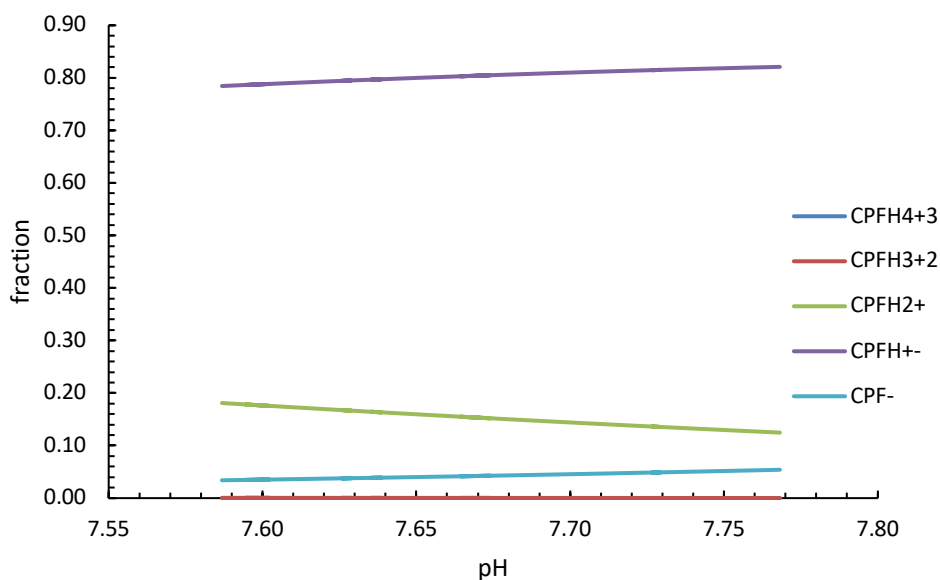


Figure 8.1.2 The distribution of CPF speciation at pH 7.60 – 7.77 ± 0.01.

From the distribution diagram presented in Figure 8.1.2, it can be determined that predominate speciation of CPF in solution with TPGS-750M is the zwitterionic CPFH⁺⁻ which is approximately 80% of all CPF present in solution. This is followed by the monoprotic CPFH₂⁺ and negatively charged CPF⁻. However, it is important to calculate binding constants for all five CPF species because it is possible that the smallest amount of the species present in solution, CPFH₄³⁺, could have the greatest binding with the TPGS-750M. It is also possible that the zwitterionic species could contribute the greatest to the fluorescence intensity obtained earlier. This will be determined through the binding equations and figures.

Similarly, to the data obtained of anthracene and TPGS-750M, the cac was determined when TPGS-750M was combined with CPF. This is shown in Figure 8.1.3.

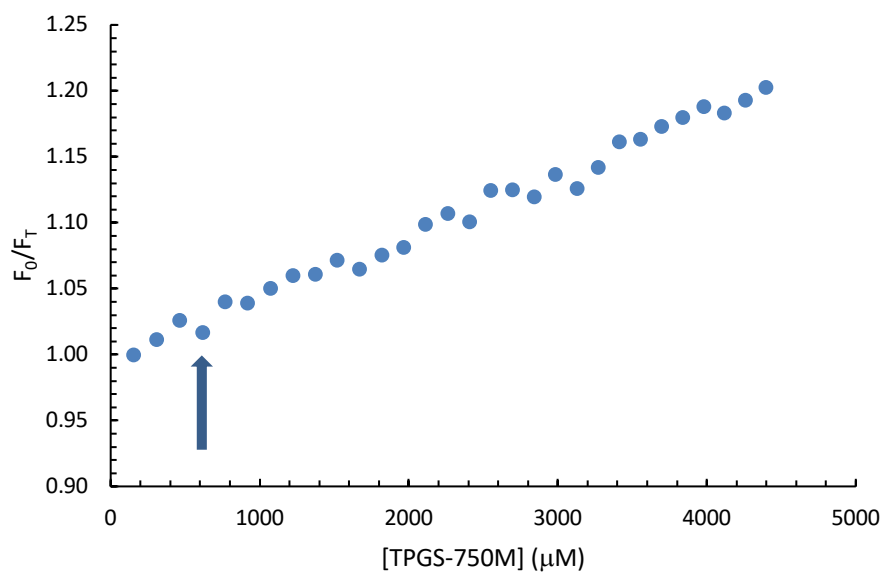


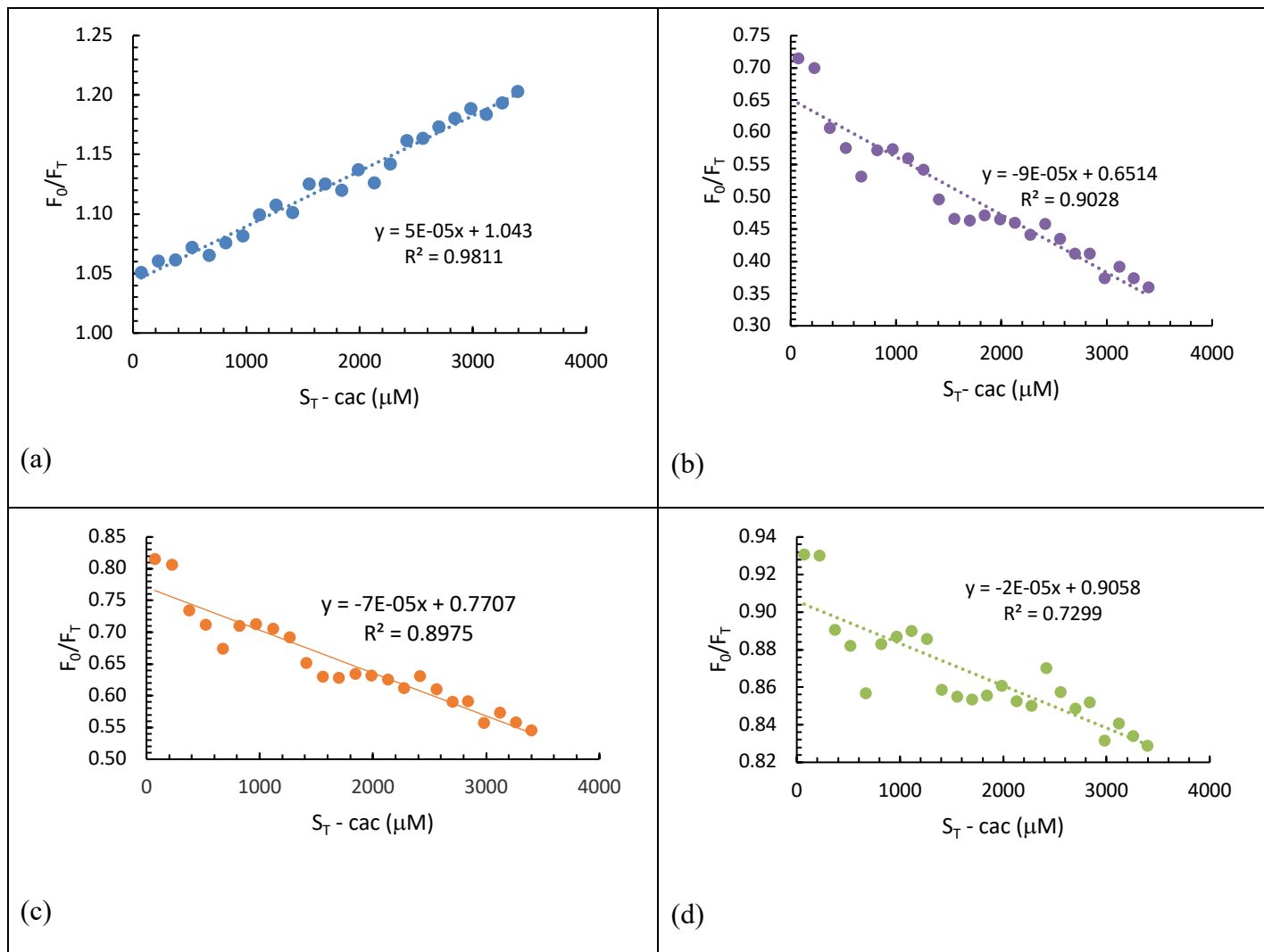
Figure 8.1.3 The determination of the experimental cac for TPGS-750M.

From Figure 8.1.3, it can be observed that the cac is lower than 1512 μM, which was the cac determined when TPGS-750M was combined with anthracene. Therefore, the cac used for the binding analysis was 1000 μM.

The upcoming plots pertain to the binding of CPF with TPGS-750M in the preaggregate and postaggregate phase for binding constants K_{11} and K_{n1}/n , respectively. The binding was determined using Equation 1.3.12 which is expressed below.

$$\frac{F_0}{F_T} = 1 + K_{11}S + \left(\frac{K_{n1}}{n}\right)(S_{T-cac})$$

α was applied to the fluorescence to account for all five species of CPF in order to precisely determine the magnitude binding.



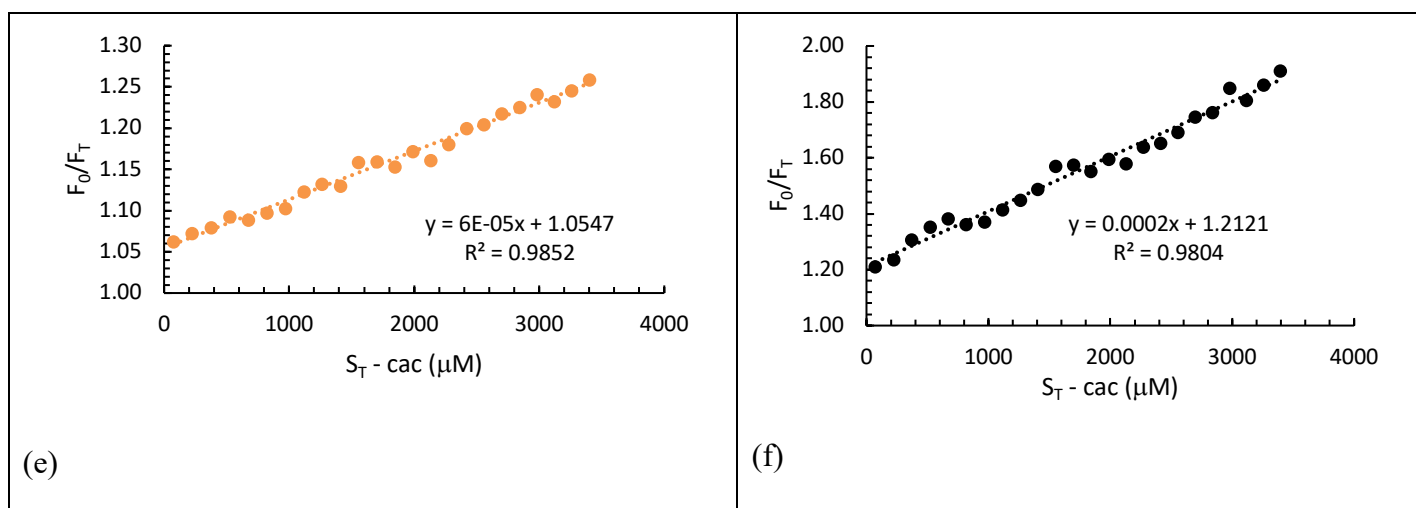


Figure 8.1.4 The equation $F_0/F_T = 1 + K_{11}[S] + (K_{n1}/n)(S_T - \text{cac})$ was used to determine K_{11} and K_{n1} . (F_0/F_T) versus $[S_T - \text{cac}]$ with no speciation of CPF (a) CPFH_4^{+3} (b) CPFH_3^{+2} (c), CPFH_2^+ (d), CPFH^{+-} (e) and CPF^- (f) at 25°C.

The positive slope obtained from Figure 8.1.4 (a) displays a positive binding for K_{n1}/n . From an initial comparison of the R^2 value of 0.9811 displays a high agreement to the binding model. Interestingly, for CPFH_4^{+3} (Figure 8.1.4 (b)), the slope is negative which implies no binding in the postaggregate region. The R^2 value was 9028. Similarly, Figure 8.1.4 (c) also has a negative slope which correlates to negative binding of K_{n1}/n and the R^2 value of this plot is 0.8975.

CPFH_2^+ is the second most abundant species in solution. However, the negative slope is indicative of no binding for this species of CPF. The R^2 value was 0.7299 showing less agreement compared to the other species of CPF.

The data obtained from Figure 8.1.4 (e) is the closest to the data obtained to when no speciation of CPF is considered. Therefore, while the CPFH^{+-} speciation is the greatest present in solution, it is the highest fluorescence emitting species.

In Figure 8.1.4 (f) for the CPF⁻ species, there appears to be binding in the pseudophase of TPGS-750M. The R² value from the figure above suggests an agreement to the F₀/F_T model.

8.1.2 Evaluation of CPF-TPGS-750M binding constants

8.1.2.1 Determination of the preaggregate and postaggregate binding of CPF with TPGS-750M

The K₁₁ and K_{n1}/n binding constants determined are shown in Table 8.1.1. For the binding constants determined, the values listed 0 either displayed no binding, or the error in the binding constant determined was greater than the value itself. Only the zwitterionic and negative speciation of CPF displayed binding in the postaggregate region of CPF. The preaggregate binding constant K₁₁ was determined for the zwitterionic and anionic speciation of CPF as well.

Table 8.1.1 Calculated K₁₁ and K_{n1}/n binding constants of CPF and TPGS-750M at 25°C extracted from the slope and intercept of Figure 8.1.4 (a) – (e). The literature aggregation number of 41 was used to determine K_{n1}.

	No Speciation	CPFH ₄ ⁺³	CPFH ₃ ⁺²	CPFH ₂ ⁺	CPFH ⁺⁻	CPF ⁻
Slope (μM⁻¹)	(5.0 ± 0.1) x 10 ⁻⁵	(-9.0 ± 0.6) x 10 ⁵	(-7.0 ± 0.5) x 10 ⁵	(-2.3 ± 0.3) x 10 ⁵	(6.0 ± 0.2) x 10 ⁻⁵	(2.0 ± 0.06) x 10 ⁻⁴
Intercept (μM⁻¹)	1.0 ± 0.003	0.65 ± 0.01	0.80 ± 0.01	0.90 ± 0.006	1.1 ± 0.003	1.2 ± 0.01
R²	0.9811	0.9028	0.8975	0.7299	0.9852	0.9804
K₁₁ (M⁻¹)	43 ± 2	0*	0*	0*	54.7 ± 2	212 ± 6
K_{n1}/n (M⁻¹)	50 ± 1	0*	0*	0*	60 ± 2	200 ± 6
K_{n1} (M⁻¹)	2050 ± 41	0*	0*	0*	2460 ± 82	8200 ± 246

Notes: The equation $F_0/F_T = 1 + K_{11}[S] + (K_{n1}/n)(S_T - \text{cac})$ was used to determine K₁₁ and K_{n1}. *K₁₁ and K_{n1} binding was negative for CPFH₄⁺³, CPFH₃⁺², CPFH₂⁺.

8.1.2.2 *The analysis of CPF and TPGS-750M monomer and pseudophase binding*

There appeared to be measurable binding in the preaggregate phase between two CPF species, including CPFH^{+-} and CPF^- , and TPGS-750M (Table 8.1.1). The species that appeared to display measurable binding in the postaggregate phase were also CPFH^{+-} and CPF^- . The data from CPFH^{+-} resembles the data from no speciation. Therefore, CPFH^{+-} is the most fluorescence contributing species out of all five species of CPF.

TPGS-750M overall a neutral compound, therefore in theory there would be interactions with all of the species of CPF. Since a majority of the interactions occurred in the postaggregate phase, it is hypothesized that the zwitterionic species has the greatest interactions with TPGS-750M due to the positive and negative charges on the species. This would have the best interactions with the polar and nonpolar structures of TPGS-750M. However, the greatest interactions occur with CPF^- . Therefore, CPF^- is the species that migrates into the hydrophobic core of the TPGS-750M pseudophase as well as interactions with the monomer before the cac. Since CPF^- interacts the most with TPGS-750M, it occupies the space and prevents CPFH^{+-} interactions.

If accounting for the K_{n1}/n binding constant determined for neutral anthracene and TPGS-750M of 562 ± 15 , the binding of zwitterionic CPF with TPGS-750M is significantly less with a value of 60 ± 2 . From the data, there appears to be an influence of overall structural charge on the binding with TPGS-750M.

Unfortunately, there has not been binding measured of TPGS with ciprofloxacin, anthracene or similar compounds using any method. Majority of binding studies of

TPGS-750M have occurred with nanoparticles or human serum albumin to serve as a catalyst. With TPGS-750M being a relatively new surfactant, it is possible for future experiments to be conducted to further understand the interactions that occur.

CONCLUSIONS AND FUTURE OUTLOOK

9.1 Conclusion and Future Outlook

Pseudophase compounds are molecular or micellar self-assembled aggregates that form in many natural aquatic environments. Pseudophase chemistry offers distinct advantages in modeling phase distributions or complexation in water-colloid and water-surfactant systems where the phases or microemulsions cannot be physically separated to assess binding constants. For example, the interactions can be observed *in vitro* at very low concentrations.

The binding model between solute binding or partitioning in monomer-monomer and monomer-aggregate systems using fluorescence spectroscopy has been enhanced. The currently published binding models are incomplete. The majority of previous studies consisted of three constituent systems, including the fluorescent probe, solvent and micelle or aggregate but failed to account for factors such as Cl^- and O_2 quenchers. These errors can significantly influence experimental outcomes and accuracy in binding analysis. However, it can be concluded from previous studies that binding between small solutes and surfactants occurs through weak noncovalent interactions.

To analyze the interactions between CPF and the corresponding pseudophase compounds, two key equations were used to account for fluorescence enhancement (FE) and fluorescence quenching like behavior (FQ):

Equation 9.1.1 Fluorescence quenching (FQ)

$$\frac{F_0}{F_T} = 1 + K_{11}[S] + \left(\frac{K_{n1}}{n}\right)(S_T - cac)$$

Equation 9.1.2 Fluorescence enhancement (FE)

$$\frac{F_T - F_0}{C_T \cdot \alpha} = k_C + (k_{11}K_{11})[S] + k_{n1}\left(\frac{K_{n1}}{n}\right)(S_T - cac)$$

F_T is the total fluorescence intensity while F_0 is the initial fluorescence of CPF. C_T is the total concentration of CPF and α is the fractional abundance of CPF distributed among 5 acid-base conjugates present at the corresponding pH. S_T is the total surfactant concentration; n is the aggregation number and cac is the critical aggregation concentration. K_{11} and K_{n1} were the preaggregate and postaggregate binding constants, respectively while k_C , k_{11} and k_{n1} represented the fluorescence efficiency of free CPF, bound CPF in the preaggregate phase and bound CPF in the postaggregate phase. Plots of (F_0/F_T) versus $[S_T - cac]$ accounted for FQ. FE was accounted for using the plot $(F_T - F_0)/(C_T \cdot \alpha)$ versus $[S_T - cac]$.

To improve upon previous solute-surfactant binding experiments, it was important to consider the acid-base chemistry of compounds such as CPF. CPF undergoes many structural changes through proton exchange. As a result, any of five chemical species may be predominant depending on solution pH. Speciation alone can substantially influence the binding between CPF and surfactants. While literature has determined different structures of CPF and the species, they do not account for them when

calculating the binding constants. Interactions will also change as the surfactant passes the cac and becomes an aggregate. The interactions are weak and noncovalent, however once the aggregate forms, the fluorophore's binding occurs within the aggregate and outside of it. Therefore, the importance of this study was the specification of CPF speciation in solution at a certain pH and determining the interactions of each species with the pseudophase compounds.

It is also important to minimize interferences in fluorescence measurements. This is most commonly done by eliminating interfering co-quenchers in solution through purging volatile quenchers with nitrogen gas or not dissolving the fluorophore in solutions containing Cl^- . The accuracy in binding constants will increase by minimizing interfering co-quenchers in solution.

Anthracene was the model compound used to confirm the FQ binding theory with TPGS-750M. Since TPGS-750M and anthracene have no pK_a or charge, this simplified the binding theory without the need to account for α . It was determined that the binding constants in the preaggregate and postaggregate phase were $K_{11} 292 \pm 8 \text{ M}^{-1}$ and $K_{n1} 2.77 (\pm 0.05) \times 10^4 \text{ M}^{-1}$, respectively. Therefore, a majority of the anthracene likely resided within the hydrophobic core of the TPGS-750M pseudophase.

CPF was best treated as a tetraprotic compound with five species interacting individually with surfactants. All five species of CPF were included order to determine the binding constants with the pseudophase compounds. Interestingly, the most abundant species in solution did not exhibit the greatest binding in solution. The most abundant species would contribute to the total fluorescence intensity of the CPF and pseudophase

interactions. The interactions appeared to vary with pH because they were greater with Anthracene – TPGS 750M compared to CPF-TPGS - 750M where K_{n1} was $2.77 (\pm 0.05) \times 10^4 \text{ M}^{-1}$ and 2500 ± 82 respectively. That was certainly unexpected.

The binding was observed to be greater when CPF was considered a tetraprotic acid compared to a triprotic acid when bound to PFOS where the pseudophase binding constants were K_{n1} of $438.2 \pm 56 \text{ M}^{-1}$ and $175.7 \pm 14 \text{ M}^{-1}$ with CPFH^{+-} , respectively. When PFOS was added with a phosphate buffer, a white solid (PFOS-Na) would precipitate out when the concentration of PFOS was greater than or equal to 50 mM. This affected the binding with CPF. The greatest binding between all of the pseudophase compounds occurred with CPF- SDS complexation in the postaggregate phase with a K_{n1} of 1780 ± 71 for the CPFH^{+-} species.

CPFH^{+-} is the species that has the most consistent binding with all of the pseudophase compounds. This is due to the positive and negative charges on the structure, which allows the species to interact with both anionic and nonionic pseudophase compounds. While the interactions are weak, CPFH^{+-} resided within the hydrophobic core of the pseudophase compounds.

Future outlook would be to expand on more cationic pseudophase compounds to observe the effects on binding with CPF. Time resolved fluorescence (TRF) would enhance the experiments as it would determine the overall fluorescence lifetime. This would provide information on the chemical kinetics of the photodegradation and could specify the type of fluorescence interactions that occur between fluorophores and

pseudophase compounds. Dynamic light scattering (DLS) would enhance the experiments in order to determine the experimental aggregation number of each pseudophase compound. This would confirm if effects of pH and salt buffer also affected the aggregation of the pseudophase compounds.

The use of NMR to further understand the protonation and deprotonation of CPF. While the structures of the five species were established, they were not confirmed by the experimentation conducted. Delving deeper into the acid dissociation constants, the microscopic dissociation constants that make up the acid dissociation constants. The microscopic dissociation constants are fractional deprotonations and the dissociations occur at a short period of time.

The microscopic dissociation constants can also be determined through fluorescence⁷. However, something to account for would be that excited-state pK_a values are lower compared to ground-state pK_a values, which can be compared to further understand CPF acid dissociation through the Förster cycle⁹⁰. These experiments would enhance understanding the interactions that occur between CPF and other fluoroquinolones and pseudophase compounds.

REFERENCES

- (1) Maia, A. S.; Ribeiro, A. R.; Amorim, C. L.; Barreiro, J. C.; Cass, Q. B.; Castro, P. M. L.; Tiritan, M. E. Degradation of Fluoroquinolone Antibiotics and Identification of Metabolites/Transformation Products by Liquid Chromatography–Tandem Mass Spectrometry. *J. Chromatogr. A* **2014**, *1333*, 87–98. <https://doi.org/10.1016/j.chroma.2014.01.069>.
- (2) Wilkinson, J.; Hooda, P. S.; Barker, J.; Barton, S.; Swinden, J. Occurrence, Fate and Transformation of Emerging Contaminants in Water: An Overarching Review of the Field. *Environ. Pollut.* **2017**, *231*, 954–970. <https://doi.org/10.1016/j.envpol.2017.08.032>.
- (3) Liang, Y.-D.; Song, J.-F.; Yang, X.-F. Flow-Injection Chemiluminescence Determination of Fluoroquinolones by Enhancement of Weak Chemiluminescence from Peroxynitrous Acid. *Anal. Chim. Acta* **2004**, *510* (1), 21–28. <https://doi.org/10.1016/j.aca.2003.12.054>.
- (4) Nazar, M. F.; Azeem, W.; Rana, U. A.; Ashfaq, M.; Lashin, A.; Al-Arifi, N.; Rahman, H. M. A. U.; Lazim, A. M.; Mahmood, A. PH-Dependent Probing of Levofloxacin Assimilated in Surfactant Mediated Assemblies: Insights from Photoluminescent and Chromatographic Measurements. *J. Mol. Liq.* **2016**, *220*, 26–32. <https://doi.org/10.1016/j.molliq.2016.04.044>.
- (5) Golet, E. M.; Xifra, I.; Siegrist, H.; Alder, A. C.; Giger, W. Environmental Exposure Assessment of Fluoroquinolone Antibacterial Agents from Sewage to Soil. *Environ. Sci. Technol.* **2003**, *37* (15), 3243–3249. <https://doi.org/10.1021/es0264448>.
- (6) Rusu, A.; Tóth, G.; Szöcs, L.; Kökösi, J.; Kraszni, M.; Gyéresi, Á.; Noszál, B. Triprotic Site-Specific Acid–Base Equilibria and Related Properties of Fluoroquinolone Antibacterials. *J. Pharm. Biomed. Anal.* **2012**, *66*, 50–57. <https://doi.org/10.1016/j.jpba.2012.02.024>.
- (7) Huangh, Z. Fluorescence Investigation of Some Fluoroquinolones in Various Media: Ground-State Acid-Base Equilibria. *Anal. Sci.* **1997**, *4*.
- (8) Lin, C.-E.; Deng, Y.-J.; Liao, W.-S.; Sun, S.-W.; Lin, W.-Y.; Chen, C.-C. Electrophoretic Behavior and PKa Determination of Quinolones with a Piperazinyl Substituent by Capillary Zone Electrophoresis. *J. Chromatogr. A* **2004**, *1051* (1–2), 283–290. <https://doi.org/10.1016/j.chroma.2004.08.069>.
- (9) Mella, M.; Fasani, E.; Albini, A. Photochemistry of 1-Cyclopropyl-6-Fluoro-1,4-Dihydro-4-Oxo-7- (Piperazin-1-Yl)Quinoline-3-Carboxylic Acid (=Ciprofloxacin) in Aqueous Solutions. *Helv. Chim. Acta* **2001**, *84* (9), 2508. [https://doi.org/10.1002/1522-2675\(20010919\)84:9<2508::AID-HLCA2508>3.0.CO;2-Y](https://doi.org/10.1002/1522-2675(20010919)84:9<2508::AID-HLCA2508>3.0.CO;2-Y).
- (10) Stahlmann, R.; Lode, H. Toxicity of Quinolones: *Drugs* **1999**, *58* (Supplement 2), 37–42. <https://doi.org/10.2165/00003495-199958002-00007>.

- (11) Salma, A.; Thoröe-Boveleth, S.; Schmidt, T. C.; Tuerk, J. Dependence of Transformation Product Formation on PH during Photolytic and Photocatalytic Degradation of Ciprofloxacin. *J. Hazard. Mater.* **2016**, *313*, 49–59. <https://doi.org/10.1016/j.jhazmat.2016.03.010>.
- (12) Caliman, F. A.; Gavrilescu, M. Pharmaceuticals, Personal Care Products and Endocrine Disrupting Agents in the Environment - A Review. *CLEAN - Soil Air Water* **2009**, *37* (4–5), 277–303. <https://doi.org/10.1002/clen.200900038>.
- (13) Movaghati, S.; Moosavi-Movahedi, A. A.; Khodaghali, F.; Digaleh, H.; Kachooei, E.; Sheibani, N. Sodium Dodecyl Sulphate Modulates the Fibrillation of Human Serum Albumin in a Dose-Dependent Manner and Impacts the PC12 Cells Retraction. *Colloids Surf. B Biointerfaces* **2014**, *122*, 341–349. <https://doi.org/10.1016/j.colsurfb.2014.07.002>.
- (14) Singer, M. M.; Tjeerdema, R. S. Fate and Effects of the Surfactant Sodium Dodecyl Sulfate. In *Reviews of Environmental Contamination and Toxicology*; Ware, G. W., Ed.; Springer New York, 1993; pp 95–149.
- (15) Hartley, G. S. State of Solution of Colloidal Electrolytes. *Q. Rev. Chem. Soc.* **1948**, *2* (2), 152. <https://doi.org/10.1039/qr9480200152>.
- (16) Falbe, J. *Surfactants in Consumer Products: Theory, Technology and Application*; Springer-Verlag, 1987.
- (17) Lehmler, H.-J. Synthesis of Environmentally Relevant Fluorinated Surfactants—a Review. *Chemosphere* **2005**, *58* (11), 1471–1496. <https://doi.org/10.1016/j.chemosphere.2004.11.078>.
- (18) Hansen, K. J.; Johnson, H. O.; Eldridge, J. S.; Butenhoff, J. L.; Dick, L. A. Quantitative Characterization of Trace Levels of PFOS and PFOA in the Tennessee River. *Environ. Sci. Technol.* **2002**, *36* (8), 1681–1685. <https://doi.org/10.1021/es010780r>.
- (19) Wang, F.; Liu, C.; Shih, K. Adsorption Behavior of Perfluorooctanesulfonate (PFOS) and Perfluorooctanoate (PFOA) on Boehmite. *Chemosphere* **2012**, *89* (8), 1009–1014. <https://doi.org/10.1016/j.chemosphere.2012.06.071>.
- (20) Qian, J.; Shen, M.; Wang, P.; Wang, C.; Li, K.; Liu, J.; Lu, B.; Tian, X. Perfluorooctane Sulfonate Adsorption on Powder Activated Carbon: Effect of Phosphate (P) Competition, PH, and Temperature. *Chemosphere* **2017**, *182*, 215–222. <https://doi.org/10.1016/j.chemosphere.2017.05.033>.
- (21) Bull, S.; Burnett, K.; Vassaux, K.; Ashdown, L.; Brown, T.; Rushton, L. Extensive Literature Search and Provision of Summaries of Studies Related to the Oral Toxicity of Perfluoroalkylated Substances (PFASs), Their Precursors and Potential Replacements in Experimental Animals and Humans. Area 1: Data on Toxicokinetics (Absorption, Distribution, Metabolism, Excretion) in in Vitro Studies, Experimental Animals and Humans. Area 2: Data on Toxicity in Experimental Animals. Area 3: Data on Observations in Humans. *EFSA Support. Publ.* **2014**, *11* (4). <https://doi.org/10.2903/sp.efsa.2014.EN-572>.
- (22) Perfluoroalkylated Substances: PFOA, PFOS and PFOSA Evaluation of Health Hazards and Proposal of a Health Based Quality Criterion for Drinking Water, Soil and Ground Water. 2015.

- (23) Drinking Water Health Advisory for Perfluorooctane Sulfonate (PFOS). **2016**, 88.
- (24) Zhang, X.; Chen, L.; Fei, X.-C.; Ma, Y.-S.; Gao, H.-W. Binding of PFOS to Serum Albumin and DNA: Insight into the Molecular Toxicity of Perfluorochemicals. *BMC Mol. Biol.* **2009**, *10* (1), 16. <https://doi.org/10.1186/1471-2199-10-16>.
- (25) Chen, Y.-M.; Guo, L.-H. Fluorescence Study on Site-Specific Binding of Perfluoroalkyl Acids to Human Serum Albumin. *Arch. Toxicol.* **2009**, *83* (3), 255–261. <https://doi.org/10.1007/s00204-008-0359-x>.
- (26) Lipshutz, B. H.; Bošković, Z.; Crowe, C. S.; Davis, V. K.; Whittemore, H. C.; Vosburg, D. A.; Wenzel, A. G. “Click” and Olefin Metathesis Chemistry in Water at Room Temperature Enabled by Biodegradable Micelles. *J. Chem. Educ.* **2013**, *90* (11), 1514–1517. <https://doi.org/10.1021/ed300893u>.
- (27) Andersson, M. P.; Gallou, F.; Klumphu, P.; Takale, B. S.; Lipshutz, B. H. Structure of Nanoparticles Derived from Designer Surfactant TPGS-750-M in Water, As Used in Organic Synthesis. *Chem. - Eur. J.* **2018**, *24* (26), 6778–6786. <https://doi.org/10.1002/chem.201705524>.
- (28) Puig-Rigall, J.; Grillo, I.; Dreiss, C. A.; González-Gaitano, G. Structural and Spectroscopic Characterization of TPGS Micelles: Disruptive Role of Cyclodextrins and Kinetic Pathways. *Langmuir* **2017**, *33* (19), 4737–4747. <https://doi.org/10.1021/acs.langmuir.7b00701>.
- (29) Lipshutz, B. H.; Ghorai, S. Transitioning Organic Synthesis from Organic Solvents to Water. What’s Your E Factor? *Green Chem* **2014**, *16* (8), 3660–3679. <https://doi.org/10.1039/C4GC00503A>.
- (30) Sadoqi, M.; Lau-Cam, C. A.; Wu, S. H. Investigation of the Micellar Properties of the Tocopheryl Polyethylene Glycol Succinate Surfactants TPGS 400 and TPGS 1000 by Steady State Fluorometry. *J. Colloid Interface Sci.* **2009**, *333* (2), 585–589. <https://doi.org/10.1016/j.jcis.2009.01.048>.
- (31) Lipshutz, B. H.; Subir, G. Green Chemistry in the Introductory Organic Laboratory. **2015**, *48* (1), 23–24.
- (32) Boggs, J. M. Myelin Basic Protein: A Multifunctional Protein. *Cell. Mol. Life Sci.* **2006**, *63* (17), 1945–1961. <https://doi.org/10.1007/s00018-006-6094-7>.
- (33) Hashim, G. A. Myelin Basic Protein: Structure, Function and Antigenic Determinants. *Immunol. Rev.* **1978**, *39* (1), 60–107. <https://doi.org/10.1111/j.1600-065X.1978.tb00397.x>.
- (34) Di Salvo, C.; Barreca, D.; Laganà, G.; di Bella, M.; Tellone, E.; Ficarra, S.; Bellocco, E. Myelin Basic Protein: Structural Characterization of Spherulites Formation and Preventive Action of Trehalose. *Int. J. Biol. Macromol.* **2013**, *57*, 63–68. <https://doi.org/10.1016/j.ijbiomac.2013.02.022>.
- (35) Jones, A. J. S.; Rumsby, M. G. Interaction of the Myelin Basic Protein with the Anionic Detergent Sodium Dodecyl Sulphate. *Biochem. J.* **1978**, *169* (2), 281–285. <https://doi.org/10.1042/bj1690281>.
- (36) Randall, C. S.; Zand, R. Spectroscopic Assessment of Secondary and Tertiary Structure in Myelin Basic Protein. *Biochemistry* **1985**, *24* (8), 1998–2004. <https://doi.org/10.1021/bi00329a030>.

- (37) Kalyanasundaram, K. *Photochemistry in Microheterogeneous Systems*; Academic Press Inc, 1987.
- (38) Turro, N. J.; Lee, P. C. C. Perfluorinated “Mini” Micelles: Energy Transfer from Benzophenone and Determination of Aggregation Number. *J. Phys. Chem.* **1982**, *86* (17), 3367–3371. <https://doi.org/10.1021/j100214a020>.
- (39) Shtykov, S. N.; Smirnova, T. D.; Bylinkin, Yu. G.; Kalashnikova, N. V.; Zhemerichkin, D. A. Determination of Ciprofloxacin and Enrofloxacin by the Sensitized Fluorescence of Europium in the Presence of the Second Ligand and Micelles of Anionic Surfactants. *J. Anal. Chem.* **2007**, *62* (2), 136–140. <https://doi.org/10.1134/S1061934807020062>.
- (40) Nazar, M. F.; Azeem, W.; Kayani, A.; Zubair, M.; John, P.; Mahmood, A.; Ashfaq, M.; Zafar, M. N.; Sumrra, S. H.; Zafar, M. N. PH-Dependent Antibiotic Gatifloxacin Interacting with Cationic Surfactant: Insights from Spectroscopic and Chromatographic Measurements. *J. Solut. Chem.* **2019**, *48* (7), 936–948. <https://doi.org/10.1007/s10953-018-0811-3>.
- (41) Khan, A. M.; Shah, S. S. Fluorescence Spectra Behavior of Ciprofloxacin HCl in Aqueous Medium and Its Interaction with Sodium Dodecyl Sulfate. *J. Dispers. Sci. Technol.* **2009**, *30* (7), 997–1002. <https://doi.org/10.1080/01932690802701523>.
- (42) Yang, R.; Fu, Y.; Li, L.-D.; Liu, J.-M. Medium Effects on Fluorescence of Ciprofloxacin Hydrochloride. *Spectrochim. Acta. A. Mol. Biomol. Spectrosc.* **2003**, *59* (12), 2723–2732. [https://doi.org/10.1016/s1386-1425\(03\)00059-3](https://doi.org/10.1016/s1386-1425(03)00059-3).
- (43) Roelants, E.; De Schryver, F. C. Parameters Affecting Aqueous Micelles of CTAC, TTAC, and DTAC Probed by Fluorescence Quenching. *Langmuir* **1987**, *3* (2), 209–214. <https://doi.org/10.1021/la00074a011>.
- (44) Söderman, O.; Stilbs, P.; Price, W. S. NMR Studies of Surfactants: NMR Studies of Surfactants. *Concepts Magn. Reson. Part A* **2004**, *23A* (2), 121–135. <https://doi.org/10.1002/cmr.a.20022>.
- (45) Furó, I. NMR Spectroscopy of Micelles and Related Systems. *J. Mol. Liq.* **2005**, *117* (1–3), 117–137. <https://doi.org/10.1016/j.molliq.2004.08.010>.
- (46) Söderman, O.; Stilbs, P. NMR Studies of Complex Surfactant Systems. *Prog. Nucl. Magn. Reson. Spectrosc.* **1994**, *26*, 445–482. [https://doi.org/10.1016/0079-6565\(94\)80013-8](https://doi.org/10.1016/0079-6565(94)80013-8).
- (47) Sharma, R.; Mahajan, S.; Mahajan, R. K. Surface Adsorption and Mixed Micelle Formation of Surface Active Ionic Liquid in Cationic Surfactants: Conductivity, Surface Tension, Fluorescence and NMR Studies. *Colloids Surf. Physicochem. Eng. Asp.* **2013**, *427*, 62–75. <https://doi.org/10.1016/j.colsurfa.2013.03.023>.
- (48) Khan, A. M.; Shah, S. S. PH Induced Partitioning and Interactions of Ciprofloxacin Hydrochloride with Anionic Surfactant Sodium Dodecyl Sulfate Using Ultraviolet and Fourier Transformed Infrared Spectroscopy Study. *J. Dispers. Sci. Technol.* **2009**, *30* (9), 1247–1254. <https://doi.org/10.1080/01932690902735058>.

- (49) Misra, P. K.; Mishra, B. K.; Behera, G. B. Micellization of Ionic Surfactants in Tetrahydrofuran-Water and Acetonitrile-Water Mixed-Solvent Systems. *Colloids Surf.* **1991**, 57 (1), 1–10. [https://doi.org/10.1016/0166-6622\(91\)80175-N](https://doi.org/10.1016/0166-6622(91)80175-N).
- (50) Zięba, A.; Maślankiewicz, A.; Sitkowski, J. ¹H, ¹³C And ¹⁵N NMR Spectra of Ciprofloxacin. *Magn. Reson. Chem.* **2004**, 42 (10), 903–904. <https://doi.org/10.1002/mrc.1468>.
- (51) Harris, D. C. *Quantitative Chemical Analysis*, 8th ed.; W.H. Freeman and Co: New York, 2010.
- (52) Polster, J.; Lachmann, H. *Spectrometric Titrations*; VHC, 1989.
- (53) Anslyn, E. V.; Dougherty, D. A. *Modern Physical Organic Chemistry*; University Science: Sausalito, CA, 2006.
- (54) Benesi, H. A.; Hildebrand, J. H. A Spectrophotometric Investigation of the Interaction of Iodine with Aromatic Hydrocarbons. *J. Am. Chem. Soc.* **1949**, 71 (8), 2703–2707. <https://doi.org/10.1021/ja01176a030>.
- (55) Scott, R. Some Comments on the Benesi-Hildebrand Equation. *Recl. Trav. Chim. Pays-Bas* **1956**, 75 (7), 787–789.
- (56) de La Guardia, M.; Peris-Cardells, E.; Sancenón, J.; Carrión, J. L.; Pramauro, E. Fluorimetric Determination of Binding Constants between Micelles and Chemical Systems. *Microchem. J.* **1991**, 44 (2), 193–200. [https://doi.org/10.1016/0026-265x\(91\)90098-a](https://doi.org/10.1016/0026-265x(91)90098-a).
- (57) Encinas, M. V.; Lissi, E. A. Evaluation of Partition Constants in Compartmentalised Systems from Fluorescence Quenching Data. *Chem. Phys. Lett.* **1982**, 91 (1), 55–57. [https://doi.org/10.1016/0009-2614\(82\)87031-0](https://doi.org/10.1016/0009-2614(82)87031-0).
- (58) van de Weert, M.; Stella, L. Fluorescence Quenching and Ligand Binding: A Critical Discussion of a Popular Methodology. *J. Mol. Struct.* **2011**, 998 (1–3), 144–150. <https://doi.org/10.1016/j.molstruc.2011.05.023>.
- (59) Banipal, T. S.; Kaur, R.; Banipal, P. K. Effect of Sodium Chloride on the Interactions of Ciprofloxacin Hydrochloride with Sodium Dodecyl Sulfate and Hexadecyl Trimethylammonium Bromide: Conductometric and Spectroscopic Approach. *J. Mol. Liq.* **2018**, 255, 113–121. <https://doi.org/10.1016/j.molliq.2018.01.089>.
- (60) Eljack, M. D.; Wilson, R. E.; Hussam, A.; Khan, S. U. Development of an Equilibrium Headspace Gas Chromatographic Method for the Measurement of Noncovalent Association and Partitioning of N-Alkylbenzenes at Infinite Dilution in Fulvic Acid Pseudophase. *J. Chromatogr. A* **2015**, 1383, 1–7. <https://doi.org/10.1016/j.chroma.2015.01.021>.
- (61) Hussam, Abul.; Basu, S. C.; Hixon, Mark.; Olumee, Zohra. General Method for the Study of Solute-Surfactant Association Equilibria of Volatile Solutes by Head Space Gas Chromatography. *Anal. Chem.* **1995**, 67 (8), 1459–1464. <https://doi.org/10.1021/ac00104a024>.
- (62) Eljack, M.; Hussam, A. Novel Equilibrium Headspace Gas Chromatographic Technique for the Measurement of Noncovalent Association and Partition of N-Alkylbenzenes in Water/n-Dodecane and Water/1-Octanol Systems at Low Phase

- Ratio without Phase Separation. *Fluid Phase Equilibria* **2014**, *384*, 60–67. <https://doi.org/10.1016/j.fluid.2014.10.024>.
- (63) Roelants, E.; Geladé, E.; Smid, J.; De Schryver, F. C. A Study of Temperature Dependence of the Mean Aggregation Number and the Kinetic Parameters of Quenching in CTAC and TTAC Micelles. *J. Colloid Interface Sci.* **1985**, *107* (2), 337–344. [https://doi.org/10.1016/0021-9797\(85\)90186-9](https://doi.org/10.1016/0021-9797(85)90186-9).
 - (64) Nithipatikom, K.; McGown, L. B. Effects of Metal Cations on the Fluorescence Intensity of Polycyclic Aromatic Hydrocarbons in Sodium Taurocholate Micellar Solutions. *Anal. Chem.* **1988**, *60* (10), 1043–1045. <https://doi.org/10.1021/ac00161a018>.
 - (65) Schwarz, F. P.; Wasik, S. P. Fluorescence Measurements of Benzene, Naphthalene, Anthracene, Pyrene, Fluoranthene, and Benzo[e]Pyrene in Water. *Anal. Chem.* **1976**, *48* (3), 524–528. <https://doi.org/10.1021/ac60367a046>.
 - (66) Nakajima, A. Fluorescence Spectra of Anthracene and Pyrene in Water and in Aqueous Surfactant Solution. *J. Lumin.* **1977**, *15* (3), 277–282. [https://doi.org/10.1016/0022-2313\(77\)90027-8](https://doi.org/10.1016/0022-2313(77)90027-8).
 - (67) Sambursky, S.; Wolfsohn, G. On the Fluorescence and Absorption Spectra of Anthracene and Phenanthrene in Solutions. *Trans. Faraday Soc.* **1940**, *35*, 427. <https://doi.org/10.1039/tf9403500427>.
 - (68) Tigoianu, R.-I.; Airinei, A.; Dorohoi, D.-O. Solvent Influence on the Electronic Fluorescence Spectra of Anthracene. *REV CHIM* **2010**, *4*.
 - (69) Bhattacharya, S. C.; Das, H. T.; Moulik, S. P. Quenching of Fluorescence of 2-Anthracene Sulphonate by Cetylpyridinium Chloride in Micellar Solutions of Tweens, Triton X-100, Sodium Dodecylsulphate (SDS) and Cetyltrimethylammonium Bromide (CTAB). *J. Photochem. Photobiol. Chem.* **1993**, *71* (3), 257–262. [https://doi.org/10.1016/1010-6030\(93\)85007-U](https://doi.org/10.1016/1010-6030(93)85007-U).
 - (70) Guetzloff, T. F.; Rice, J. A. Micellar Nature of Humic Colloids. In *Humic and Fulvic Acids*; Gaffney, J. S., Marley, N. A., Clark, S. B., Eds.; American Chemical Society: Washington, DC, 1996; Vol. 651, pp 18–25. <https://doi.org/10.1021/bk-1996-0651.ch002>.
 - (71) Soemo, A. R.; Pemberton, J. E. Combined Quenching Mechanism of Anthracene Fluorescence by Cetylpyridinium Chloride in Sodium Dodecyl Sulfate Micelles. *J. Fluoresc.* **2014**, *24* (2), 295–299. <https://doi.org/10.1007/s10895-013-1319-2>.
 - (72) Pownall, H. J.; Smith, L. C. Fluorescence Quenching of Anthracene in Charged Micelles by Pyridinium and Iodide Ions. *Biochemistry* **1974**, *13* (12), 2594–2597. <https://doi.org/10.1021/bi00709a019>.
 - (73) Van Doorslaer, X.; Dewulf, J.; Van Langenhove, H.; Demeestere, K. Fluoroquinolone Antibiotics: An Emerging Class of Environmental Micropollutants. *Sci. Total Environ.* **2014**, *500–501*, 250–269. <https://doi.org/10.1016/j.scitotenv.2014.08.075>.
 - (74) Xiao, R.; He, Z.; Diaz-Rivera, D.; Pee, G. Y.; Weavers, L. K. Sonochemical Degradation of Ciprofloxacin and Ibuprofen in the Presence of Matrix Organic Compounds. *Ultrason. Sonochem.* **2014**, *21* (1), 428–435. <https://doi.org/10.1016/j.ultsonch.2013.06.012>.

- (75) De Bel, E.; Dewulf, J.; Witte, B. D.; Van Langenhove, H.; Janssen, C. Influence of PH on the Sonolysis of Ciprofloxacin: Biodegradability, Ecotoxicity and Antibiotic Activity of Its Degradation Products. *Chemosphere* **2009**, 77 (2), 291–295. <https://doi.org/10.1016/j.chemosphere.2009.07.033>.
- (76) Qiang, Z.; Adams, C. Potentiometric Determination of Acid Dissociation Constants (PKa) for Human and Veterinary Antibiotics. *Water Res.* **2004**, 38 (12), 2874–2890. <https://doi.org/10.1016/j.watres.2004.03.017>.
- (77) Babić, S.; Horvat, A. J. M.; Mutavdžić Pavlović, D.; Kaštelan-Macan, M. Determination of PKa Values of Active Pharmaceutical Ingredients. *TrAC Trends Anal. Chem.* **2007**, 26 (11), 1043–1061. <https://doi.org/10.1016/j.trac.2007.09.004>.
- (78) Gad-Allah, T. A.; Ali, M. E. M.; Badawy, M. I. Photocatalytic Oxidation of Ciprofloxacin under Simulated Sunlight. *J. Hazard. Mater.* **2011**, 186 (1), 751–755. <https://doi.org/10.1016/j.jhazmat.2010.11.066>.
- (79) Phenols, alcohols and carboxylic acids - pKa values https://www.engineeringtoolbox.com/paraffinic-benzoic-hydroxy-dioic-acids-structure-pka-carboxylic-dissociation-constant-alcohol-phenol-d_1948.html (accessed Feb 12, 2020).
- (80) Richter, B. Essentials of Heterocyclic Chemistry <https://www.scripps.edu/baran/heterocycles/Essentials1-2009.pdf> (accessed Feb 12, 2020).
- (81) Khalili, F.; Henni, A.; East, A. L. L. PKa Values of Some Piperazines at (298, 303, 313, and 323) K. *J. Chem. Eng. Data* **2009**, 54 (10), 2914–2917. <https://doi.org/10.1021/je900005c>.
- (82) Gilbert, N. World's Rivers "Awash with Dangerous Levels of Antibiotics." *The Guardian*. May 26, 2019.
- (83) Sun, S.; Wu, L.; Bai, P.; Png, C. E. Fluorescence Enhancement in Visible Light: Dielectric or Noble Metal? *Phys. Chem. Chem. Phys.* **2016**, 18 (28), 19324–19335. <https://doi.org/10.1039/C6CP03303B>.
- (84) Anger, P.; Bharadwaj, P.; Novotny, L. Enhancement and Quenching of Single-Molecule Fluorescence. *Phys. Rev. Lett.* **2006**, 96 (11). <https://doi.org/10.1103/PhysRevLett.96.113002>.
- (85) Hua, J.; Jiao, Y.; Wang, M.; Yang, Y. Determination of Norfloxacin or Ciprofloxacin by Carbon Dots Fluorescence Enhancement Using Magnetic Nanoparticles as Adsorbent. *Microchim. Acta* **2018**, 185 (2). <https://doi.org/10.1007/s00604-018-2685-x>.
- (86) Wang, H.; Wang, Y.; Yan, H.; Zhang, J.; Thomas, R. K. Binding of Sodium Dodecyl Sulfate with Linear and Branched Polyethyleneimines in Aqueous Solution at Different PH Values. *Langmuir* **2006**, 22 (4), 1526–1533. <https://doi.org/10.1021/la051988j>.
- (87) Lampert, D. J.; Frisch, M. A.; Speitel, G. E. Removal of Perfluorooctanoic Acid and Perfluorooctane Sulfonate from Wastewater by Ion Exchange. *Pract. Period. Hazard. Toxic Radioact. Waste Manag.* **2007**, 11 (1), 60–68. [https://doi.org/10.1061/\(ASCE\)1090-025X\(2007\)11:1\(60\)](https://doi.org/10.1061/(ASCE)1090-025X(2007)11:1(60)).

- (88) *Perfluorooctane Sulfonate in Drinking Water*; Canada, 2016.
- (89) Jones, A. J. S.; Rumsby, M. G. THE INTRINSIC FLUORESCENCE CHARACTERISTICS OF THE MYELIN BASIC PROTEIN. *J. Neurochem.* **1975**, 25 (5), 565–572. <https://doi.org/10.1111/j.1471-4159.1975.tb04369.x>.
- (90) Marciniak, B.; Kozubek, H.; Paszyc, S. Estimation of PKa* in the First Excited Singlet State. A Physical Chemistry Experiment That Explores Acid-Base Properties in the Excited State. *J. Chem. Educ.* **1992**, 69 (3), 247. <https://doi.org/10.1021/ed069p247>.

BIOGRAPHY

Carol A. Ajjan was born in Washington, DC and graduated from Yorktown High School, Arlington, Virginia, in 2011. She received her Bachelor of Science in 2015 and PhD in 2020 in Chemistry from George Mason University.